Wind Tunnel Parametric Study of Kite Performance for Power Generation

Master of Science Thesis

Cranfield University

MSc Aerospace Dynamics

Alex Rementeria Zalduegui

August 19th, 2019

Abstract

Little has been studied about the aerodynamic characteristics of fully-flexible kites. High deformability, high anhedral and low aspect ratio are some of the features that make these lifting devices differ from conventional aeroplanes. With the emergence of the novel technology of *Airborne Wind Energy* (AWE), a promising wind power alternative involving the use of kites, it is considered necessary to widen the understanding on kite aerodynamics as they are key to a proper optimisation of the technology.

The still young state of the art of AWE and the relative little attention that kites have received through history have made necessary to first build a complete literature review on the topic.

Wind tunnel tests of a scaled, four-line ram-air inflatable kite have been undertaken at Cranfield University. The experimental setup allowed to measure the aerodynamic coefficients at several control-input configurations. A parametric study of different wing anhedrals and pull of brakes is done over a range of wind speeds. The tests have shown stability issues of the kite, which has adversely affected the quality and quantity of the extracted data. Having that in mind, maximum L/D values over 4 are obtained, which is in agreement with the typical performance of fully-flexible, low aspect ratio wings. The anhedral is seen to decrease the lift coefficient, and the brakes are confirmed to be effective in worsening performance (reducing L/D).

A surface vorticity solver is used to build a parametric study similar to that of the experimental approach. The validation of the numerical method has been only possible qualitatively, where the trends in lift and drag coefficients under a change in anhedral match with the experimental.

All in all, it is suggested that future work focuses on the stability problem and in the field of the *Fluid Structure Interaction*.

Acknowledgements

In first instance, I would like to thank Professor Kevin Garry for introducing the aerodynamics to a mechanical engineer. He also attended my concerns in the initial stages of the project, and guided me into a topic that has been a constant motivator itself. I think there is still a lot to learnt in the department about the flight of the kite, and I am thankful he made me responsible for introducing the AWE technology to them.

I am also grateful for the infinite patience of the wind tunnel technicians Lynton Banks-Davies and Karl Gerhard during the tests, and also for their teaching on the things that are not written in textbooks. It was a pleasure to spend three days with such experienced persons.

I want to thank Dr. Vivek Ahuja for the continuous email exchange across the ocean during the weeks I was doing the numerical approach. He answered every doubt and query with a real predisposition to help.

For the optimism-boost that the email contact supposed, I want to thank Rachel Leuthold. I am very grateful she introduced me to the AWEC, and I am willing to get to know more about the AWE community.

My personal thanks go to Elena and Nahi for helping me gain perspective in the hard moments, and to my friends in Cranfield, the every-day support. Finally, I want to thank my family, to whom I owe this and every step.

Contents

List of Figures

List of Tables

Nomenclature

Abbreviations

AWE	Airborne Wind Energy
$AWEC$	Airborne Wind Energy Conference
$AWES$	Airborne Wind Energy System
$B.C.$	Before Christ
LE	Leading Edge
ppm	Part Per Million
TE	Trailing Edge

Symbols

$\alpha,\ AoA$	Angle of Attack	$[deg]$
ρ	Air Density	$[kg/m^3]$
θ	Handle Pitch Angle	$[deg]$
A	Wing Area	$[m^2]$
a	Axial Induction Factor (Betz efficiency)	$[-]$
A_s	Swept Area	$[m^2]$
C_D	Drag Coefficient	$[-]$
C_L	Lift Coefficient	$[-]$
$C_M,\ C_{My}$	Pitching Moment Coefficient	$[-]$

C_P	Pressure Coefficient	$[-]$
CD	Drag Coefficient (numerical approach)	$[-]$
CDi	Pressure Drag Coefficient (numerical approach)	$[-]$
CDo	Skin Friction Drag Coefficient (numerical approach)	$[-]$
CL	Lift Coefficient (numerical approach)	$[-]$
CM	Pitching Moment Coefficient (numerical approach)	$[-]$
D	Drag Force	$[N]$
e	Load Speed to Wind Speed Ratio	$[-]$
L	Lift Force	$[N]$
l	Line Lateral/Spanwise Spacing	$[cm]$
L/D	Lift to Drag ratio	$[-]$
M_x	Rolling Moment	$[Nm]$
M_y	Pitching Moment	$[Nm]$
M_z	Yawing Moment	$[Nm]$
P	Power	$[N * m/s]$
P_w	Wind Power Density	$[N * m/s]$
P_{max}	Maximum Power	$[N * m/s]$
q	Dynamic Pressure	$[Pa]$
T	Line Tension	$[N]$
V_C	Crosswind Velocity	$[m/s]$
V_L	Load (reel-out) velocity	$[m/s]$
V_W	Wind Speed	$[m/s]$
V_{rel}	Relative airspeed	$[m/s]$

Chapter 1

Introduction

1.1 Context of the Problem

The majority of the scientific community agrees that there is a causality between the concentration of greenhouse gases in the atmosphere and a global warming that leads to a climate change. The human activity after the industrial revolution has increased the emission of gases like CO_2 up to levels high enough to create a generalised social concern on climate change. CO_2 concentrations of the last 420,000 years are recorded in Figure 1.1. The sudden increase up to year 2007 is clearly off the previous trends of glacial and warm periods (min. and max. CO_2 concentrations, respectively). The CO_2 concentration at July 2019 was 411.77 ppm, which is out of the presented chart, and this value is still increasing.

The main source of these greenhouse gases is the use of fossil fuels. This alternative is cheap to extract and has a high energetic value per volume unit. It is easy to transport and "ready to use". Fossil fuels are attractive, but are limited and produce high emissions.

There is a clear need to change both the energy consumption and production. The transition to renewable energy sources is necessary if the ever-increasing energetic demand of the human society is to be satisfied in a sustainable way.

Wind energy has shown a good potential, which makes the industry of wind turbines increase every year. There is however an alternative to the conventional technology, it has been defined as *Airborne Wind Energy* (AWE) and it involves the use of tethered flying devices, or kites, for wind energy harvesting. The kite is a lifting body that, tethered to the ground by a line, can

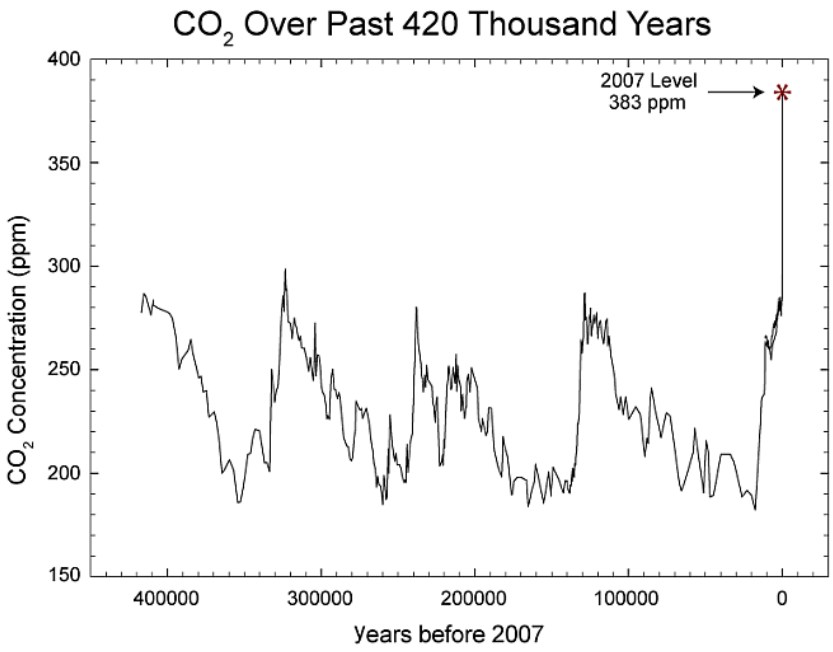

Figure 1.1: Atmospheric CO_2 concentrations over the last 420,000 years. Source: *GLOBALVIEW + CO2 (Mauna Loa & South Pole readings), Nature 399 (Petit et.al. 1999).*

rise and fly in the atmosphere under wind pressure. The most typical mechanism is based on a kite that creates sufficient aerodynamic force to both sustain itself and to create an extra pull that is then converted into electricity. A more detailed review of AWES is given in Chapter 2.3.

The AWE technology is only a few decades old, and has been put into practice in the last decade. Today there is a small range of companies that effectively fly full-scale power kites in the prototype state, and the first commercial AWE systems (AWES) are about to come.

There is various reasons why AWES are competitive, or can be in the recent future. First, the kites can be flown at much higher altitudes than the operation altitude of the tallest wind turbines. Due to the atmospheric boundary layer, wind speed increases with altitude, so the kite sees a higher wind energy input (Figure 1.2b). The equation relating wind speed with available wind power is the following.

$$P = \frac{1}{2}\rho A {V_W}^3$$

It can be seen that the power is directly proportional to the cube of the wind speed, which overcomes the decrease in air density with altitude. The high altitude that AWES can reach is therefore a very attractive feature.

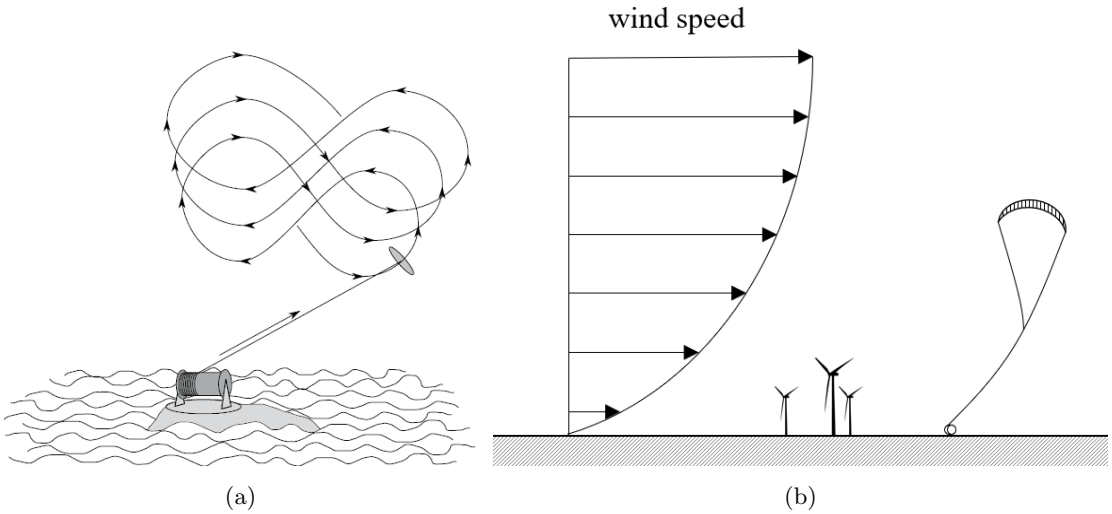

Figure 1.2: (a) "8"-shape patterns by the kite during the reel-out phase of an AWES. Source: *Estimation of the mechanical energy output of the kite wind generator (Argatov et.al., 2009).* (b) The existence of atmospheric boundary layer means a higher wind speed is seen by the AWE kite.

The initial cost involved in AWES is also smaller, specially because of the lack of a structure to sustain the power-generating device. Thus in the future it could become more competitive than the conventional wind turbines in front of the cheap fossil fuels. The maintenance of AWES is also cheaper, an advantage for the offshore application.

1.2 Motivation

AWE is a novel technology still in the research/prototype state. The behaviour of fully-flexible kites has been scarcely studied because of the little attention they have received until a past few decades. The characteristics of an AWES involving flexible kites have the following characteristics that make them differ from the more studied conventional aeroplanes:

- A high deformability creating a highly coupled system of aerodynamic forces and wing shape.
- High anhedral and low aspect ratio of the majority of flexible kites.

- Complex dynamic system with extra constrains due to the tether lines.
- Complex flight patterns, typically "8"-shaped and an additional displacement due to the reel-out. The relative orientation of kite and airflow are constantly changing.

These characteristics make the control of AWES to be one of the most demanding challenges of the area. Therefore there is a need to better understand the aerodynamic characteristics of such a system to allow a comprehensive optimisation process.

The aerodynamic characteristics are an important part of the optimisation of AWES. Apart from being directly related to the amount of pull generated, the performance of the kite (L/D ratio) is a key parameter to optimise. As will be explained in later sections, L/D dictates the motion of the kite. Thus it can be seen as an input for the optimisation of flight pattern and angle of attack of the kite, among others.

All in all, an aerodynamic study of the kite is considered valuable in order to widen the still scarce literature available. The wind tunnel facilities in Cranfield University are a good chance of starting an experimental research line in this emerging technology. As this is the first project related to the topic, a complete literature review is also considered vital.

1.3 Aims and Objectives

Aim

Implement an analytically supported experimental method that will, along with a complete literature review on the topic, serve as a basis for the understanding of the aerodynamic characteristics of power-kites.

Objectives

- Build a self-standing literature review on the use of kites for wind power generation. The literature review should serve as a base for future research, and include both a review of the novel technology and a state of the art of the research on the aerodynamic characteristics.
- Plan and implement an experimental methodology in a wind tunnel that will allow the measurement of aerodynamic loads acting on a fully-flexible scaled kite.

- With the wind tunnel tests, build a parametric study accounting for the effects of wind speed, input pitch angle and wing anhedral.
- Validate a numerical analysis (most likely a Potential Method) with the wind tunnel results. The numerical method should account for the characteristics of a high-anhedral, low-aspect-ratio and high-thickness wing.
- With the numerical method, build a similar parametric study in parallel to the experimental one.

Chapter 2

Literature Review

The aim of this chapter is to give an introduction to the actual state of the use of tethered flying objects as an alternative way of harvesting wind energy, as well as to explain the knowledge gained until the date on the flight of kites.

The literature review is intended to be self-standing and to serve as a basis for future work. For the sake of completeness it will therefore include topics further from the scope of the project.

2.1 Definition of kite

To begin with it is necessary to clarify what a kite is, since popular belief differs from what this work considers to be a kite.

A good example is seen in Oxford's definition: "*a toy consisting of a light frame with thin material stretched over it, flown in the wind at the end of a long string*".

A more precise definition is given in [1]: "*A heavier-than-air machine held to the earth by means of a flexible line and capable of rising to a positive angle with the horizon as the result of forces created by wind-pressure*".

The latter fits better to the context of AWES. Apart from extending its possible applications (could be a toy or an engineering tool), it covers any tethered and non-self-powered flying object independently of their material and geometry. Thus a simple flat rigged fabric, tethered

parafoils and parachutes, and even tethered rigid gliders fit into the definition. As explained in Chapter 2.3 AWE technology includes a wide range of different flying objects valid for wind energy harvesting.

2.2 The evolution of kites through history

It is a fact that the scientific interest on kites has been small in comparison with that of more conventional flying objects. However kites have been used by humans for more than two thousand years, which means a more profound knowledge should have been accumulated through history, allowing a more successful study of the physics of their flight.

A possible explanation for this apparent contradiction is that the society sees the kites as no more than toys (a definition given above is indicative). It is also true that the relatively small cost involved in their construction has reduced the necessity of applying systematic design tools.

As these are only hypotheses, the author finds of much interest to first look back at the history of kites in order to uncover the reasons that drove the kites to differ from the path of the rest of aviation.

2.2.1 The origins

One of the most complete and reliable reviews about the history of kites is given by Clive Hart (1967) [1]. It is generally agreed that kites originated in China. There is evidence that kites were known 2,200 years ago, but probably were also used back to 1000 B.C. [2]. Hart introduces the hypothesis that the first kites were an extension of banners, which in many places were made to fly attached to lines. If the banners were stiffened by rods to make them more visible, he states, the similarity with a kite would become evident.

Chinese folklore is full of references to the use of kites, and even if not necessarily reliable, they indicate that kites were known. The most popular story dates back to 196 B.C., where General Han Hsin presumably flew a kite towards the walls of the palace he was to raid to know the exact distance from his troops. That way he was able to dig a tunnel with the length of the line and successfully get into the palace.

Even if they began as military instruments, kites took a strong spiritual connotation. They became a source of superstitions and gave way to popular ceremonies and traditions such as the Kite's Day (still celebrated). Needless to say that the symbolism implicit in kites would also serve as military strategy.

During the first millennium after their invention kites spread across Asia and Oceania. There is plenty of kite design varieties coming from Korea, Japan, India, Polynesia and other islands. Not only designs, but also new applications were given to the kite (apart from the omnipresent link with gods): kite fighting contests, their use as aid for fishing and meteorology purposes, and as transport of material or even men.

Figure 2.1: A Maori *birdman* kite that reminds to a long-span contemporary aircraft. Wingspan 2.08 m.

2.2.2 Spread to the West

The introduction of kites in Europe is ambiguous in respect to the dates, and various cultures have certainly influenced their development. Figure 2.2 sketched by Hart helps to understand the spread of the kite from eastern countries before 1600.

It is the Romans that gave the earliest prototype of a concept of western kite (around year 200). Dragon shaped windsocks were made to fly by letting the air inflate the hollow figure, a mechanism similar to the ram-air inflatable kites nowadays (see Figure 2.5 (b) and (c)). These devices had no lifting surfaces and could not sustain above the tether point, thus according to the definition given above these were no proper kites. Nevertheless they served as a basis

for later variations firstly recorded in drawings from the 14th and 15th centuries. These kites, also windsocks in nature, did have wings (and thus lifting surfaces) attached to the flying figures.

On the other hand, Marco Polo brought notice of the art of kite making from his long stay in China, but remained as no more than curious stories. The same concept of kite also spread from Asia to the north of Africa as early as the 9th century. According to Hart, it is probable that the relationships across the Mediterranean Sea allowed the introduction of eastern kite designs in Europe.

From these two different concepts, the one coming from Asia took relevance thanks to the trading routes (mainly Dutch sailors), letting the windsock design unused with time. By the 18th century kite flying was popular among the European society.

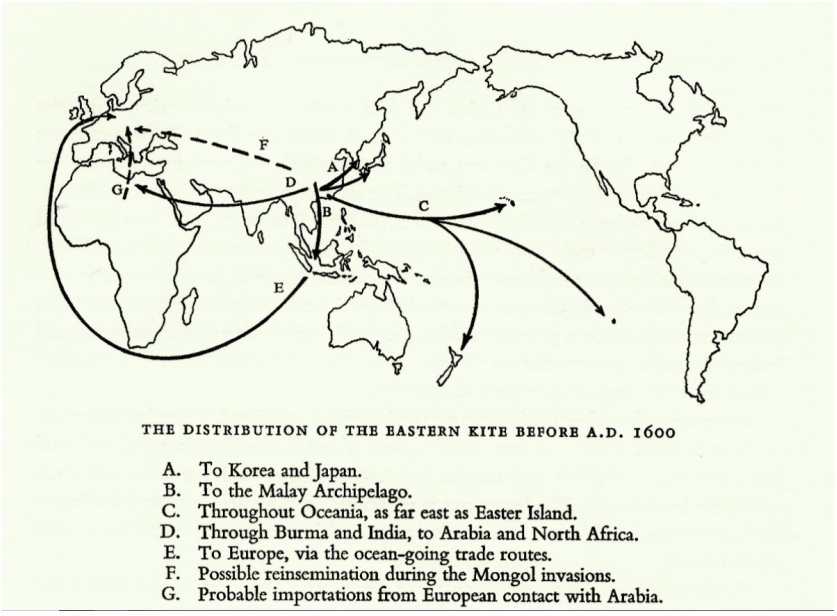

Figure 2.2: Sketch of the spread of kites from China before 1600. Source: *Kites: An historical survey (Hart, 1967)*

It is therefore clear that kites were well known in a considerable part of the world 300 years ago. Their use, however, was mainly limited to leisure and scattered practical uses, and their designs were a result of hundreds of years of hand-craft. Note that neither the first lighter-than-air flying device nor the first aircraft were still invented at the date.

Figure 2.3: Early illustration of the popularized diamond-shaped kites in Europe, from *The Mysteryes of Nature and Art.* England, 1634.

2.2.3 The kite as a research tool

During the 18th century the kite was first used for scientific purposes in the West.

In 1749 Alexander Wilson proposed to measure the temperature of the air in the higher regions of the atmosphere by arranging several kites to a single line and attaching a thermometer to the highest one. This is also the first record of such a configuration of kites, and a precursor of the actual *Laddermill* configuration, a concept developed by Delft University of Technology (mentioned in Chapter 2.5.1).

It was in 1752, only four years later, that the most famous experiment involving kites took place. Benjamin Franklin, with the aid of a kite similar to that in Figure 2.3 and a stormy day, managed to prove that lightnings are in essence electricity. There were other scientists contemporary to Franklin that made their own tests with kites [1], spreading their use as a research tool.

During the 19th century meteorological observations originated, but as in 1783 the first lighter-

than-air flying device was invented, the attention of the scientific community was directed towards these new machines. That is one clear account of the decrease in interest on kites due to an alternative development in aviation.

It can be said, however, that kites re-gained the interest of the community this time. They ended up showing a better potential for meteorological purposes (1880s - 1930s). Also by the end of the 19th century new designs originated such as the Eddy's bow kite and Hargrave's box kite (Figure 2.4a), which would have a more reliable flight than the previous ones. Kite designs became bigger for the purpose of lifting humans, for which a considerable amount of records is available (see Hart [1], Chapter 7).

As Hobbs states [3], during the decades previous to the invention of the aeroplane a considerable qualitative understanding on the flight of the kite was gained, even if no aerodynamic studies were undertaken. An example of the state of the art in that period is Marvin (1897) [4]. Here the forces acting on a flying tethered kite are considered, and general stability issues are discussed.

2.2.4 Origins of the aeroplane and decay of the kite

Soon the introduction of power by propellers allowed the development of the first aircraft prototypes. The basis for their lifting surfaces was without doubt coming from kite designs.

A clear example of the transition from the kite to the aircraft is that of the design of Hargrave in 1894. It was essentially the same shape as his box kite (Figure 2.4a), with an engine added to it. A line would connect it to the ground so that it launched as a kite, with no engine power. Once in flight the power would be set on and the line picked up to begin flying toward the wind. However, there is no evidence that the device was brought into practice [1].

Note the similarity of the design in Figure 2.4a with a biplane, with the exception of the vertical surfaces closing the "box". They gave stability to the device, but also made it less manoeuvrable. Later aeroplanes would get rid of them and transfer the stability issues to the control input of the pilot.

In close relation is the wing warping that Wright Brothers introduced in 1899. It was their

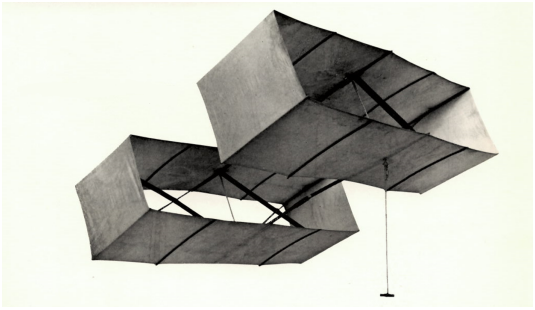

(a) Hargrave's box kite. Source: *Kites: An historical survey (Hart, 1967)*

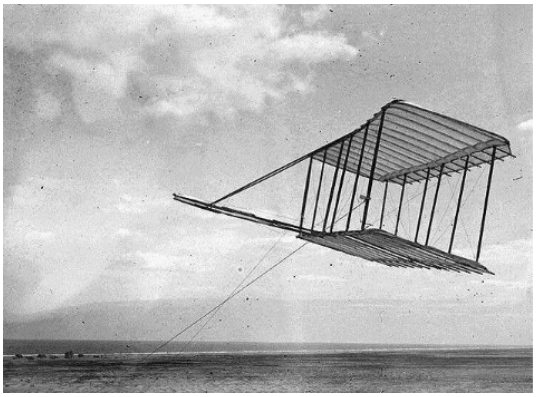

(b) Wright Brothers' Glider No. 1. A glider flown as a kite (1900)

Figure 2.4: Precursors of the first aeroplanes

first prototype, a glider that was, in fact, flown as a kite (*Glider No. 1)*. The design was similar to the box kite but without the stabilizing vertical surfaces, and thus consisted of two horizontal flat surfaces (Figure 2.4b). The warping was imposed by pulling the control lines asymmetrically, achieving a similar effect to that of ailerons nowadays.

In 1903 Wright Brothers designed and built the first heavier-than-air powered aircraft that could effectively fly. The development of the understanding on aerodynamics between the end of the 19th and the beginning of the 20th century was finally successfully applied to a real aircraft.

Kites did not have the potential that aeroplanes had. They had opened the way to the modern aviation, and had been a crucial part of its beginnings, but the increasing interest on the aeroplane finally shadowed the path of the kite for the first half of the 20th century.

2.2.5 Last decades: increased interest

Even if kites were no longer object of the leading research in applied aerodynamics during the 20th century, major contributions were made to what is considered the modern kite. The knowledge gained with the development of the aeroplane also helped to the first serious aerodynamic analysis on kites.

As can be expected the kite was used for military purposes during the first half of the century. As a result the earliest wind tunnel tests were undertaken with the Cody war kite (a winged box kite) and variants between 1938-1942. Jackson (1942) [5] successfully measures the performance of various Cody kite designs including the effects of wind speed, bridle length and different kite geometry configurations.

In 1948 Francis M. Rogallo patented a delta-shaped fully flexible kite which flew with no rigid frames. The design, known today as the parawing, was simple, highly manoeuvrable and had a high glide ratio. Its good performance attracted the attention of the U.S. space programme, who saw the high glide ratio as an opportunity for landing manned spacecraft after atmospheric re-entry. Together with Rogallo they carried out several wind tunnel tests with improved glider designs at Langley (Figure 2.5a). Finally the idea was replaced by advanced parachute descent systems for landing, but still an extensive set of wind tunnel tests was undertaken:

- The original report by Rogallo et al. (1960) [6] involves wind tunnel tests of aluminium-alloy models at subsonic and supersonic speeds for several angles of attack and wing configurations. Real flight tests at low speeds are also done for the analysis of deployment characteristics. Overall, the performance of such a glider is said to meet the requirements for the re-entry flight, maintaining the maximum temperatures at about 800°C.

- In 1963 Polhamus and Naeseth present a report [7] involving wind tunnel tests with several parawing models with different configurations of camber, twist and aspect ratios. A high aspect ratio, and the zero-camber, zero-twist configuration are concluded to be preferable for performance.

- Rogallo et al. [8] presents a complete overview of the data obtained from wind tunnel tests during the previous years for different wing designs. Fully flexible kite models are included this time.

- There is a list of reports available from the period of 1967-1971 involving experimental assessment of the parawing and the development of its design and understanding [1]. An interesting report is that of Libbey, Ware and Naeseth (1967) [9], where a fully flexible parawing is analyzed in a wind tunnel in terms of L/D, C_L,C_D, C_M over a range of

[1] link: `http://2e5.com/kite/nasa/reports/`

angles of attack, as well as longitudinal and directional static stability and the effect of line length.

Another design that set the basis for high-performance kites is that of the parafoil, invented by Domina C. Jalbert in 1964. The parafoil is a fully flexible kite that is self inflated with wind pressure by openings along the leading edge (as windsocks in medieval Europe). Jalbert adopted the idea of wing aerofoil sections for his kite, a shape that was applied to the vertical ribs that separate the multiple inflated cells. As a result, one of the most efficient kites to the date was invented (see Figure 2.5b).

The most comprehensive analysis on parafoils is made by John D. Nicolaides in 1970s:

- Nicolaides, Speelman and Menard (1970) [10] give a review of the applications of parafoils: cargo delivery, manned flight and tethered flight. In addition, some wind tunnel tests and free flight tests are collected to show the good performance (L/D over 4 for AR of 2-3) and the reliability of its deployment and stability.
- Nicolaides (1971) [11], carries out an extensive set of wind tunnel tests, both in Notre Dame University and NASA Langley. A total of 13 different parafoils are tested: 4 scaled models (fabric, rigid and semi-rigid materials) and 9 full-scale models (all fabric), with varying surface area and AR.
- Nicolaides and Tragarz (1971) [12] collects previous wind tunnel tests and compares the results of flight performance with estimated values and with real flight tests to conclude a considerable agreement between them.

Also during the 1970s a new kite design was developed, the flexifoil. It is similar to the parafoil in almost every aspect, but generally with an increased AR and a spanwise curvature (or anhedral), as seen in Figure 2.5c. It needs to be said that the line between the definitions of parafoil and flexifoil is diffuse, and that flexifoils are often called parafoils. This is a widely used design nowadays in kite-surf sport and gliding activities. The kite tested in the 8x6 Wind Tunnel at Cranfield University is of this nature.

By the end of 1970s a firm base was set on the understanding of kites. The modern, efficient kites were already invented, their performance was experimentally studied and some designs had even gone through an extensive optimization process. It was discovered that kites are a

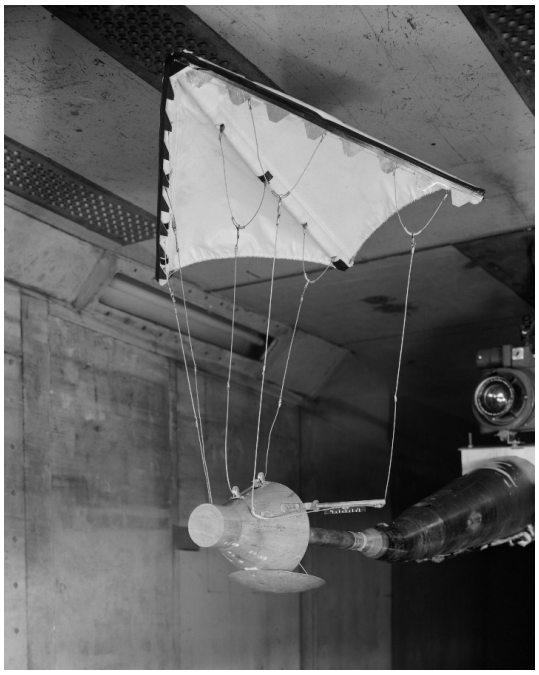

(a) A stiffened version of Rogallo's parawing in a wind tunnel test for Gemini recovery programme (1961). Source: *NASA*

(b) Parafoil. Source:

(c) A prototype *X-38 emergency reentry vehicle* approaching and landing with a large scale parawing (1999). Source: *NASA*

Figure 2.5: Modern kites

cheap but reliable flying device capable of creating considerable amounts of lift with a reasonable ratio to drag. Their potential was now more clear, and the energetic crisis added the interest in new energy source alternatives: the first ideas of the Airborne Wind Energy (AWE) arose [13].

It was in 1980 that Miles L. Loyd proposed "*a concept for large-scale wind power production by means of aerodynamically efficient kites*" [14]. Here, Loyd suggests that a kite (any tethered lifting device) flying crosswind in a closed loop can generate a high power output. The concept of crosswind motion is novel here and thus worth to explain: the kite, rather than flying static, is steered in circles in a plane normal to the wind direction (similar to wind turbine blades). That way the relative airspeed of the kite increases well above the wind speed, resulting in a higher aerodynamic load. Figure 2.6 is a sketch of the velocities and forces involved in such a mechanism.

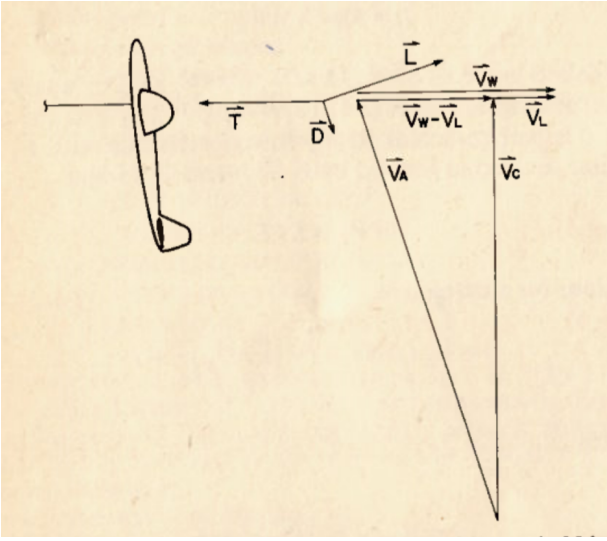

Figure 2.6: Forces and velocities on a kite in crosswind motion (no weight, no line drag). Crosswind velocity (V_C) is added to the wind velocity (V_W) to increase the relative airspeed (V_A). If work is to be created a load velocity (V_L) is substracted in the wind direction. Source: *Crosswind Kite Power (Loyd, 1980)*

The conversion of the wind power input, according to Loyd, can be done either by adding turbines to the kite or in the ground with the mechanical pull of the line. These two concepts are defined as *drag power* and *lift power* respectively. Figure 2.7 shows the results of a simplistic theoretical analysis comparing the different approaches for kite power generation. Even

if neither tether drag nor system's weight and efficiencies are considered in the calculations, the comparison is useful for understanding the potential of the two crosswind motions over the static flight.

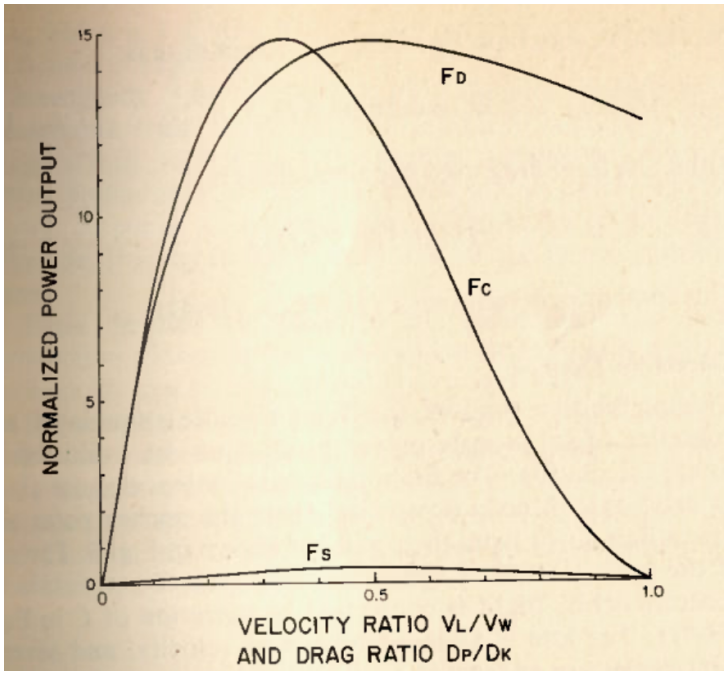

Figure 2.7: Power output comparison for: drag power crosswind (F_D), lift power crosswind (F_C) and static flight (F_S), where D_P/D_K is the ratio of output drag power to kite drag. L/D=10 for all cases. Source: *Crosswind Kite Power (Loyd, 1980)*

In the same paper Loyd presents a more detailed analytical approach and estimates the power output that a tethered C-5A aircraft would give. Even if results are somehow optimistic, a power of 6.7 MW is achieved, much higher than the available power of a wind turbine unit in 1980s.

Such encouraging results gave the foundations for the AWES technology. Since then, and specially in the last decades, the interest in this application of kites has increased. The most recent research on the topic is covered in Chapters 2.4 and 2.5, but first a more in depth review of the AWES is given for the better understanding of the context in which today's research is involved.

2.3 Airborne Wind Energy Systems (AWES)

The term *Airborne Wind Energy Systems* (AWES) was introduced in the last few decades to cover the emerging technologies involving wind energy harvesting by means of tethered lifting devices, i. e., kites. This chapter is intended to give a complete review composed of: a classification of the technologies, the physics behind the different systems, their potential as a renewable energy source and the main challenges to face, as well as a review of the actual state of companies and universities.

2.3.1 Classification of AWES

The general purpose of an AWES is that of converting wind energy into electricity, as conventional wind turbines do. To the date two main configurations are conceived, the *Ground-Gen* systems (GG-AWES) and the *Fly-Gen* systems (FG-AWES). Figure 2.8 is a sketch of these two concepts.

Ground-Gen AWES transform the wind power into a mechanical pull that is transmitted through the tether to the ground, were a drum connected to a generator converts the mechanical torque into electrical power. Cherubini, et al. (2015) [15] further classifies the GG-AWES into *Fixed-Ground-Station* GG-AWES and *Moving-Ground-Station* GG-AWES. The first converts the pull into electricity in a fixed station in the ground, while the second converts it in a ground station in motion. The most widely used technology is the Fixed-Ground-Station GG-AWES due to the simplicity of the system.

Fly-Gen AWES make use of generators attached to the kite itself, so that wind power is directly converted into electricity with no need of pull or work. The electricity is then transported to the ground by an extra tether line.

Going back to Loyd (1980) and his seminal concept of AWES, there is a match worth to mention. His *lift power* system is what now is defined as Ground-Gen AWES, because the force creating the pull to the line is the lift of the kite. On the other hand, the *drag power* system is equivalent to the Fly-Gen AWES because it is the drag that generates power in the kite's generators.

One difference between GG and FG is that in GG-AWES work is needed to give motion to

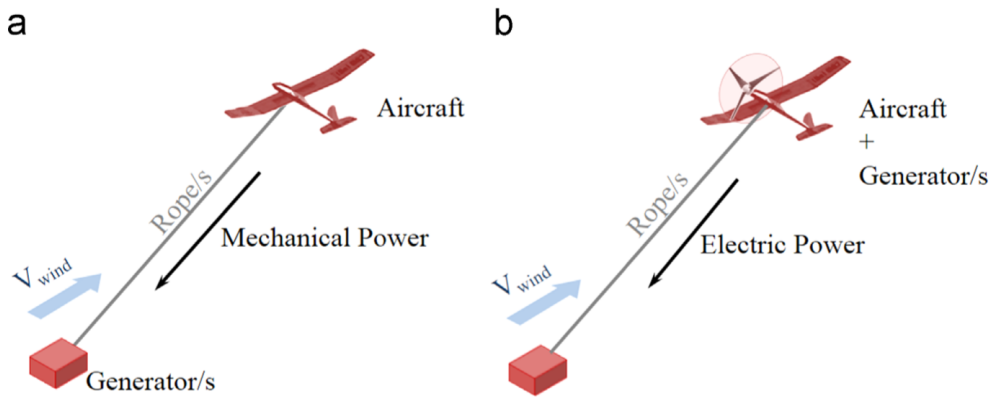

Figure 2.8: *Ground-Gen* (a) and *Fly-Gen* (b) AWES concepts with their respective transmission of power. Source: *Airborne Wind Energy Systems: A review of the technologies (Cherubini, et. al. (2015))*

the generator. In Moving-Ground-Station GG-AWES that condition is satisfied by the displacement of the ground station. In the case of the Fixed-Ground-Station GG-AWES, that means the line or tether needs to be reeled-out to effectively produce electricity. For the sake of repeatability, it is of interest that the hole process is cyclic, so a reel-in phase is necessary to recover the kite to its initial position (Figure 2.9). As a result, a pumping cycle is created where a fraction of it spends energy. It needs to be ensured that this fraction takes less energy from the system than the reel-out phase gives. To ensure that, a small pull coming from the kite is wanted during the reel-in. This can be achieved by reducing the angle of attack of the kite, forcing a stall or by changing its aerodynamic characteristics to reduce lift. In the case of a non-rigid ram-air parafoil, for example, the aerodynamic shape can be intentionally worsened.

Therefore there is a disadvantage in the power output of the Fixed-Ground-Station GG-AWES. They give a pumping output, which makes necessary the use of batteries or capacities to maintain a constant electricity supply. An alternative and effective solution is to fly several kites to cover the gaps in the output signal, as pistons typically do in an internal combustion engine.

In contrast, Moving-Ground-Station GG-AWES and FG-AWES have the advantage of giving a more constant power output. The disadvantages of the FG-AWES are the increased weight due to the in-flight generators and the electricity-driving line, as well as the complexity inherent in such a flying system. A Moving-Ground-Station system is also more complex, and

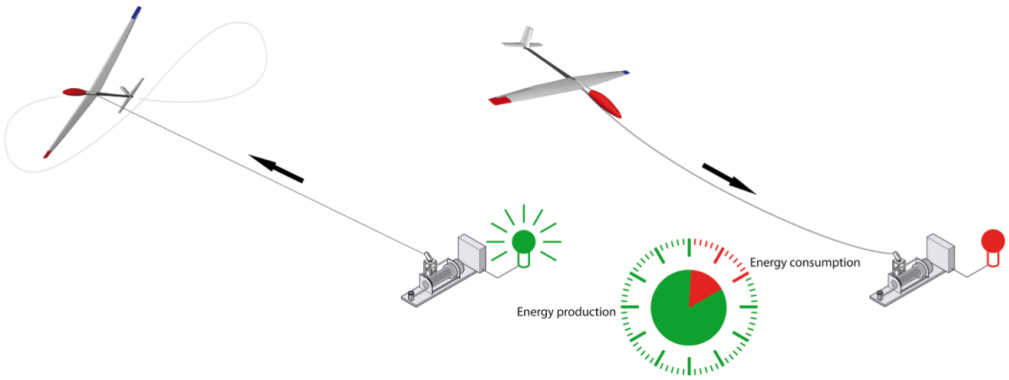

Figure 2.9: Reel-out (left) and reel-in (right) phases in the pumping cycle of a Fixed-Ground-Station GG-AWES. Source: *The PowerPlane an Airborne Wind Energy System Conceptual Operations (Sieberling and Ruijterkamp, 2011)*

to the date the simplicity of the Fixed-Ground-Station devices is preferred.

All the configurations fly crosswind to take the advantage of the increased relative airspeed. Typically an "8"-shaped flight pattern is adopted (Figure 2.9, left). There is a clear improvement in terms of power output, as stated by Loyd, and it opens the possibility to large scale power production. There is, however, certain FG-AWES designed to fly static (e. g., companies *Sky Windpower, Altaeros Energies, Omnidea*).

The kites used today among the Ground-Gen AWES are both rigid and non-rigid devices. [15] classifies them as follows:

- Leading Edge Inflatable (LEI) kites: They are non-rigid, composed of a single fabric surface and an inflated (no intakes) leading edge that adds stiffness to the kite. They are simple in design, easy to take-off and land but have scalability issues. The LE tube can be supported by extra lines to gain aerodynamic performance.
- Foil kites (flexifoils): The advantage of these kites, as well as their parafoil predecessors, relays on the aerodynamically efficient aerofoil-shaped section. The ram-air intakes in the leading edge inflate the cavity between the upper and lower surfaces giving the kite a stiffened, curved wing shape. They are scalable, highly manoeuvrable and have a good performance.

- Delta kites: They are made out of fabric and stiffened by a structure. They show a better aerodynamic performance than previous ones, but the structure brings increased weight.

- Gliders: The best aerodynamic performance is achieved by rigid-wing gliders, with the drawback of increased weight. An advantage over the fabric kites is their durability. Rigid gliders have a durability in the order of years, against the order of hundreds of hours of fabric kites [15].

The kites among the Air-Gen AWES can be classified in three main groups, according to [15]. Note that all of them have attached turbines:

- Rigid gliders or frames creating lift by means of wings. Their performance is good, with the drawback of the increased weight.

- Devices creating lift with the same turbines used for power generation. The advantage here is that there is no need of extra lifting surfaces. As the turbines are creating the lift, they do not point directly to the wind and so efficiency is lost.

- Lighter-than-air flying devices. Even if they do not fulfil the definition of kites, they are currently being used by companies for power generation, so it is worth to include them.

2.3.2 The simplified power equation

As has been seen there is a wide range of alternatives in the AWES, a technology that is emerging and still in the initial phases of development as a renewable energy source. One reason for the rapid increase in interest over the last decades is the potential of the technology: considerable power outputs with minimum cost.

A list of companies and the power outputs achieved in the market is given in Chapter 2.3.3. But first, for a theoretical understanding of the potential of AWES an explanation of the very basics of the governing physics is considered necessary.

The first record of simplified equations to obtain the maximum theoretical power output of AWE systems is given by Loyd [14]. Both *lift mode* (GG) and *drag mode* (FG) are studied. The assumptions made here are:

- Kite mass is neglected

- No line drag and mass are considered
- Betz efficiency and power conversion/transmission efficiencies are neglected
- Kite velocity is constant
- Only aerodynamic forces and tether tension are considered

A kite flying crosswind in lift mode is considered as showed in Figure 2.10.

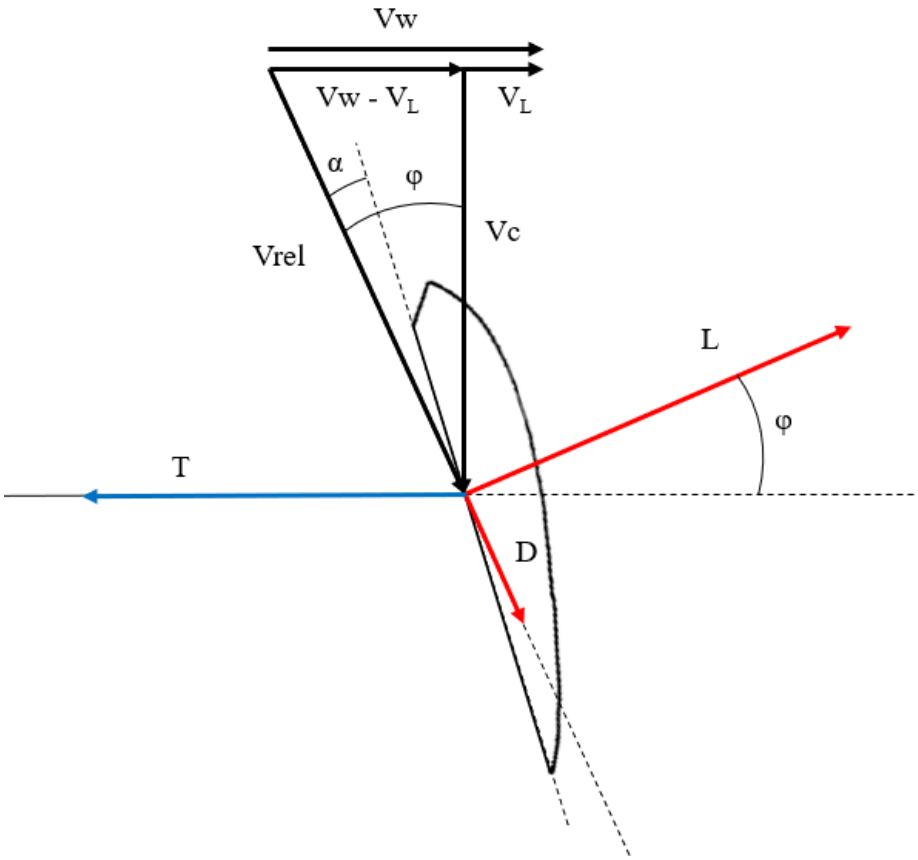

Figure 2.10: Forces and velocities in a wing flying crosswind. Wind velocity (V_W), reel-out velocity (V_L), crosswind velocity (V_C) and relative airspeed (V_{rel}); lift (L), drag (D) and tether tension (T); angle of attack (α).

As velocities are constant, equilibrium is satisfied in the direction parallel to the crosswind velocity:

$$\begin{aligned} Dcos\varphi &= Lsin\varphi \\ \frac{L}{D} &= \frac{C_L}{C_D} = \frac{cos\varphi}{sin\varphi} \end{aligned} \tag{2.1}$$

The same trigonometrical relation is satisfied for the velocities:

$$\frac{L}{D} = \frac{V_C}{V_W - V_L} \tag{2.2}$$

Note that the magnitude of the L/D ratio is dictating the relations in the velocity field.

Loyd makes the assumption that L/D is high enough to meet $V_C \approx V_{rel}$. This can be applied to rigid-winged kites with good performance, but non-rigid kites do not typically exceed L/D values of 6. The continuation here is therefore made for any L/D.

Introducing the trigonometrical relation $V_C = V_{rel} cos\varphi$, Eq. 2.2 becomes:

$$V_{rel} = (V_W - V_L)(L/D)\frac{1}{cos\varphi} \tag{2.3}$$

Now,

$$\begin{aligned} L &= \frac{1}{2}\rho A C_L {V_{rel}}^2 \\ D &= \frac{1}{2}\rho A C_D {V_{rel}}^2 \end{aligned} \tag{2.4}$$

Substituting Eq. 2.3 into Eq. 2.4 gives:

$$\begin{aligned} L &= \frac{1}{2}\rho A C_L (V_W - V_L)^2 (L/D)^2 \frac{1}{cos^2\varphi} \\ D &= \frac{1}{2}\rho A C_D (V_W - V_L)^2 (L/D)^2 \frac{1}{cos^2\varphi} \end{aligned} \tag{2.5}$$

Applying the equilibrium in the tether direction:

$$T = Lcos\varphi + Dsin\varphi \tag{2.6}$$

Now, substituting Eq. 2.5 into Eq. 2.6 and simplified using of Eq. 2.1, the following expression arises:

$$T = \frac{1}{2}\rho A C_L (V_W - V_L)^2 (L/D)^2 \frac{1}{cos\varphi} + \frac{1}{2}\rho A C_L (V_W - V_L)^2 \frac{1}{cos\varphi} \tag{2.7}$$

The term $cos\varphi$ can be written as a function of (L/D). For this the trigonometrical relation $sin^2\varphi + cos^2\varphi = 1$ is used in combination with Eq. 2.1 [16]:

$$\begin{aligned} cos^2\varphi &= 1 - sin^2\varphi = 1 - \frac{cos^2\varphi}{(L/D)^2} \\ cos^2\varphi\left[1 + \frac{1}{(L/D)^2}\right] &= 1 \\ cos\varphi &= \sqrt{\frac{(L/D)^2}{1 + (L/D)^2}} \end{aligned} \tag{2.8}$$

Hence Eq. 2.7, after rearranging, can be rewritten as:

$$T = \frac{1}{2}\rho A C_L (V_W - V_L)^2 \underbrace{\sqrt{\frac{1 + (L/D)^2}{(L/D)^2}}\left[(L/D)^2 + 1\right]}_{\text{H=f(L/D)}} \tag{2.9}$$

The power output of the system is computed as the work done by the tether tension T (note that the rate of change of the displacement creating work is V_L):

$$P = TV_L \tag{2.10}$$

Hence the power equation can be obtained substituting Eq. 2.9 into Eq. 2.10:

$$P = \frac{1}{2}\rho A C_L (V_W - V_L)^2 H V_L \tag{2.11}$$

In order to obtain the maximum achievable theoretical power, Eq. 2.11 is differentiated over V_L and equalled to zero, giving:

$$P_{max} = \frac{1}{2}\rho A C_L \frac{4}{27} {V_W}^3 H \tag{2.12}$$

,where

$$V_L = \frac{1}{3}V_W$$

Thus the same values as Loyd are obtained, with the difference in the definition of H. Note that for high values of L/D, H tends to the expression $(L/D)^2$ as in Loyd. The main conclusion that Loyd obtained from Eq. 2.12 is that to maximise the power output the values of L/D and C_L have to be maximised.

Another expression for the power equation relies on the wind input power density, P_w, such as:

$$P = P_w A C_L F \tag{2.13}$$

,where

$$P_w = \frac{1}{2}\rho {V_W}^3$$

and F is a function of the flight mode, in this case lifting crosswind mode (F_L).

Equalling the two power equations (Eq. 2.11 and Eq. 2.13) the function F_L is obtained, and Eq. 2.13 becomes:

$$P = \left(\frac{1}{2}\rho A {V_W}^3\right) C_L \underbrace{H \frac{V_L}{V_W}\left(1 - \frac{V_L}{V_W}\right)^2}_{\text{FL}} \tag{2.14}$$

Again, the same expression as in Loyd is obtained.

For a more in depth analysis of the power equation in lift mode, the following literature is recommended: [16] [17]. Here new features have been added, such as variable wind speed with altitude, line drag or the gravity and centrifugal effects.

It is also worth to make a note on the Betz efficiency, or the effect of the velocity reduction that the kite induces to the air past the swept area. As stated above, it was neglected by Loyd, and the induction factor has been considered *"not applicable to kites"* by other recent authors. However, De Lellis et al. (2018) [18] claims the Betz efficiency to be essential also in AWES technology, and Leuthold et al. (2017) [19] proved that at least the axial induction factor is relevant. Kheiri et al. (2018) [20] includes the axial induction factor (a) in Eq. 2.14 as:

$$P = \left(\frac{1}{2}\rho A_s {V_w}^3\right) C_L \frac{{C_L}^2}{C_D} e(1-e)^2(1-a^2) \tag{2.15}$$

,where C_L/C_D is high, A_s is the ring shaped surface swept by the kite and

$$e = \frac{V_L}{V_W}$$

In the same paper it is stated that for Eq. 2.15, "*for example, neglecting a 5% induction factor results in nearly 10% power overestimation*".

In the case of drag mode, V_L becomes zero as no work is needed along the tether. Then, the function F_D would become:

$$F_D = H(D_P/D_K)/(1 + D_P/D_K)^3 \tag{2.16}$$

where D_P is the drag producing power by means of turbines and D_K is the drag of the kite.

Once the basic power equations have been given, they can be applied to theoretical case studies, with no in-depth analysis on the viability of such configurations, but to quantitatively understand the potential of the AWES. Note that these calculations are optimistic (no weight, line drag, efficiency...). First a lift mode (GG) AWES is studied, and then a drag mode (FG) AWES.

First the parafoil of the NASA X-38 re-entry test program is used (Figure 2.5c). The 5500 ft^2 kite is chosen from the experimental tests [21]. An L/D of 3 and a C_L of 0.5 are obtained. According to the literature, the future AWES could typically fly at altitudes of 1000 meters [15]. For this study an altitude of 3000 ft (914 m) is taken. With the aid of International Standard Atmosphere (ISA) data, an air-density of 1.12 kg/m^3 is obtained. Wind speed (V_W) is considered 30 m/s. As maximum power output is of interest, as explained before, $V_L = 1/3V_W$. Then, Eq. 2.12 gives:

$$P_{max} = \frac{1}{2}\rho A C_L \frac{4}{27} {V_W}^3 \sqrt{\frac{1 + (L/D)^2}{(L/D)^2}} \left[(L/D)^2 + 1\right] = 6MW \tag{2.17}$$

Even if the practical power output is certainly lower than 6MW, it can well be in the order of the megawatt. This value is promising for a single unit of AWES with such a low L/D.

Loyd also made theoretical estimations with an ideal tethered *C-5A* aircraft ($L/D = 20$). He obtained a value of 22 MW with a wind speed of 10 m/s using the power equations above for drag mode. A more realistic study in the same paper including weight and tether drag gives a power output of 6.7 MW, a third of the ideal case.

2.3.3 Companies and University research

The relatively small costs involved in AWE systems has allowed small, interdisciplinary companies to flourish over the last decade. The most complete review of the companies involved in the emerging market is given in [15]. Table 2.1 and Table 2.2 are extracted from that paper to summarize the technology developed by companies in Ground-Gen (GG) AWES and Fly-Gen (FG) AWES respectively.

Some of the most attractive technologies are collected here for a better insight into the practicality of AWES.

KiteGen Research (Italy)
This company exploits Fixed-Ground-Station GG-AWES by means of LEI and semi-rigid kites connected to the ground by two separate and controllable lines. Its patented "*KiteGen Stem*" model has a nominal power of 3 MW [22]. During the reel-out or power generation phase the kite follows an "8"-shaped flight pattern. On the other hand, an asymmetric stall forced by pulling one of the lines allows a reel-in phase with minimum lift. *KiteGen* has a promising view of its technology towards the future, and is also developing offshore AWE systems, a very attractive field.

SkySails Power (Germany)
It is of most interest their application of flexible kites as auxiliary propulsion systems for cargo ships. It is claimed to reduce an average of 10-15 % of fuel consumption, with peak reductions of up to 50 % [23]. The company is currently developing mobile-ground and offshore GG-AWES with nominal power outputs around the MW.

Ampyx Power (Netherlands)
This company uses automated rigid gliders with on-board sensors and actuators as a GG-AWES. As stated in [15], it is one of the few companies to achieve a fully automated sequence of take-off, pumping cycles and landing. For the climb a propulsion system is implemented. *Ampyx Power* is currently designing its first commercial prototype, the *AP-4*, a 2 MW offshore system ready for 2024.

Table 2.1: A classification of companies developing Ground-Gen (GG) AWES. Source: *Airborne Wind Energy Systems: a review of the technologies (Cherubini, et. al., 2015)*

Ground-Gen HAWECs								
Fixed/Moving		Airborne System	Company	Power Class	Main force	Actuators		N. Ropes
						On ground	Airborne	
Fixed ground station - Pumping System		Leading edge inflatable kite	KiteGen Stem	kW	Lift	x		2
			WindLift	kW	Lift	x		3
			Kitenergy	kW	Lift	x		2
			Swiss Kite Power 2	kW	Lift	x		3
			KitePower	kW	Lift		x	1
			Swiss Kite Power 1	kW	Lift		x	1
		Foil kite	SkySails Power	kW-MW	Lift		x	1
			EnerKite	kW	Lift	x		3
		Delta Kite	EnerKite	kW	Lift	x		3
		Swept Rigid Wing	EnerKite	kW	Lift	x		3
		Glider	Ampyx Power	kW-MW	Lift		x	1
			e-Kite	kW	Lift	x		2
			Kitemill	kW	Lift		x	1
		Glider with rotors	TwingTec	kW	Lift		x	2
		Semi-rigid Wing	KiteGen Stem	MW	Lift	x		2
		Parachute	GuangdongTech	MW	Drag		x	2
		Aerostat	Omnidea	kW	Magnus effect		x	2
Moving ground station	- Rail	Leading edge inflatable kite	KiteGen Rail Carousel	MW-GW	Lift	x		2
			Kitenergy	MW	Lift	x		2
		Foil kite	NTS		Lift	x		4
	-Axial	Leading edge inflatable kite	KiteGen Carousel	MW	Lift	x		2

Table 2.2: A classification of companies developing Fly-Gen (FG) AWES. Source: *Airborne Wind Energy Systems: a review of the technologies (Cherubini, et. al., 2015)*

Fly-Gen HAWECs				
General system description	Company	Flying principle	Type	Energy generation system
Turbines on a tethered aircraft	Makani Power	Wings lift	Crosswind	6/8 turbines
	Joby Energy	Wings lift	Crosswind	Several turbines
Tethered quadcopter	Sky Windpower	Rotors thrust	Non-crosswind	4 turbines
Turbine on a lighter than the air balloon	Altaeros Energies	Buoyancy	Non-crosswind	1 turbine
Magnus Effect turbine	Omnidea	Buoyancy	Non-crosswind	Buoyant wind turbine

Makani Power (USA)

In contrast with the previous companies, this uses a rigid glider with on-board turbines (GF-AWES). Take-off is achieved with the aid of the turbines operated as propellers. In the power generation phase the kite flies crosswind in a circular path with fixed line length. Now owned by *Google*, it is developing a 28 m wingspan, 600 KW prototype with 8 on-board turbines. As many other companies, *Makani Power* is planning a future commercial, offshore AWES. The device will be a 65m span, 5 MW glider with 6 on-board turbines.

Delft University of Technology (Netherlands)

It is also worth to mention the research line that has been carried out in Delft University of Technology for the last two decades and started by the former astronaut Proff. Ockels. A 20 KW LEI kite was developed with automated launch and landing. In 2016 the company *KitePower* was founded as a result of the research in Delft, and currently a commercial 100 KW AWES is being developed [24]. In the last decades a considerable amount of studies have been carried out, a fact that is supported by all the references in this project that belong to Delft University researchers.

Airborne Wind Energy Confernce (AWEC)

The *Airborne Wind Energy Conference* took place for the first time in 2009, and has been held every 1-2 years since then [25]. Every aspect involving AWES is covered in this conference, from structures, materials, aerodynamics, flight dynamics and control to regulations, political, environmental challenges and economics and financing. The conference is constantly growing as a part of the AWES community, hosting university researchers, companies and investors.

2.3.4 Important features, challenges and opportunities

The active control

One of the key components that allow a practical implementation of AWES is the automatic control of the system. During the power generation phase the direction of the kite with respect to the wind is constantly changing, so an active control helps in maintaining the optimal flight characteristics by adjusting the angle of attack or the turning rates.

In systems with reel-out phase the weight and the drag of the tether line is constantly growing, so corrections have to be done to maintain the optimal flight. For the reel-in phase the efficiency of the kite has to be reduced to spend the minimum energy to recover to the initial position.

In addition, the variance of wind speed with altitude or simply the variance of the wind speed with time also changes the properties of the flight and must be corrected automatically. It is also of interest that the take-off and landing phases are automated if large scale power plants are to be done in the future.

All in all, there is a clear demand of an active control system that maximizes the efficiency of the AWES. As a result, an extensive research is being done in the recent years. A more in depth review of the work done in the topic is given in Chapter 2.4.

Offshore AWES

It has been seen that several companies are developing commercial Offshore AWES. It is an attractive opportunity because of various reasons. First, the exploitable areas in the continent, specially in Europe, are now reduced. The wind in the sea is more constant and has in general a higher kinetic energy to harvest. The main drawback of the offshore alternative

is that installation, maintenance and electricity transport costs rise dramatically for conventional wind turbines. However, the simplicity inherent to the AWES makes them cheaper, and a very good candidate for offshore harvesting.

There is good opportunities in the scalability of certain kites, e.g. the foil kite. An offshore AWES plant with large-scale kites, taking into account the good potential of the systems as well as the relative low cost in their implementation, could become one of the most attractive renewable energy sources.

Ecological and environmental impact

There is very scarce literature on the ecological and environmental impact of the novel technology of AWES.

According to the ecological impact, Bruinzeel et al. (2018) [26] estimates an average bird mortality of 2-13 per year by collision with a tethered aircraft and 11 by collision with a tether line. These numbers are translated from regular Environmental Impact Assessments (EIA). It is justified that the impacts of tethered aircraft are similar to that of conventional aircraft at certain manoeuvres, and tether line impacts are related to power line databases. Also, the values are obtained with a conservative conversion to the constant operation of AWES (24 h a day, all year round). For AWES working only by day the combined (aircraft + tether) mortality numbers are reduced to 5-15 per year. The latter is said to be similar to the mortality of conventional wind turbines, an average of 7 per year.

However, these values are estimates coming from statistics of other human activities, and not necessarily precise. For the validation of the study, as stated in the article, the installment of impact-triggered cameras in the AWES could help.

The disturbance, rather than the mortality, is claimed to have its origin in the noise, so in the case of AWES the effect would be little (as with gliders).

Furthermore, and up to the knowledge of the author, the ecological impact of non-rigid kites has yet not been covered.

According to the environmental impact, it will most likely be measurable only with the im-

plementation of large-scale AWE farms. The impact of taking kinetic energy from the wind is still not studied for AWES as it is for conventional wind turbines. For the case of conventional wind power, Wang and Prinn (2010) [27] claims that the turbines-induced reduction in wind speed close to the surface decreases the atmospheric vertical turbulent transport rate, thus warming the surface. However, AWES have a different impact: they induce a smaller reduction in wind speed (small Betz efficiency) and they do it in a wider area. This leads to the idea that the impact in climate through the wind speed reduction is even smaller for the AWES than for conventional wind power. On the other hand Miller et al. (2011) [28], in a study of the impact of taking kinetic energy from high altitude jet streams, states:

"*the common expression for instantaneous wind power* $1/2\rho V^3$ *merely characterizes the transport of kinetic energy by the flow, but not the generation rate of kinetic energy*"

Even if jet streams are far higher than the actual target for AWES (10km vs 1km), it gives a more sustainable point of view of wind energy harvesting. There is a high availability of wind power in the atmosphere, but the rate of kinetic energy generation is limited, as well as the vertical kinetic energy flux (or re-energizing) in the atmospheric boundary layer [29]. This could mean an upper limit for future large-scale AWE power production.

That said, the conclusion is that further study needs to be done to better understand the ecological and environmental impact of AWES.

2.4 Research on: AWES dynamic modelling, control and stability

One of the main challenges when building an AWE system is the control of the trajectory of the kite and other parameters to ensure an optimal power output. For that, a correct dynamic modelling of the kite-tether system is necessary.

It has to be said that the model can become very complex if realistic effects such as kite shape and deformation, wind variance, tether drag and length variance, inertial forces, etc. are included. First the most simplistic dynamic models are given along with several assumptions, and more detailed studies are given later.

Williams et al. (2007) [30] gives the basic equations of motion for what is now called a Fixed-Ground-Station GG-AWES. Here the tether is assumed to be a rigid line with mass $\rho_0 L_0$, where ρ_0 is the tether density per unit length and L_0 the tether length. The kite is assumed to be a point mass (m_k) flown downwind in a three-dimensional semi-spherical domain. Figure 2.11 shows the spherical coordinate system used here: L is the radial distance in the tether direction, θ is the angle of the tether with the vertical inside the wind plane, and ϕ is the angle out of the wind plane (also called "crosswind" component).

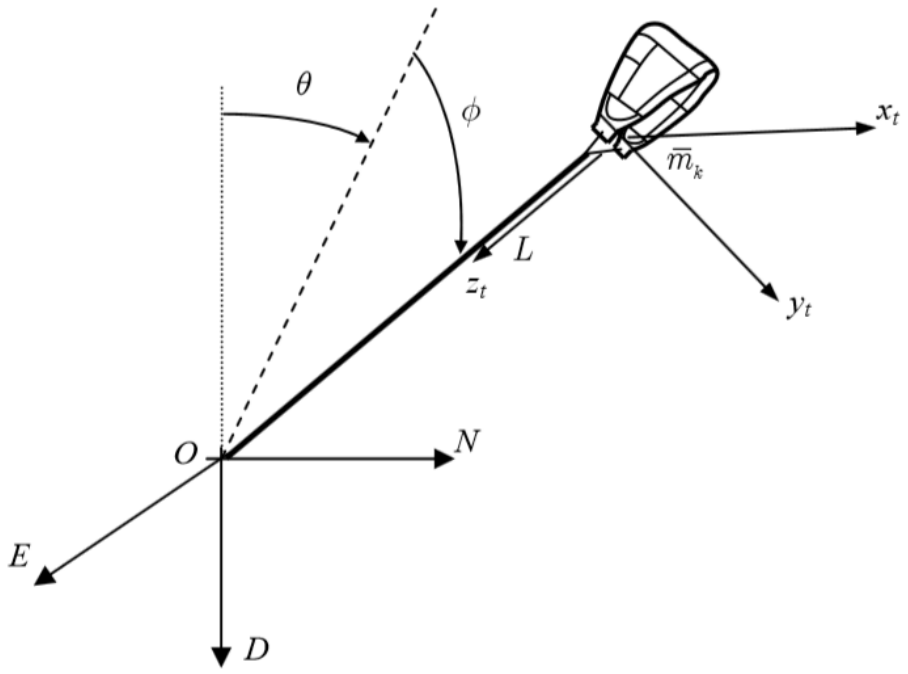

Figure 2.11: Spherical coordinates in a kite-tether system fixed to the ground. Source: *Modeling, Simulation, and Testing of Surf Kites for Power Generation (Williams et. al., 2008)*

With an approach using Lagrange equations, the equations for the kite-tether motion result in:

$$(m_k + \frac{1}{3}\rho_0 L)L^2\ddot{\theta}cos^2\phi + 2(m_k + \frac{1}{2}\rho_0 L)L\dot{L}\dot{\theta}cos^2\phi$$
$$- 2(m_k + \frac{1}{3}\rho_0 L)L^2\dot{\theta}\dot{\phi}sin\phi cos\phi - (m_k + \frac{1}{2}\rho_0 L)gLcos\phi sin\theta = {Q_\theta}^k + {Q_\theta}^t \quad (2.18)$$

$$(m_k + \frac{1}{3}\rho_0 L)L^2\ddot{\theta} + 2(m_k + \frac{1}{2}\rho_0 L)L\dot{L}\dot{\theta}$$
$$+ (m_k + \frac{1}{3}\rho_0 L)L^2\dot{\theta}^2 sin\phi cos\phi - (m_k + \frac{1}{2}\rho_0 L)gLsin\phi cos\theta = {Q_\phi}^k + {Q_\phi}^t \quad (2.19)$$

$$(m_k + \rho_0 L)\ddot{L} + \frac{1}{2}\rho_0\dot{L}^2 - (m_k + \frac{1}{2}\rho_0 L)L\dot{\phi}^2$$
$$- (m_k + \frac{1}{2}\rho_0 L)L\dot{\theta}^2 cos^2\phi + (m_k + \rho_0 L)gcos\phi cos\theta = {Q_L}^k - T \quad (2.20)$$

, where g is the earth's gravity, T is the tether tension and Q are the torques coming from aerodynamic forces (see equations 19-21 in [30]). Superscripts k and t refer to the kite and the tether respectively.

Note that the equations are uncoupled and that they take into account the tether length variation with time.

This first approach takes the kite as a point mass. This means the attitude dynamics, the aerodynamics inside the kite and the deformations are not taken into account. More detailed modelling options are presented in [31] and listed below. For a review of these models with their respective advantages and disadvantages, see [32].

- Rigid Body Model: The attitude of the kite is added (pitch, yaw, roll), resulting in a 6 degrees-of-freedom model with higher fidelity for posterior simulation. The previous equations of motion (Eq. 2.18-2.20) are derived when the inertia of the kite is considered to be negligible in comparison with the hole system.
- Multi-Plate Flexible Model: In the case of non-rigid kites the deformation modes are important if a detailed study is to be done. The most simple way of modelling this is

dividing the kite geometry in several flat plates with independent position and pitch and roll angles, hinged to each other in some elected point. A disadvantage is that the hinge forces have not a physical meaning. An example of the application such a model is [33].

- Finite Element Methods (FEM): This method comes with a high computational cost, but discretizes the kite in a much higher detail, allowing simulations closer to the reality. Kite deformation can be computed with the highest accuracy available.

For the case of the Rigid Body Model, the same paper develops a procedure for the calculation of forces and moments acting in the system taking into account the moments of inertia of the kite.

Another study [34] builds a dynamic model of a kite attached to the ground with two lines. The kite model is a rigid one, with one tether line connected to each tip. The tethers are assumed not to have effects of inertia, flexibility and elasticity, and the wind velocity and direction are considered constant. With these assumptions in mind two analyses are made, one with constant tether length and the other with varying tether length.

The main conclusion in the constant-length model is that, if kite is designed correctly, no additional control input is needed to satisfy a stable crosswind flight pattern. The important design parameter to look at is the roll response to sideslip ($C_{l\beta}$). As shown in Figure 2.12 there is a wind-velocity-dependent threshold in the value of $C_{l\beta}$. Kites with values below the $C_{l\beta,min}$ will follow a stable periodic pattern and would need no active control in this dynamic model. For the reel-out model an unstable periodic flight is found for values of $C_{l\beta}$ beyond a threshold. As a general conclusion it can be said that even if the model is not of the highest fidelity, it shows that the roll response to side-slip can be an important design parameter to take into account for stability.

Van der Vlugt et al. (2019) [35] gives a recent dynamic model taking the hole pumping cycle. The phases of traction, retraction and transition are included. The mass is assumed to be small enough to neglect the inertial forces and build a quasi-steady equilibrium of gravity, aerodynamic and tension forces. This first assumption means the launch and landing phases are out of the scope of the paper. The other assumptions are: tether is inelastic (but not straight), kite has constant aerodynamic properties and wind speed and density vary with

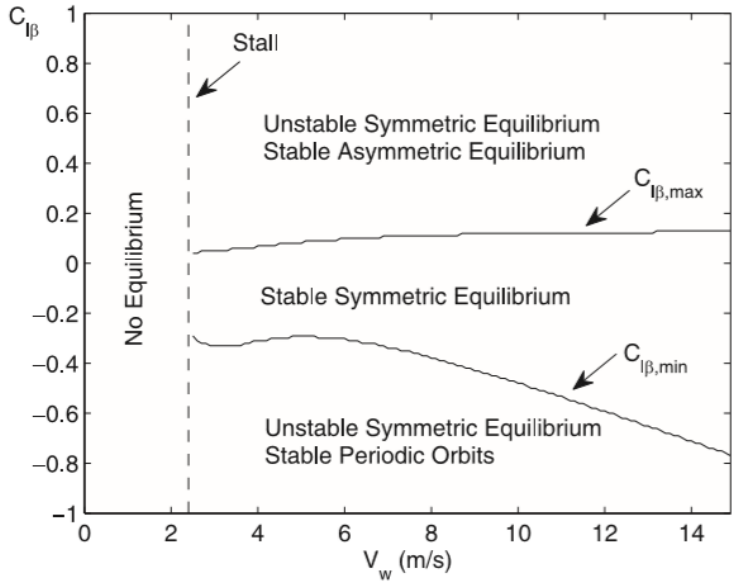

(a)

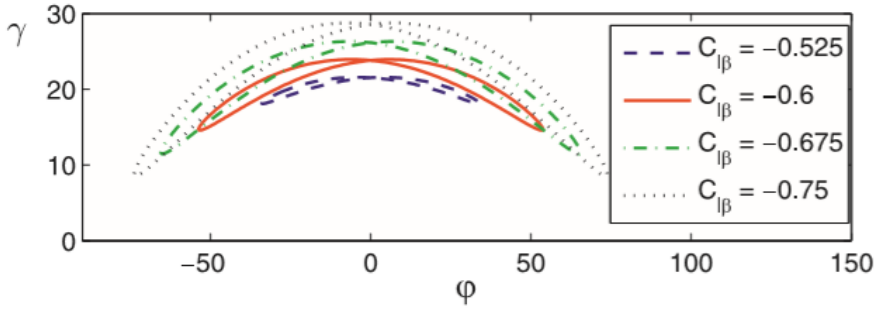

(b)

Figure 2.12: Results of the constant-tether-length model. (a) Roll to side-slip derivative ($C_{|\beta}$) vs wind speed (V_W) with simulated thresholds giving different stability conditions. (b) Angle with horizontal plane (γ) vs angle out of the wind plane (ϕ) for different $C_{|\beta}$ values inside the *Stable Periodic Orbits* region. Source: *Modeling and dynamics of a two-line kite (Sanchez-Arriaga et. al., 2017)*

altitude but not with time. The power equation is computed without and with gravity (point mass) for each flight phase, and then a mean value is calculated. The model is further validated with flight test data of a pumping cycle with the Delft University 20 KW LEI kite. As an example Figure 2.13 compares the flight pattern of the dynamic model (with and without gravity) and the flight test. The agreement is good in the traction and transition phases, and the addition of gravity improves the agreement in the retraction phase.

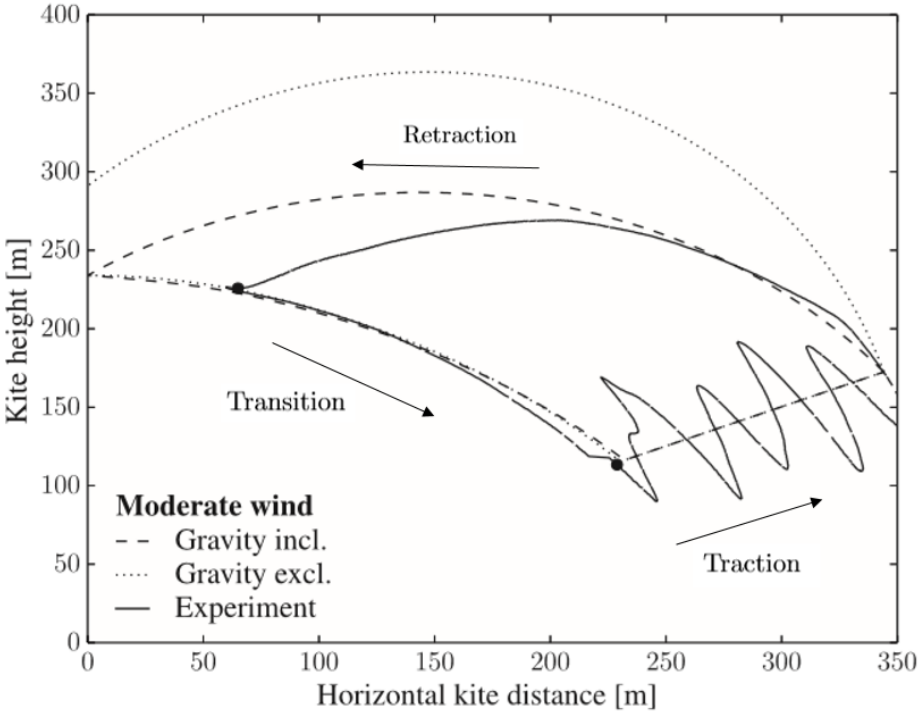

Figure 2.13: Two-dimensional projection of the displacement of the kite. Comparison between model with gravity, model without gravity and experimental data. Source: *Quasi-steady model of a pumping kite power system (van der Vlugt et. al., 2019)*

It has been seen that the most accurate model is that of FEM. It allows to account for the deformations of the kite in chord-wise and span-wise directions. However, introducing flexibility to the kite model means a Fluid-Structure Interaction (FSI) study needs to be done. FSI problems rely on the coupling between the aerodynamic loads and the deformations. In other words, the aerodynamic forces will affect the shape of the solid, which in turn will change the previous aerodynamic forces. The interaction between the two has to be computed in an iterative process by the FSI solvers. For an introduction to FSI and a review of the kite FSI models see Chapter 3 in [36]. A complete FSI implementation for AWES with a LEI kite is

done in [37]. Here a FEM model is built and put into an FSI solver (see Figure 2.14).

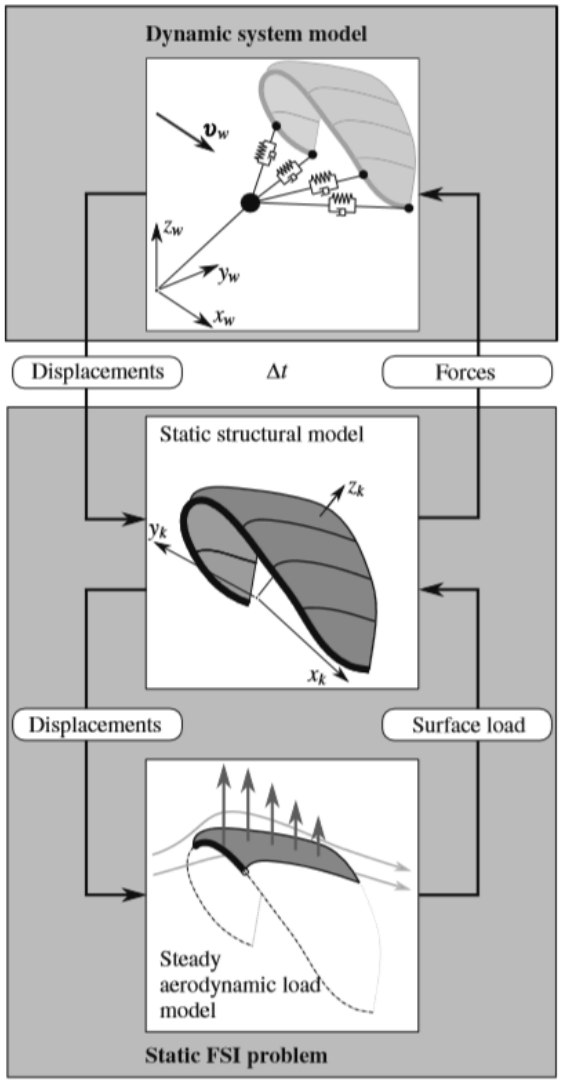

(a)

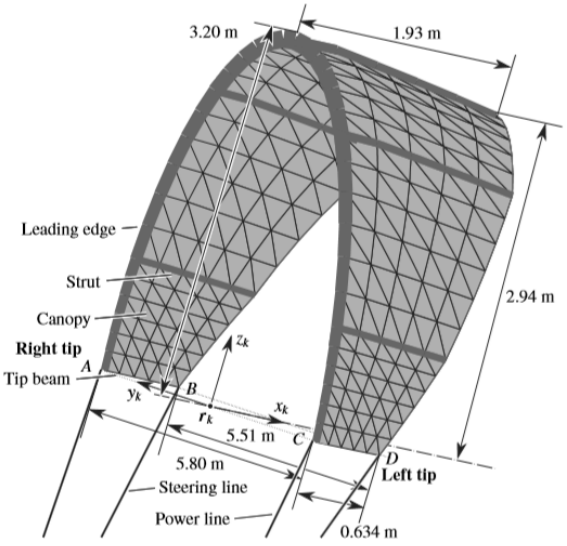

(b)

Figure 2.14: (a) FSI structure scheme. (b) FEM model with named kite components and dimensions. Source: *Dynamic Nonlinear Aeroelastic Model of a Kite for Power Generation (Bosch et. al., 2014)*

As a practical case, the application of the active control in the *SkySails* kites for cargo ship towing is explained in [38]. The hole explanation is given through the equations of motion, dynamics, and the design of the implemented control system.

Another practical implementation of an automatic control is that of [39] with the Delft Uni-

versity 40 KW LEI kite. Again, the architecture of the control system is explained. The implementation is said to be satisfactory for 15 flights of 2 hours-length each.

2.5 Research on: Aerodynamics of kites

It is clear that there is an increasing demand on the optimization of AWES. It has also been seen that the power output is directly related to L/D and C_L, and so a complete study on performance optimization is of interest. However, the aerodynamic characteristics of non-rigid kites have not been as studied as conventional aircraft. It is the deformability, the non-planar wing shape and the added tether-constrains that make kites behave different. Here a collection of the available literature on the aerodynamic characteristics of kites is given to serve as a basis for both the current project and further work.

2.5.1 Experimental research

Even if research on AWE technology is in its first stages, military applications of the kite as a gliding parachute led to early aerodynamic studies that serve as a basis for actual development of AWES.

Den Boer (1982) [40] records wind tunnel measurements for a semi-rigid sailwing model. The model had a rigid, elliptical LE cylinder and two fabric sails attached to it serving as the upper and the lower surfaces of the wing (Figure 2.15). The experiment aimed to analyze only two-dimensional aerodynamics. Tests were carried at several angles of attack and independent LE-bar rotation angles, as well as different sail lengths. The effect of dynamic pressure on the wing shape was analyzed by applying two wind speeds, 23 m/s and 34 m/s. The results were encouraging because C_L/C_D values up to 88 were obtained with C_L between 0.8 and 1.9. The wing deformation under wind pressure was established to be relevant and not negligible.

A very comprehensive study of the aerodynamic characteristics of paragliders is that of Babinsky (1999) [41]. Wind tunnel tests of a semi-rigid ram-air paraglider model were undertaken for a two-dimensional analysis. The wing had a rigid inner structure and a fabric covering, and ram-air intakes as well as typical parafoil cells were emulated. A smaller rigid model was also tested for comparison of the effects of flexibility and for measuring the ram-air intake

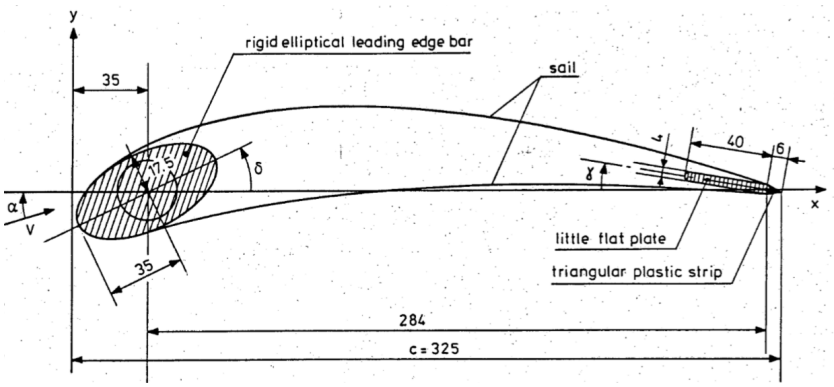

Figure 2.15: Section of the wind tunnel model tested by den Boer. Source: *Numerical & experimental investigation of the aerodynamics of double membrane sailwing airfoil sections (den Boer, 1982)*

drag. An extensive study was done, including the following conclusions:

- The intake drag is dominated by the intake size, and there is a very little dependence on the angle of attack. Babinsky also modified the empirical estimation of intake drag given by Ware and Hassell in 1969, drastically reducing its value.

  $$C_{D,Hassell\&Ware} = 0.5\frac{h}{c} \;\Rightarrow\; C_{D,Babinsky} = 0.07\frac{h}{c}$$

  were h is the height of the intake and c the reference chord. It is seen that the intake drag is an order of magnitude smaller in Babinsky's formulation.

- C_L vs AoA (α) curve has a lower intercept compared to rigid wings, a smaller slope of the linear trend and, in the words of Babinsky, a "*soft stall*" at higher values of α. For a better understanding of these characteristics a plot given in that paper is shown in Figure 2.16. This forces the kite to fly at higher α for the same lift, thus having a penalty in drag.

- Two separation zones appear, one in the LE due to the intake and the other in the TE (Figure 2.17). The LE bubble is detected in the Cp distributions. It is evident in the cell centers, and it is non-existent in the ribs. Cp distribution also shows a higher suction in the LE upper surface in the ribs than in the cell centers. The TE separation wake appears much sooner in the ribs (42% chord) than in the cell centers (80% chord). It is concluded that it is the ribs that pull the TE separation forward.

- Wing deformation is measured with a $\pm 10\%$ error by superposition of images. The thickness vs chord map shows that, when deformed, the maximum thickness moves

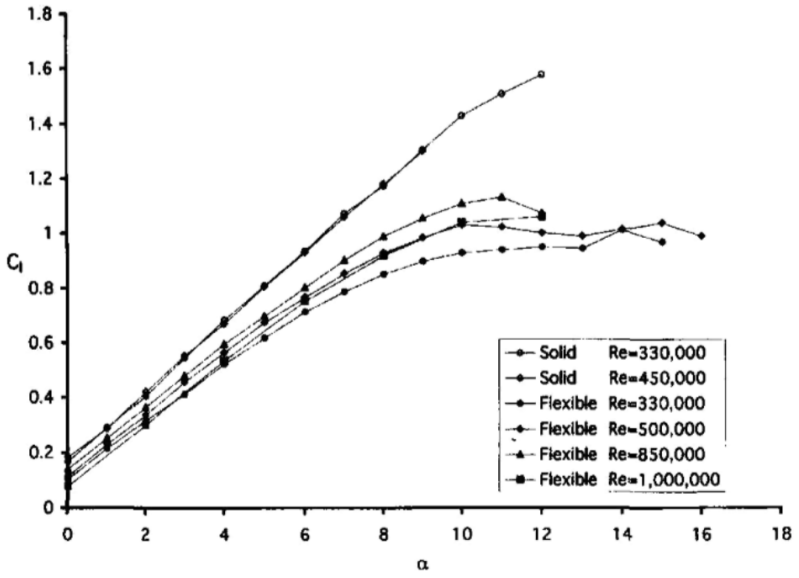

Figure 2.16: C_L vs α plot at different Re numbers. Comparison of rigid and flexible wings. Source: *The aerodynamic performance of paragliders (Babinsky 1999)*

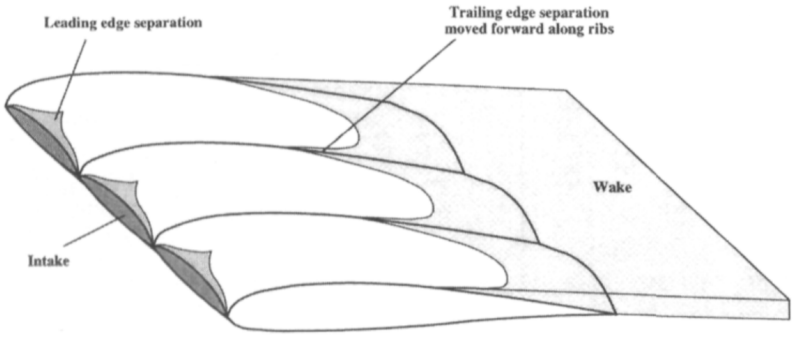

Figure 2.17: Schematic LE and TE separation areas. Source: *The aerodynamic performance of paragliders (Babinsky 1999)*

backward in chord direction, thickness increases by up to 25% and the curvature in the LE decreases. It is clear that the deformation is a source of penalties in lift and TE separation.

Similar conclusions on the C_L vs α chart in Figure 2.16 are taken by [11] in his parafoil test program (see Chapter 2.2.5).

A more recent but related study is [42]. Again, a semi-rigid wind tunnel model of a ram-air

parafoil is tested with rigid structure and fabric covering as upper and lower surfaces. The results in overall performance ($C_L, C_D, L/D$) are similar to the ones in previous tests explained in this Chapter, which helps in settling and extending the available aerodynamic data. But a concept that has yet not been mentioned here is introduced: the durability of the fabric. As explained in the paper, the pressure difference between the inner and the outer volumes changes the permeability of the fabric. Thus, the tests lack repeatability if the fabric is of first-use. However, the paper ensures the canopy is put under wind pressure sufficient time to have a stabilized permeability. The best account for this effect is seen in the L/D parameter in Figure 2.18, which plots the maximum L/D, C_L and C_D obtained over the usage in time. A reduction of 12% in L/D (5.75 to 5.07) is seen after 213 minutes of usage. As a conclusion, it can be said that the usage increases permeability ($\propto$ porosity), which in turn reduces performance.

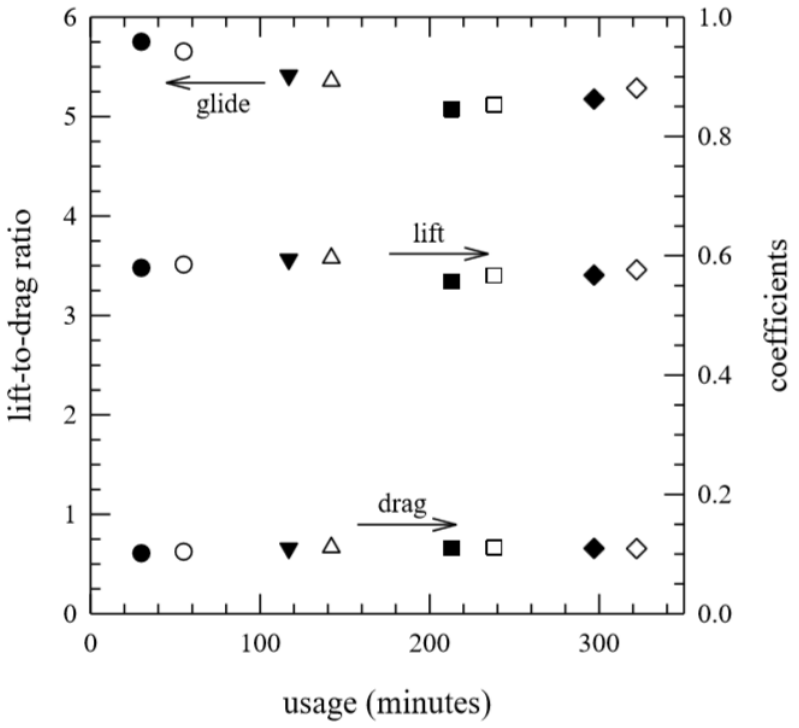

Figure 2.18: L/D (*glide*), C_L and C_D against usage of the wing model in time. Source: *Aerodynamic investigations of a Ram-Air parachute canopy and an Airdrop System (Desabrais et. al., 2015)*

Another interesting mention in the same paper is that of the separation bubble found downwind the LE intake in the lower surface. Both smoke flow visualization and real flight tests

qualitatively showed this phenomenon. It is said to be due to a reversed flow originated by a stagnation point inside or at the LE intake.

Up to this point the wind tunnel tests with semi-rigid models have been covered. There is however some literature involving wind tunnel tests with rigid kite models and real-flexible kites.

According to the study of rigid models, [43] tests a 1/8 scale rigid paraglider into a wind tunnel. A set of different angles of attack and sideslip angles are tested. The results at low sideslip and positive lift are similar to those of conventional planar wings, and the ones with high sideslip angles and negative lift are considered not representative of the aerodynamics of real kites. It is clear that under the latter conditions the deformations would make the kite collapse of change its shape in a considerable way, showing a completely different performance. In addition, the point at $C_L = 0.3$ is found to give a stable pitching moment equilibrium related to the principle of pendulum used in paragliding.

de Wachter (2008) [44] makes a study of a real full-scale flexible ram-air kite in two wind tunnels. One concern is said to be the lateral/directional stability of the kite, which is designed to steer and fly crosswind but had to maintain its position towards the wind direction in the wind tunnel. The solution is found by constraining the kite with rigid bars in the adequate equilibrium point (AoA) at each flight condition. Without the bars the kite would show a dutch roll mode. The results of the wind tunnel tests at approximately 8, 12 and 16 m/s are given in C_L vs brake position, L/D vs brake position and C_L vs C_D charts. C_L values of 0.7-1.3 and maximum L/D of 6.5-8 are obtained. Thermography tests give results of laminar-to-turbulent flow transition. A photogrametry technique is seen to be very useful at analyzing the effects of several deformation modes such as: ballooning, LE and TE deformations, wing anhedral under dynamic pressure, and local AoA. A wash-in is detected, where the tips have a higher AoA than the root (said to give better manoeuvrability). The effect of dynamic pressure on spanwise anhedral is that of flattening the root and moving the tips further apart. Finally some thoughts about the wind tunnel wall effects are given. The walls are said to obstruct the downwash induced by wake vortices, thus having higher lift and lower drag, as well as further deforming the kite.

As some literature defend [45] [46], wind tunnel tests with real all-flexible kites are not very

reliable for the study of the performance of full-scale AWES power kites. Some of the reasons are the scalability of the fabric, the difference in turbulence intensity with atmospheric flight and the lateral/directional stability issues. That is why more extensive literature is available for real flight tests than for wind tunnel tests with flexible models.

Hobbs (1990) [47] flies many different kites and studies the aerodynamic performance of each design. It is of interest the set of plots recorded in the paper with C_L vs C_D plots for each kite flown, eight in total (Figure 2.19). The Cody kite and the parafoil are compared with previous wind tunnel data (Jackson [5] and Nicolaides [**Nicolaides1971**] respectively).

The gliding parafoil (or flexifoil) in Figure 2.5c is part of a NASA test program for the re-entry of crew in a lifting vehicle from the International Space Station. Various papers are available studying the aerodynamics and performance of flight tests with a large scale parafoil. Iacomini et al. (1999) [48] analyses the longitudinal aerodynamics of the parafoil-tether-payload system in steady state flight, giving values of C_L, C_D and L/D as functions of parafoil flap deflection and angle of attack. Iacomini et al. (1999) , in a separate paper [49], analyses the lateral/directional aerodynamics and the turn performance of the same set of tests. [21] assesses the scalability of the parafoil aerodynamics by comparing the 5500 ft^2 flight tests with later tests with a 7500 ft^2 parafoil. The hole set of data collected serves as a basis for further flight simulation.

Another flight test program for the landing of space capsules is that involving the *Test Vehicle ALEX*, a paraglider-payload system. Jann (2001) [50] is the last of three papers covering the different flight tests undertaken, the components of the ALEX vehicle and the results obtained with their respective data identification, as well as the development of a dynamic model and control system for autonomous landing.

Delft University of Technology has also several flight tests with full-scale kites. The nature of these tests is closer to the development of AWES than the flight tests mentioned above. Some literature for the flight tests are [31] [32] [51] and [46]. For a more in depth insight into the Laddermill concept mentioned in some of these, see Ockels (2001) [52].

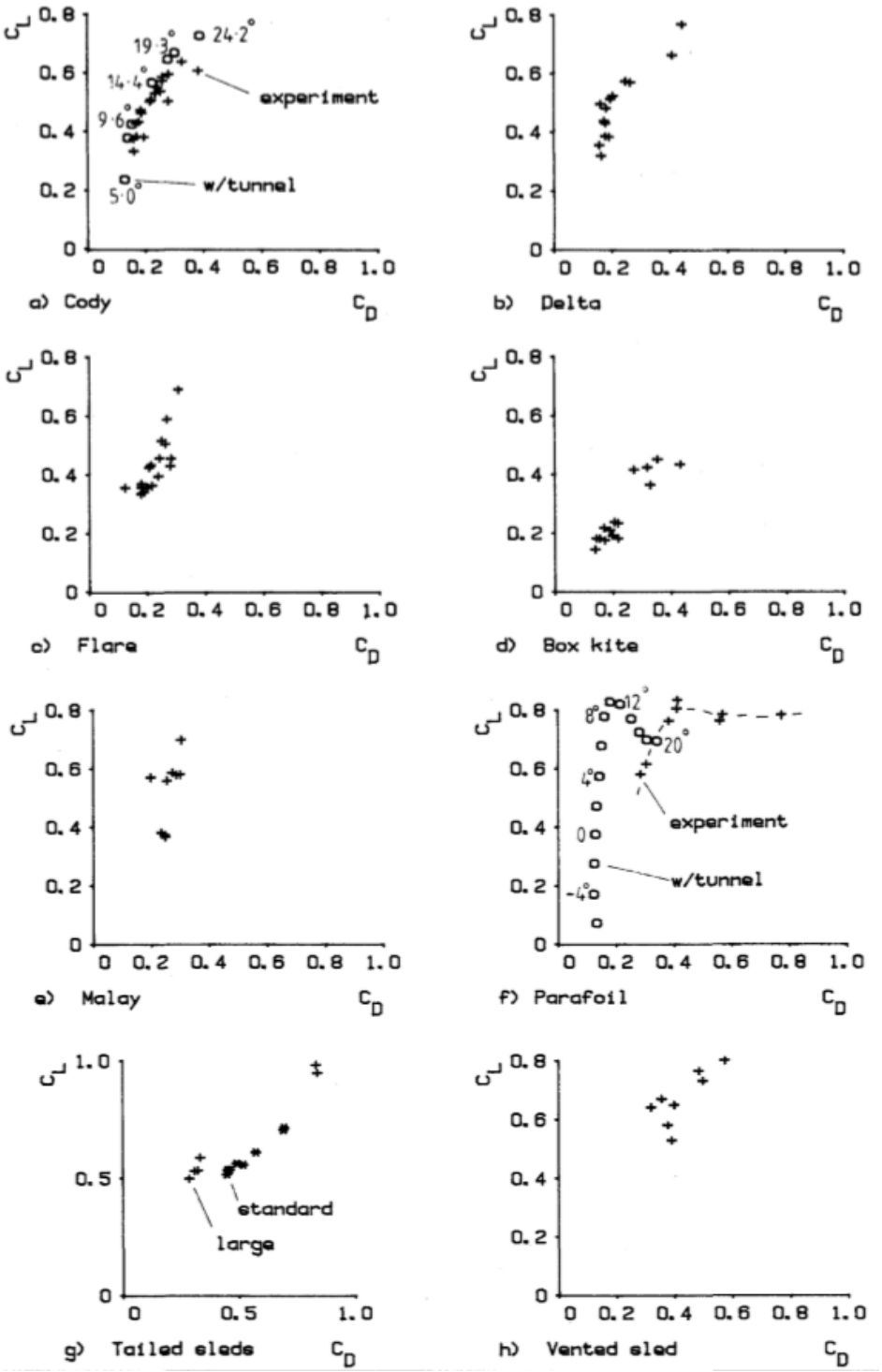

Figure 2.19: C_L vs C_D plots for flight tests with different kite types. Cody (a) and parafoil (f) are compared with wind tunnel data from the literature. Source: *Kite performance measurements in natural wind (Hobbs, 1990)*

2.5.2 Analytical research

The growing demand on kite design optimization for applications in AWES has led to several analytical approaches, from simple modified Lifting Line Theory (LLT) to RANS solvers. An analytical approach leads to the knowledge of preliminary aerodynamic coefficients, which help in developing the dynamic models explained in Chapter 2.4.

The challenge of implementing low order potential methods (LLT, VLM, Panel Methods) to kites relies on the non-conventional geometry of most of these: non-planar shape, low aspect ratio and a relatively high thickness to chord. As LLT is designed for planar wings with high aspect ratio, some modifications need to be done to the method. Gonzalez (1993) [53] implements the Multhopp LLT procedure for non-planar wings (i. e. spanwise curved wings) departing from an extended LLT developed by Weissinger for low aspect ratio wings. The horseshoe vortex filaments are placed in a spanwise arched line, and extend with infinite length downwind in the chordwise direction (Figure 2.20a). The results obtained are compared with a Vortex Lattice Method (VLM) for curved wings, and the agreement is found to be good with an error of 10% in the lift curve slope and lift distribution. In addition, the effects of wing taper, aspect ratio and spanwise curvature are collected in three plots of the lift distribution. The curvature is seen to decrease the lift along the span, as seen in Figure 2.20b.

Jann (2003) [54] also develops a modified LLT for curved wings. Similarly to Gonzalez, it concludes that the curvature in a wing decreases the lift distribution (to 92% of a planar wing of same AR). Here the curvature is said to give side forces of 15% of the magnitude of the total lift. The results of force and moment derivatives are compared with both a VLM and real flight tests (ALEX flight tests in Chapter 2.5.1). In the latter validation, some derivatives result to be similar, while the rest are said to be different due to the simplifications made in the theoretical approach (rigid body, zero-thickness, separation and viscous effects neglected).

De Solminihac et al. (2018) [55] develops a Fluid Structure Interaction (FSI) method by coupling a structural model (FEM constrained in the four corners) and a 3D non-linear LLT model that iteratively compute the structural forces & displacements along with aerodynamic forces. The method is then implemented to a 35 m^2 LEI kite.

The Vortex Lattice Methods (VLM) account for the chordwise distribution of aerodynamical

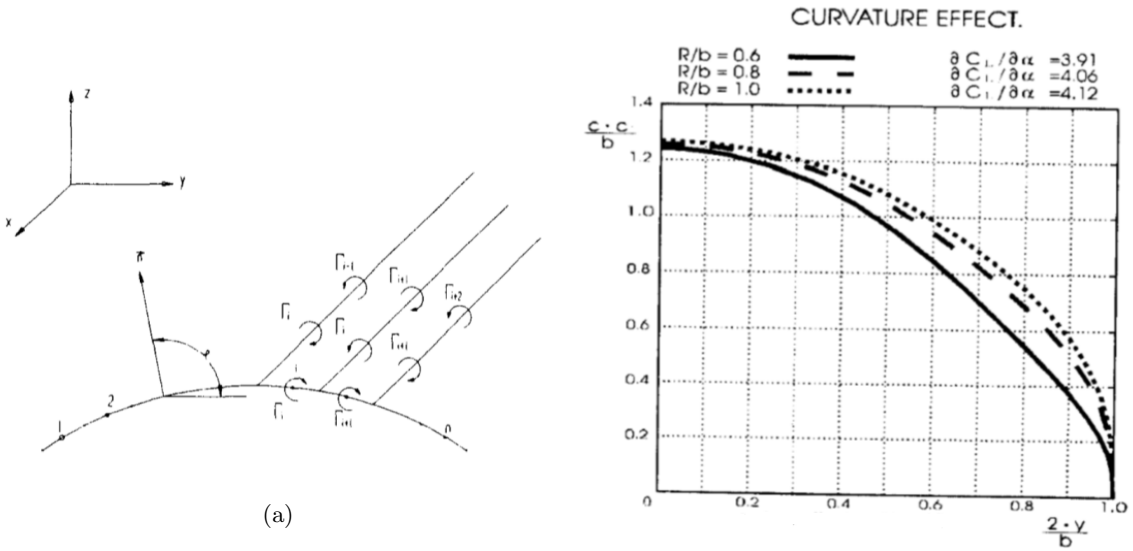

(a)

(b)

Figure 2.20: (a) Horseshoe vortices on a curved spanwise line. (b) Lift distribution, effect of spanwise curvature as a function of the ratio line-length/span (R/b). Source: *Prandtl Theory Applied to Paraglider Aerodynamics (Gonzalez, 1993)*

forces. Still computationally cheap, these methods give more accurate results than the LLT. A reference for the implementation of a VLM is Gaunaa et al. (2011) [56]. Here a hybrid method is developed including a VLM and 2D airfoil section coefficients. The VLM is said to be valid for computing low aspect ratio, spanwise curved wings, while the 2D airfoil study adds the effects of airfoil thickness and viscous effects. The results of the hybrid method are generally more in accordance with CFD results than just the VLM method.

A further step in the complexity of potential methods is the application of Panel Methods with panels around the upper and lower surfaces of the kite to take into account the thickness of the object. The distribution of the panels allows to consider the chordwise pressure distributions, low aspect ratios, and in a 3D case also the spanwise curvature. Leuthold (2015) [36] suggests a Multiple Wake Panel Method that takes into consideration more than one wake vortex sheets. That way, not only the trailing edge wake but other separation regions can be modelled (in a LEI kite, for example, the regions behind the LE tube, or in a Ram-Air kite the areas behind the LE intakes). A limitation of the proposed method is the accuracy in modelling the reattachment of the flow. However, an extension of the code given by [57] gives a solution for the reattachment problem.

A literature for the build of a 3D Panel Method in *Matlab* is [58]. An alternative and powerful option for the analysis of arbitrary geometry inputs is the Panel Method software PANAIR. A review of this and additional Panel Method software is given in [59].

Panel Methods were the highest fidelity analytical methods before computational methods (CFD) became practical. Today the highest fidelity is achieved with CFD, with the drawback of increased time cost. Several literature include a CFD analysis of kites with RANS solvers, whether as the main subject of study or as a way of validating other analytical approaches [44] [56] [60] [61] .

Chapter 3

Wind Tunnel Tests

3.1 Preliminary Considerations

It has been seen that the literature includes a wide range of experimental approaches for the determination of the aerodynamic characteristics of kites. In the case of non-rigid kites, the following three factors can be identified to classify the experiments (for rigid kites, points 2 and 3 apply):

1. Is the tested object a flexible kite, a semi-rigid model or a rigid model?
2. Is the kite full-scale or a scaled model?
3. Are the tests carried out in the free atmosphere or in a wind tunnel?

Having in mind that the practical application is that of AWES, the highest fidelity is achieved with flight tests of a full-scale, flexible kite with similar motion to the power generation case, typically crosswind. These tests, however, are only possible once the design process is mature enough to efficiently fly a controllable kite. The companies listed in Chapter 2.3.3 are a good example of entities that can undertake these tests. Other flight tests seen in the literature with a lower fidelity to AWES are the kite-glider test programmes. The aerodynamics of a gliding canopy can be similar to the kites used in AWES, but the motion and the constrains of the system differ completely. A simple alternative is to fly scaled flexible kites typically designed for other applications such as leisure. The problem here arises from sclalability issues and a design that is not optimised for power generation. Overall, flight tests are ideal in the sense that they account for the atmospheric turbulence and a crosswind motion is possible to test. More similar flight conditions can be obtained in a flight test, but it is a challenge from

the control and measuring point of view.

Wind tunnels offer a more controlled environment, but the kite needs to be static in the test section. There is typically no availability to test full-scale kites because of the big section that would be needed. This brings scalability issues (explained below). The literature shows that most of the scaled kite models tested in wind tunnels were semi-rigid. This is a good choice for measuring flexible kites, since the effects of deformation can be partially calculated while the structural shape is stiff and well defined. The highest fidelity regarding deformation modes would be achieved by fully flexible models.

The starting point to decide what experimental approach to follow is to remind the scope of the experiments. They aim to study the aerodynamic characteristics of a flexible kite as well as its response to a control input. In addition, the experimental setup aims to be the first of a continued research on kite aerodynamics for AWE technologies.

Having that in mind, the flight tests are discarded, first because there is not a proper equipment available for the measurement of loads, and second because of repeatability issues. Regarding the latter, it is of more interest to implement a wind tunnel test technique in the available 8x6 Wind Tunnel of Cranfield University and give start to a continued and more comprehensive aerodynamic study of kites in a controlled and repeatable environment. The size of the wind tunnel only allows the use of scaled kites, so scalability effects need to be taken into account. According to whether to use a rigid, semi-rigid or fully flexible model, first a rigid model of adjustable spanwise curvature was considered, but the practical solutions for the building of the model were not satisfactory enough. The availability in the market of economically affordable, low-spanned, fully flexible ram-air kites for leisure purposes led to the decision of testing a real inflatable scaled kite into the wind tunnel. Details of both the wind tunnel and the tested kite are given below.

3.2 The Wind Tunnel

The experimental tests were undertaken into the 8x6 Low Speed Wind Tunnel (LSWT) at Cranfield University. The working section of this closed-loop wind tunnel is rectangular, 2.4 meters wide and 1.8 meters high. The applicable air speed into the working section has a

maximum of 50 m/s. A planview of the wind tunnel is given in Figure 3.1.

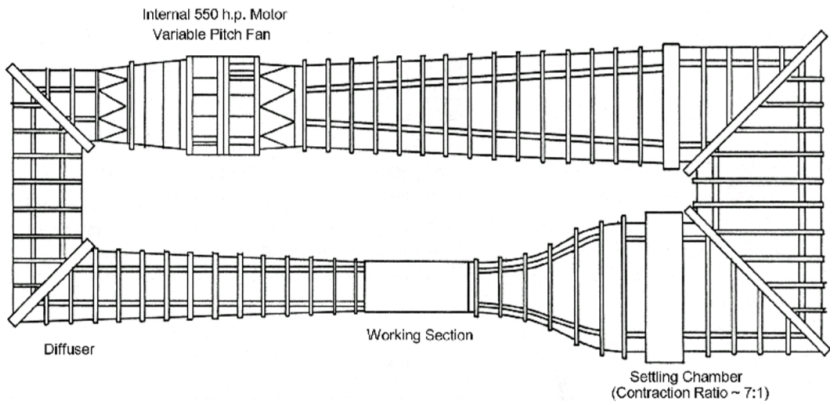

Figure 3.1: Planview of the 8x6 wind tunnel at Cranfield University.

A six-component strain-gauge balance system is externally installed above the working section roof. It allows measurements of forces and moments with their respective standard deviations in all three dimensions .

The relatively high area of the working section made the 8x6 LSWT the most suitable for testing the kite. Being this the biggest working section available for the tests, the dimensions of the kite had to be considered prior to its purchase. A 30% width margin was also applied, which reduced the maximum possible span of the kite to 1.7 meters. The wind speed range available also had to cover the designed speed range of the kite.

3.3 The Kite Model

Before the purchase of the kite, several decisions had to be made regarding the type of canopy, tether lines distribution, physical dimensions and budget for the project:

The most common (and thus available) types of canopy are the ram-air parafoil and the leading-edge inflatable (LEI). As mentioned previously, the ram-air parafoil shape usually has better aerodynamic performance and is scalable up to an order of magnitude higher than the LEI kites. They are thus more adequate for high power output applications, which makes the wind tunnel analysis of a ram-air kite preferable. Furthermore, the author considers of more interest to analyse a wing with aerofoil-shaped sections. Its aerodynamics can be more easily

compared to conventional planar wings to isolate the effect of spanwise curvature (anhedral), and there is more opportunity to build an analytical approach with software constrained to conventional wing shapes. Therefore a ram-air parafoil shaped kite was preferred for the wind tunnel tests.

According to the configuration of tether lines it was considered a requirement that the kite had four lines. Compared to the two-line kite, the four-line kite allows a more complete set of control inputs such as activating the breaks by pulling the two trailing edge lines or easily inputing the asymmetric flight, as well as having the kite more constrained to instability fluctuations.

As the practical case to analyse is the use of kites for wind power generation, the dimensions of the kite had to be as big as possible in order to minimize scaling effects such as:

- Reynolds number. This non-dimensional number is predominant in low speed aerodynamics and is directly proportional to a reference length of the flying object. A bigger model would give a closer Re number to the full scale case.
- Deformation. If the kite is too small in size (considering the fabric material and thickness are similar) it will most likely show different deformation characteristics. Therefore the deformation of the kite must be scaled too, which brings an extra design challenge [46].
- General design properties. As the scaled kites available in the market are more of a leisure flying object, smallest kites are directed to the beginner users and tend to be simpler in design, easier to fly (further from the optimal performance) and may have cheaper materials.

Regarding the budget, it is clear that one advantage of the kites is that they are cheap to build. The simplest kite had 1.2 meters span (with two lines) and costed £27. The price of the kites in the market was found to be proportional to their size and it also varied from one to another manufacturer.

All in all, the kite of interest had a ram-air parafoil canopy, four lines and it was the biggest in size that at the same time fulfilled the dimensional constrains of the 8x6 LSWT.

As a result the *Cross Power Kite Quattro 1.5* was selected for the wind tunnel tests. A

summarized list of the scaled ram-air kites found by the author is shown in Table 3.1 as a guide to the state of the art of the market of scaled inflatable kites.

Table 3.1: A summary of scaled ram-air kites available on: https://www.kiteworld.co.uk/

Manufacturer	Model	Span [m]	Price [£]	Wind range (min/max) [m/s]	Lines
Cross Power Kites	*Air*	1.2	29	2.7/13.9	2
		1.5	37.5	2.2/13.9	
		1.8	45	2.2/13.9	
		2.1	58	1.8/13.9	
		2.5	72	1.8/10.7	
	Boarder	1.5	49	2.2/13.9	2
		1.8	61	2.2/13.9	
		2.1	80	1.8/13.9	
		2.5	87	1.8/10.7	
	Quattro	**1.5**	**113**	**2.7/13.4**	**4**
		2.5	129	2.2/13.4	
		3.5	148	2.2/12.5	
		4.5	165	2.2/12.5	
Prism Power Kites	*Synapse*	1.4	50	2.7/11.2	2
		1.7	75	2.2/11.2	
		2	95	1.8/11.2	
	Tantrum	2.2	110	2.2/11.2	2
		2.5	140	1.8/11.2	
Spiderkites Power Kites	*Amigo*	1.35	30	2.7/12.5	2
		1.75	43	2.2/12.5	
		2.05	55	2.2/12.5	
	Amigo DC	1.35	49	2.7/12.5	2
		1.75	68	2.7/12.5	
		2.05	75	2.7/12.5	

3.3.1 Cross Power Quattro 1.5

The *Cross Power Kite Quattro 1.5* is a four-line ram-air kite. It is controlled by two bars, each one attached to the LE and TE lines of one side. The LE lines are the ones that sustain the entire kite connected along the lower surface, the leading edge line and the tips. So they are responsible for giving the shape and for transmitting the majority of the aerodynamic loads. There is no real necessity of the TE lines for a stable flight, whose utility is that of bending the surface at the trailing edge to break the aerofoil shape and reduce the aerody-

namic performance of the canopy. These TE lines are commonly named breaks.

The lower and the upper surfaces of the canopy are connected by cross sectional, aerofoil-shaped ribs, also made out of fabric, that will give the aerofoil shape to the inflated kite. These sections have holes in them to let the air distribute uniformly through all the cells. The spacings between the ribs are called cells. Air pressure inside the cells causes the ballooning effect between the ribs.

Geometry characteristics (flattened)	
Area (S)	1.3 m^2
Span (b)	2.08 m
AR (b^2/S)	3.33
Root chord (c_{root})	780 mm
Tip chord (c_{tip})	280 mm
Taper ratio (c_{tip}/c_{root})	0.36

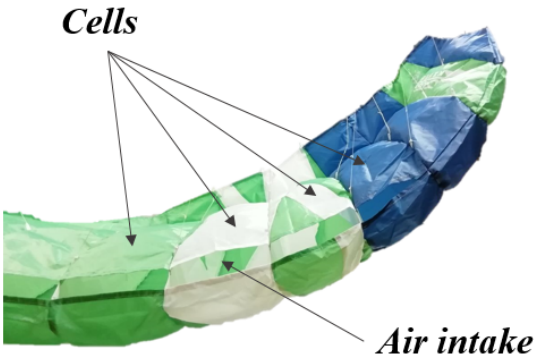

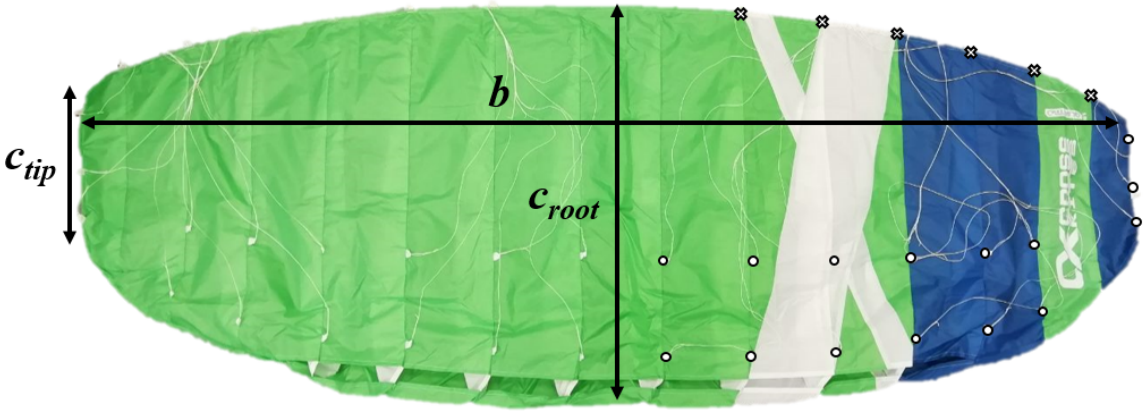

Figure 3.2: Planview and frontview of the CrossKites Quattro 1.5 with flattened geometry characteristics. Circles denote LE line connections, crosses denote TE line connections.

A planview of the flattened kite is shown in Figure 3.2. The LE line is opened with ram-air intakes and has an elliptic shape. The shape of the TE line is a circular arch. The main two-dimensional geometry characteristics are also listed the figure.

According to the airfoil-shaped sections, no similarities were found with typical airfoils. How-

ever, the shape of the root rib was taken from digital photographs and is given in Figure 3.3. This geometry must not been taken as an accurate reproduction, and it may not be representative of the shape of all the airfoil sections in the wing. However, it gives information about the thickness to chord ratio and the location of the maximum thickness at the root.

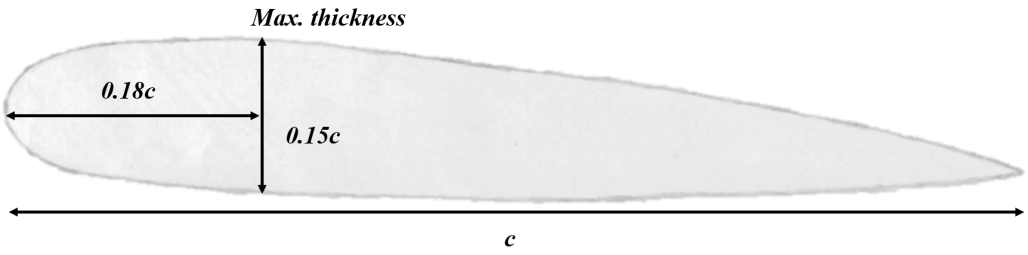

Figure 3.3: Airfoil section in the root.

The spanwise curvature, or anhedral, is another important feature of the kite, but it is one of the variables changing in the experiment, so no exact value is given here. Just note that the high anhedral values of the kite give a reduced projected span in comparison with the flattened geometry, making it closer to the upper limit of 1.7 meters span allowed in the wind tunnel. The effect of the anhedral on the aerodynamic loads is explained in later Chapters.

3.4 Methodology

3.4.1 Experimental Setup

The kite is hanged upside down inside the wind tunnel in order to facilitate launching. The four lines of the kite are connected to an adjustable H frame that emulates the input control bars. Figure 3.4 is a picture taken inside the wind tunnel and downwind from the kite. Figure 3.5 is a sketch showing the disposition of the H frame as well as the main input parameters that can be modified: the pitch angle of the horizontal bar and the spanwise or lateral distance between the handles sustaining the kite lines. The adjustment of different pitch angles and lateral spacings is done manually from run to run.

Tests at different wind speeds were undertaken for each configuration of fixed pitch angle and spanwise spacing. The lower boundary of the speed range was set to around 2.4 m/s, enough for the kite to inflate. The wind speeds being so low, it was difficult to set it to a fixed value

Figure 3.4: The kite hanged from the H frame inside the wind tunnel.

repeatedly, and instead the rotation speed of the fan was fixed to 40 rpm for the lowest speed on all the tests. The upper boundary of the wind range was set to that allowed by the stability of the kite. This value varied from test to test, and ranged from ∼5 m/s (60 rpm) to ∼10 m/s (100 rpm). The wind speed ranges for each run are given in more detail in Chapter 3.5.1.

For each run the forces and moments in the three directions were measured with a strain-gauge balance system located above the wind tunnel test section roof. The H frame transferred the loads from the kite to the balance. The output was a complete record of lift (L), drag (D), sideforce (S), pitching moment (My), yawing moment (Mz) and rolling moment (Mx) for each run. Note that the loads were measured in a mathematical point (P) in the middle of the test section. A sketch of the location of each element in the XZ plane is given in Figure 3.6. The distances between the balance (O), the measuring point (P) and the H frame (H) had to be taken for the correction of the pitching moments (My). The corrections are as follows:

$$\begin{aligned} L_H &= L_P \\ D_H &= D_P \\ M_{y,H} &= M_{y,P} + D_P\, h - L_P\, d \end{aligned} \tag{3.1}$$

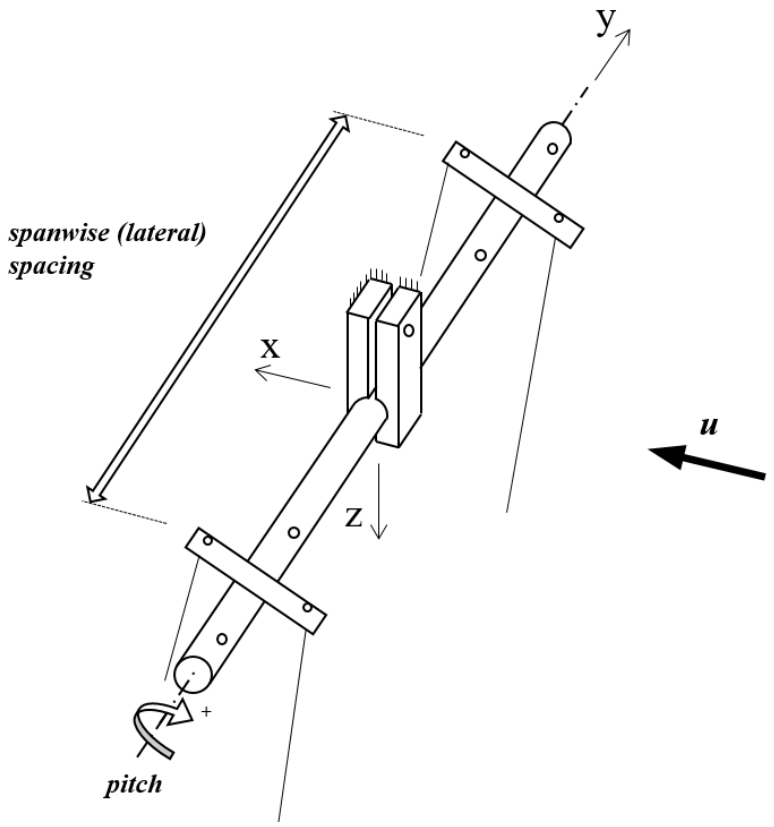

Figure 3.5: Sketch of the H frame that sustains the kite upside down. Pitch angle and spanwise distance are the adjustable input parameters.

In addition, photos were taken with two digital cameras, one inside the wind tunnel (downwind, frontal photos) and the other one in the control room (lateral photos). Apart from helping to have a record of the stability of the kite, the lateral photos allowed to measure the angle of the lines for each run. The frontal photos helped in recording the development of the spanwise curvature of the kite.

3.4.2 A note on stability

As the kite is designed to fly in the open atmosphere, a major concern was its adaptability to a wind tunnel test. An important step was therefore that of finding the ideal flight configuration in terms of control pitch angle, spanwise separation and wind speed.

The kite showed stability issues when rising the wind speed. More specifically, it steered

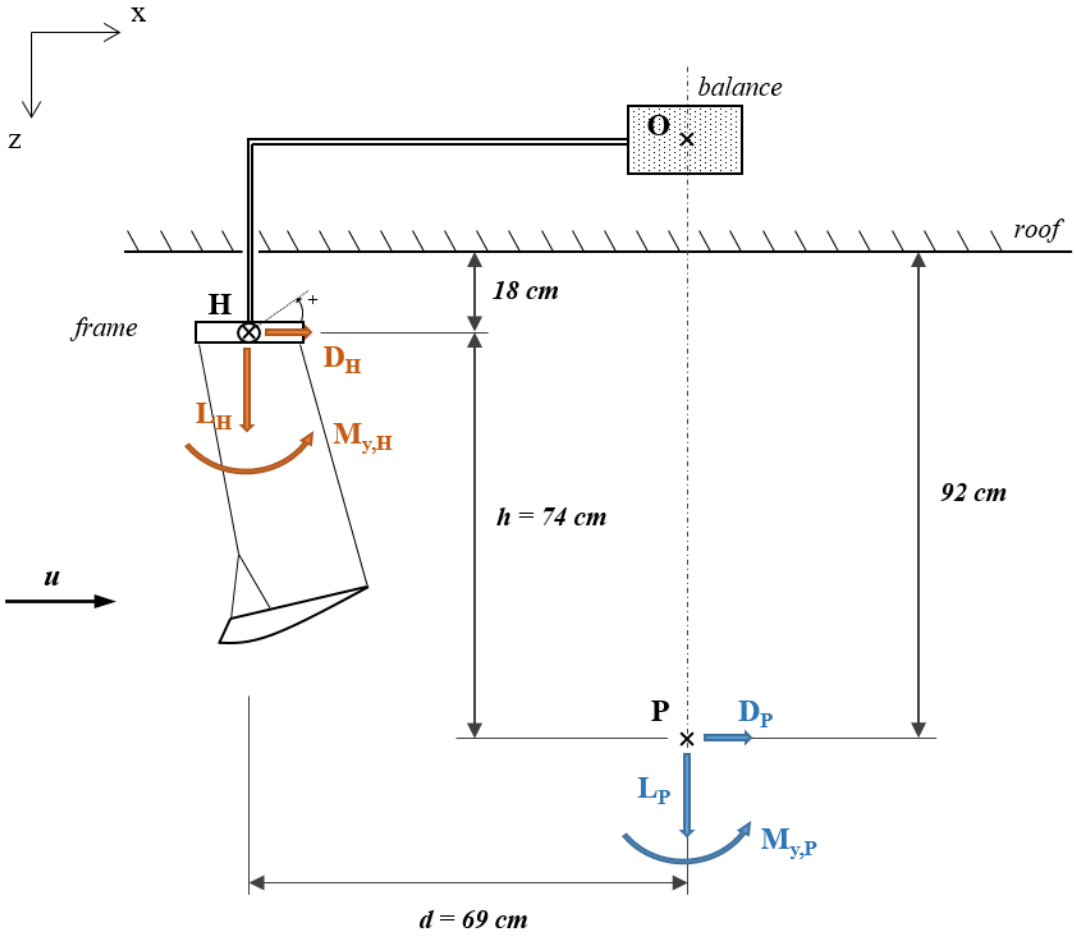

Figure 3.6: XZ-plane distances between H frame and point P. XZ-plane forces and moments in point P and the equivalent in point H.

around the vertical axis and because of the constrain that the tether lines imposed it turned again to end up yawing and rolling in "8" shape cicles. A further increase in wind speed made the amplitude of these oscillations to diverge and it forced to stop the run.

Attempts were made to increase the stability of the kite at the highest velocities, such as folding the wing tips inwards to reduce the wake interaction with the walls or attaching the kite to the walls by means of two extra lines, one on each side of the test section. The first solution showed no improvement in stability, it rather worsened it. A possible reason for this is the reduced vertical surfaces acting as yaw stabilizers. The second solution avoided the kite to increase the amplitude of its fluctuations, but did not fully eliminate them. A way of avoiding instabilities would be adding more tension to the extra lines attached to the

walls, which would eliminate any possibility of lateral displacement, but would also transfer not-measured-loads to the walls.

Due to the lack of a practical solution in the short term, the tests were finally carried out as intended in the beginning. The only feature seen to increase lateral/directional stability was the application of brakes (tense TE lines). The brakes are designed to make the kite fly out of the maximum-performance point, but they had to be applied for the sake of stability. From pure observation some direct conclusions were found regarding the effect of applying brakes:

- Instabilities still happen, but at higher wind speeds.
- The kite does not fully inflate because the brakes bend part of the surface close to the TE. Performance is most likely worsened.

Figure 3.7: Schematic view of the change in airfoil shape when brakes are applied.

- There is a clear connection between the inflation of the kite and the stability. As soon as the brakes are no longer pulled the kite inflates and instabilities arise.

It was concluded that it is not possible to have both a stable flight and a fully inflated geometry with that kite and in that wind tunnel. That is why the application of brakes was considered necessary if a set of results was to be obtained, even if they were not representing the flight of the fully inflated kite. In essence, it was preferred to have lower quality results than not having any. The discussion is therefore given under this consideration, and even if the results will not quantitatively match those of typical kite aerodynamic characteristics, a parametric study is still possible.

The stability issue is considered an essential part of the future work.

3.4.3 Tests

As it has been mentioned before, the main output values of the experimental setup are the aerodynamic forces and moments given by the kite in all the three dimensions and with the H frame as reference. The inputs or variables to analyse, on the other hand, are the wind speed (or dynamic pressure), the spanwise curvature of the kite, and the pitch angle of the input handle bars.

Having those variables in mind, the following procedure has been carried out:

1. With no wind and without the kite being hung, manually set a spanwise distance of the handle bars in the H frame. There are 4 spanwise distances available: 61cm, 75cm, 90cm and 105cm.

2. Manually set the desired pitch angle to the handle bars with the aid of an inclinometer. The two bars are independent, so both symmetric and asymmetric configurations are allowed.

3. Hang the kite to the H frame. A LE and a TE line are attached to each handle bar. The spanwise distance of the LE and TE lines is the same, i.e., the handle bars are parallel.

4. Turn on the wind tunnel and run the test at different wind speeds. The first record is taken at a fan rotational speed of 40 rpm. This value typically gave wind speeds between 1.9 and 2.3 m/s. Then apply increments of 10 rpm until the kite shows a diverging instability. Stable fluctuations of very high amplitude are recorded and filtered in the post-processing. When the kite is diverging, set the wind speed to 0.

5. The tests in the previous step are called a Run. Repeat steps 2 to 5 until the desired Runs are tested at a fixed spanwise spacing.

6. Repeat steps 1 to 5 until the desired spanwise spacings are tested.

7. Tare corrections: run the same tests without the kite. Every combination of tested pitch angle and spanwise distance needs a tare correction at a range of wind speeds.

Note that no zero-wind measurements are included in this procedure. The reason is that the zero-wind data collected showed no loads measurable by the balance. The balance was previously calibrated for the weight of the H frame, i.e., it gives zero force and moment output values with the H frame attached. As the weight of the kite is negligible compared to the H frame, no extra weight is recorded when the kite is hanged from the handles, and no zero-wind force and moment values appear.

In addition, every time a temporal break was done, the last test before the break was repeated after it. That way it was ensured that the variations in the environment such as the air temperature and density did not change the results considerably. Note that the experiments have been undertaken over 3 days, with a weekend between the second and third day.

Table 3.2 is a list of the main sets of Runs, including Runs at 61cm, 90cm and 105cm spanwise distances with a variety of handle pitch angles (θ) for each of these cases. The positive direction for the angle θ is shown in Figures 3.5 and 3.6.

Table 3.2: Main sets of measurements. Three different spanwise spacings with various pitch angles per case. All of them are symmetric flight.

Spanwise spacing (l)					
61 cm *-SET 01-*		90 cm *-SET 02-*		105 cm *-SET 03-*	
θ	Run No. (Tare corr.)	θ	Run No. (Tare corr.)	θ	Run No. (Tare corr.)
-10 deg	*034 (035)*	-10 deg	*019 (040)*	-10 deg	*052 (051)*
0 deg	*001 (009)*	0 deg	*020 (039)*	0 deg	*053 (050)*
5 deg	*006 (010)*				
10 deg	*002 (011)*	10 deg	*021 (041)*	10 deg	*054 (048)*
15 deg	*007 (012)*	15 deg	*022 (046)*	15 deg	*055 (049)*
20 deg	*003 (013)*	20 deg	*023 (047)*		
30 deg	*004 (014)*				
40 deg	*005 (015)*				

It can be seen that the measured pitch angles are not the same for every set. The tests could

not be structured or planified from the beginning because the behaviour of the kite was not known and it was found to be unstable. Thus a considerable part of the wind tunnel time was spent to find the ideal flight configuration for the stability issue, and lots of trial and error tests were carried out.

The *SET 01* is the one with the most complete record of handle pitch angles (θ). From here it was seen that the best flight configurations are at values of θ between -10 and 15 degrees. That is why *SET 02* and *SET 03* focus on these pitch angles.

Table 3.3: Asymmetric flight tests

Spanwise spacing (l)		
105 cm *-SET ASYM.-*		
θ left	θ right	Run No. (Tare corr.)
15 deg	10 deg	*056 (068)*
15 deg	5 deg	*058 (067)*
10 deg	5 deg	*059 (066)*
10 deg	0 deg	*060 (065)*
5 deg	0 deg	*063 (064)*

Apart from these, some additional sets were undertaken. It was of interest to analyse the aerodynamic characteristics of the asymmetric flight. The configuration of the handle bars was varied as shown in Table 3.3. The pitch angles ranged from 0 to 15 degrees, with 5 and 10 degrees of difference between the left and the right bar (reference for *left* and *right* bars is taken looking upwind from the kite). A total of 5 Runs were tested.

There is also repeated tests that allowed to make an analysis of the repeatability of the experiments. This is the case for Runs 033, 052, 053 and 054 written in Table 3.2.

Some other extra measurements were taken when the stability issue was being faced. For example, Runs 028, 029, 030 and 031 were done with the tips of the kite folded. As it has been mentioned before, this was a solution that intended to decrease the interference of the

wake with the wind tunnel walls by reducing the span of the kite.

3.4.4 Tare Corrections

As it has been mentioned, every Run needs its tare correction. The aerodynamic loads of the H frame are independently measured and then substracted to the data obtained form the kite measurements. As with the kite, the tare measurements are taken at different wind speeds for each configuration. It has also been explained that it was difficult to set the wind tunnel to fixed wind speeds, so rotation speed of the tunnel engine was fixed. Measurements at 40 to 110 rpm have been taken, which typically corresponded to 2 to 11.5 m/s wind speed.

The problem of this methodology is that it was not possible to match wind speeds of the Runs and their respective tare measurements for the substraction of loads. As a solution, a linear fit of the tare measurements was done for each Run and aerodynamic load to match interpolated values instead. Once the tare forces and moments for every wind speed are taken, they are substracted to the output values.

The aerodynamic loads of the H frame for this experiment have been very small in relation with the forces coming from the kite + H frame system.

3.4.5 Data output

The strain-gauge balance system is developed by the company *Ate Aerotech*, who also offer the software for the data acquisition. The *Balance Output Data Software* gives the output in the following format for each Run:

Data Point	Data + Time	Wind Speed [m/s]	q [Pa]	Air Temp. [°C]	P barometric
...	...	...	...	...	...
Fz (Lift) [N]	Fz St. Dev.	Fx (Drag) [N]	Fx St. Dev.	Fy (Side force) [N]	Fy St. Dev.
...	...	...	...	...	...
My (Pitch) [Nm]	My St. Dev.	Mx (Roll) [Nm]	Mx St. Dev.	Mz (Yaw) [Nm]	Mz St. Dev.
...	...	...	...	...	...

where the data points are the number of measurements at different wind speeds that are taken

in each Run. The *Data+Time* cell helps in relating the data with photos taken during the tests, which are also dated. The aerodynamic forces and moments are given with respect to the point P in the centre of the wind tunnel, as explained in Chapter 3.4.1, and with the XYZ reference system given in the same Chapter. As the XYZ reference system is fixed with the X axis in the same direction as the free stream wind speed, the Fx will always be Drag, Fz the Lift, and so on. Needless to say that the angle of attack of the model will have no effect in this relation. Finally the standard deviations of all the aerodynamic forces and moments are given.

3.5 Results and Discussion

3.5.1 Main limitation: stability

The kite has become unstable in every Run when the wind speed was raised above some point. During the tests notes were taken about the nature of the fluctuation of the kite. The kite was defined as *unstable* when the fluctuations started, and was defined as *diverging* when the amplitude of the fluctuations began rising at a fixed input rpm. It is easy to understand that the *diverging* state always supposed the end of the Runs and these points are not taken for the analysis. Some stable fluctuations also had too big amplitude to suppose a stable flight, so their results were not taken into account. Figure 3.8a is an example of a diverging kite from the side view and Figure 3.8b is an unstable case with very high fluctuation amplitude.

Table 3.4 records the wind speed range (lowest and highest wind speeds) and the note on stability for the *SET 01, SET 02* and *SET 03*. Note that the state *div* always forced to finish the undergoing test. The speed at which the state *uns* was noted is also added. If there is none, it means the kite got unstable and diverged at the same wind speed (*uns* + *div*).

The lower limit of the wind speed range does not vary much and stays between 1.8 and 2.4 m/s, while the upper limit depends on the case. The negative handle angle (θ = -10 deg) was the one that allowed a better inflation of the kite, or in other words, the configuration with less pull of breaks. That is why the diverging speed for this pitch angle is among the smallest ones for all the three sets.

According to the spanwise distance, the lowest one (*SET 01*, 61 cm) is the one that allowed measurements at higher wind speeds. An important mention here is that the use of the origi-

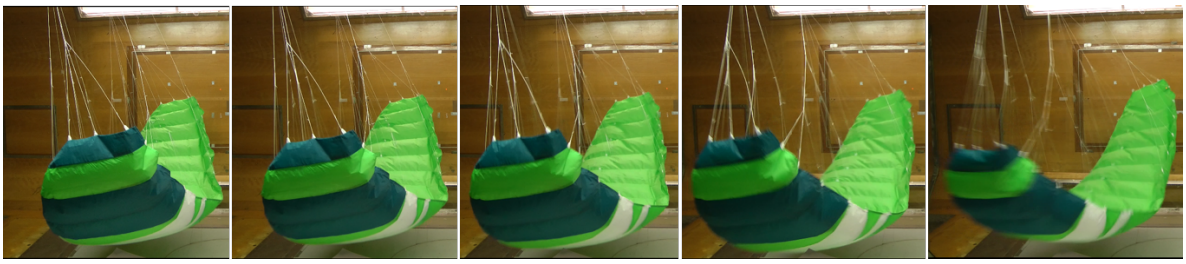

(a) Side pictures from outside the wind tunnel. Left to right, the kite is diverging. Photos taken from a video at steps every 2-3 periods of the "8"-shaped fluctuations.

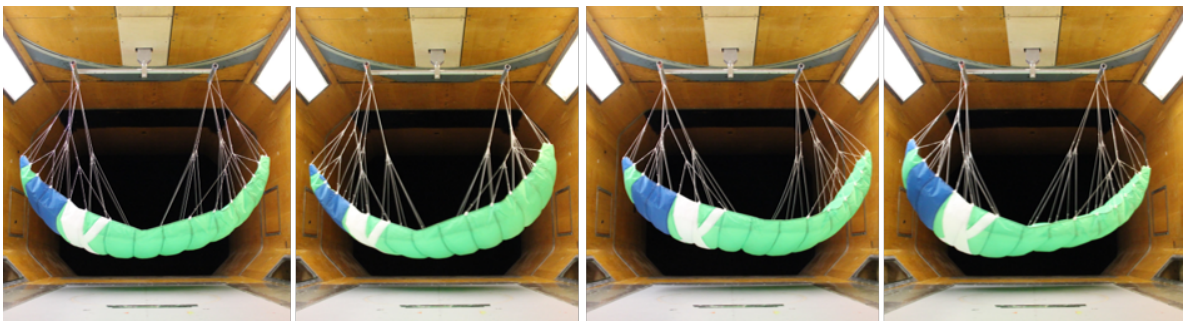

(b) Front pictures taken downwind from inside the wind tunnel. Left to right, consecutive photos of a single period of the "8"-shaped fluctuations.

Figure 3.8

nal handles of the kite (for atmospheric flight) resulted in a similar lateral spacing between the lines at the point where the lines are attached to the H frame. Therefore it can be said that the spanwise distance in *SET 01* is closer to the design spanwise distance. Another possible reason for the wider speed range in *SET 01* is that the higher curvature of the kite is creating less interference with the walls. This last hypothesis is later discussed along with the results of aerodynamic loads.

Until now the stability of the kite has been discussed from the point of observation. The *unstable* and *diverging* definitions are just indicators taken during the tests to help the author have a record of the quality of each measured point. But the output data has further information of when could the kite be fluctuating. The main indicators have been found to be the standard deviations of the forces and moments (σ). More specifically, the deviations of Sideforce (Fy), Roll moment (Mx) and Yaw moment (Mz) are the ones that most clearly increase when the kite gets unstable. These values give a sense of the variability of the measured value during the sample time (30 seconds). It is evident that a fluctuating kite will

Table 3.4: Wind speed ranges for *SET 01, SET 02* and *SET 03*. Lower limit is always 40 rpm, and upper limit is dictated by the state *div*.

SET 01 *(l = 61 cm)*				
Run	Handle angle [deg]	Rev. [rpm]	Note on Stability	Wind Speed [m/s]
034	-10	40		2.1
		60	*div*	4.9
001	0	40		2.2
		70	*uns*	6.2
		80	*div*	7.5
006	5	*40*		2.3
		80	*div*	7.5
002	10	*40*		1.9
		90	*uns*	8.6
		100	*div*	9.8
007	15	40		2.3
		70	*uns*	6.2
		110	*div*	9.7
003	20	40		2
		70	*uns*	6.1
		110	*div*	10.7
004	30	40	*uns*	1.6
		90	*div*	8

SET 02 *(l = 90 cm)*				
Run	Handle angle [deg]	Rev. [rpm]	Note on Stability	Wind Speed [m/s]
019	-10	40		2.4
		60	*div*	5.1
020	0	40		2.2
		60	*div*	5.1
021	10	40		2.3
		60	*div*	4.9
022	15	40		2.3
		70	*uns*	6.1
		80	*div*	6.8
023	20	40		2.2
		60	*uns*	4.8
		80	*div*	7.3

SET 03 *(l = 105 cm)*				
Run	Handle angle [deg]	Rev. [rpm]	Note on stability	Wind Speed [m/s]
052	-10	40		2.3
		60	*div*	5.1
053	0	40		2.1
		60	*uns*	4.9
		80	*div*	7.4
054	10	40		1.9
		60	*div*	4.8
055	15	40		1.8
		60	*uns*	4.8
		70	*div*	6

also give fluctuating forces and moments, and even if the mean values are close to zero, the standard deviations will be high in comparison with the mean.

This phenomenon has been seen to match the notes taken by observation in several cases. There seems to be a general trend: when the notes *uns* or *div* are taken, the deviations rise. An example is given in Figure 3.9. Here the dimensionless or relative standard deviation, $\sigma_{rel} = \frac{\sigma}{force,moment}$, is plotted against wind speed for the sideforce, yaw moment and roll

moments. The plot on the left ($\theta = 0$ deg) shows a rapid increase in the deviations when wind speed increases above 6 m/s. This increase matches with the *unstable* and *diverging* states of Run 001 in Table 3.4. The plot on the right ($\theta = 15$ deg) also shows an increase in the deviation, even if the trend is not so clear. The *unstable* state in Run 007 arises at 6.2 m/s, just at the point where the deviations of all the three Fy, Mz and Mx rise. The later decrease in σ_{rel} is not significant of a decrease in unstabilities, since it was never observed that a further increase in speed stabilized the kite. Note that the trends do not need to be followed as a way of measuring the level of instability, but just as an identifier. For both plots it can be said that the kite was "stable" until ∼5 m/s.

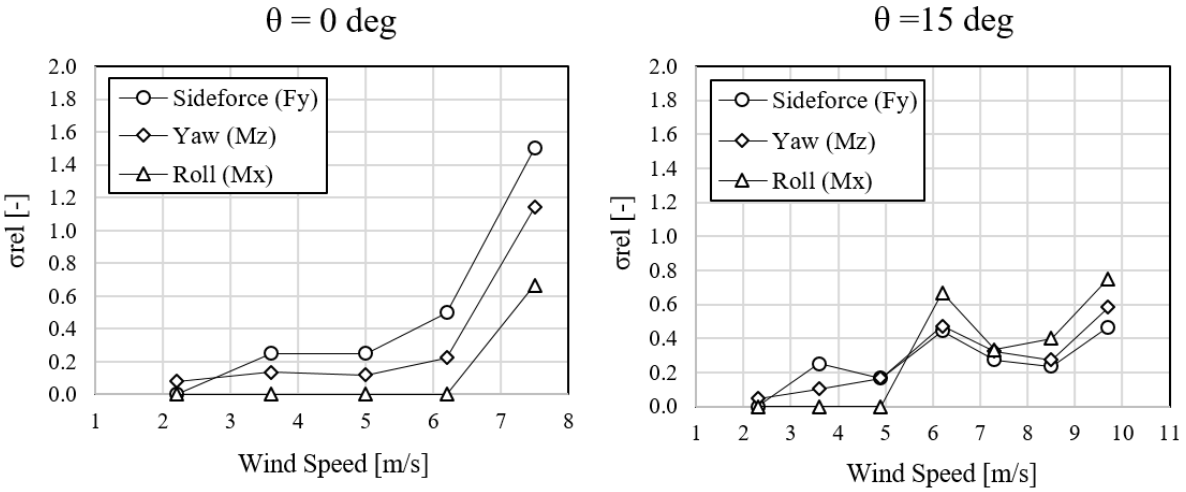

Figure 3.9: Relative standard deviation against wind speed for pitch angles 0 and 15 degrees. Both are from *SET 01*, left is Run 001 and right is Run 007.

Other flight configurations also showed a rapid increase in standard deviations from a wind speed on. Each case has its own critical velocity where the kite started to fluctuate and readings started to deviate. There are also some cases that do not match this logic, but they are few and not enough to refute the general trend seen in most of the Runs.

There is, therefore, a way of detecting the start of unstable flight for most of the Runs. This identifier can be used to see if the unstable flight has an effect on the main output loads: Lift and Drag. This analysis is done once the main output values are presented (Chapter 3.5.2).

3.5.2 Effect of wind speed on kite performance

It is of interest to look at the distribution of the Lift and Drag against the wind speed. The well known relation between the aerodynamic forces Lift (L) and Drag (D) and the wind speed written in Eq. 2.4. The force is directly related to the square of the velocity. Now, if the definition of dynamic pressure, $q = \frac{1}{2}\rho V^2$, is implemented:

$$\begin{aligned} L &= C_L\, A\, q \\ D &= C_D\, A\, q \end{aligned} \tag{3.2}$$

That is, the relation of the force with the dynamic pressure is linear if the rest of variables are constant.

According to the Reynolds number, [36] states that typical AWES kites have Re in the order of 1e6. Reynolds number during the tests has been between 0.1e6 and 0.6e6, and order of magnitude lower. Differences in laminar-to-turbulent transition and different separation scenarios are expected because the flow in the wind tunnel tests is more viscosity-driven. However, the limitations of the tests (stability) have not made possible to match Re numbers, so the difference is left as a reminder.

Lift and Lift Coefficient

First, the Lift is presented against q for Run 002 (Figure 3.10). It is also of interest to non-dimensionalise the force in the form of C_L for comparison with other tests. The C_L vs q for Run 002 is also presented in Figure 3.10. The area used to calculate each C_L is the real wing area of the kite, $A = 1.3m^2$. In the case of wings with dihedral or anhedral the projected area is usually taken since it is only the forces projected in the vertical direction that create Lift force. However, for the sake of comparison between different spanwise curvatures of the same kite, a single reference area is preferred. The C_L will therefore have information about the "efficiency" of the curved kite compared to the flattened version of the same kite.
The results are given for a single Run, but are significative of the majority of Runs: a linear, positive-sloped trend in the Lift vs q chart and a decreasing C_L with q. There are some features here that are somewhat non-conventional and need to be commented.

C_L decreases with dynamic pressure. For conventional tests with fixed, rigid wings, C_L should remain constant (or almost constant) since it is a value mainly dependant on the geometry

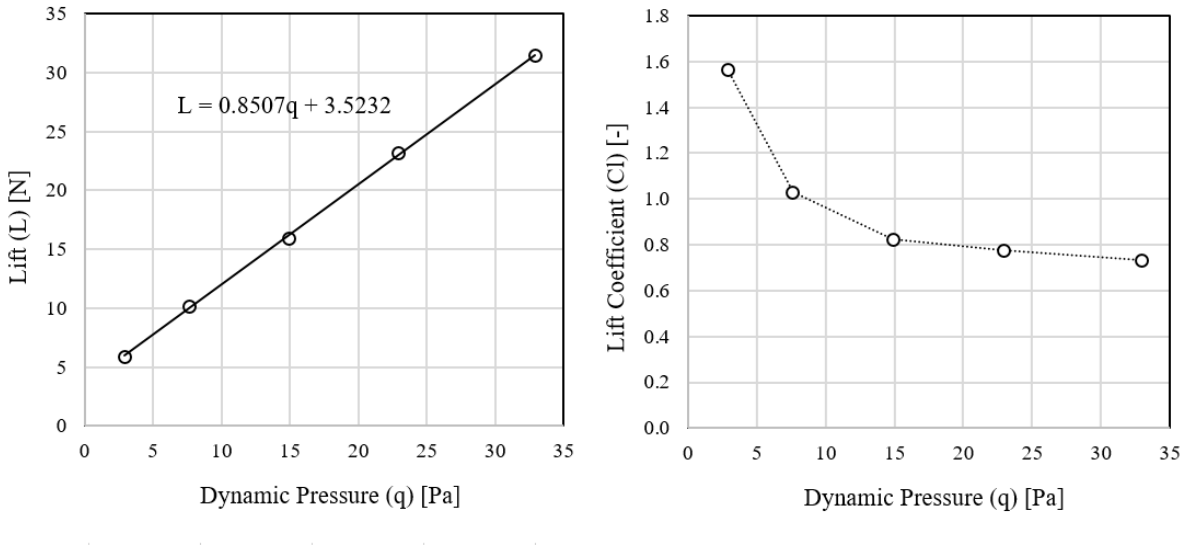

Figure 3.10: Lift vs q (left) and Lift Coefficient vs q (right) for Run 002. Pitch angle is 0 deg and spanwise spacing 61 cm.

and the angle of attack (AoA). In this experiment the AoA was seen to slightly increase with increased wind speed, so C_L could be expected to increase too. The only reason found for the rather decreasing trend is that the geometry of the kite changes. This hypothesis goes along with the Fluid Structure Interaction problem, where the aerodynamic loads alter the geometry at levels enough to induce a change in the loads.

Another feature is that the C_L values are very high. Specially at lower wind speeds, the kite must be acting as a high-lift device. That idea matches the fact that the TE brakes are creating a highly cambered wing shape. If this is correct, the extra camber created by the brakes must decrease with wind speed, since C_L also does. The brakes, however, would bring a drawback in C_D, an idea that is confirmed by Figure 3.12, where the L/D values are lower at low speeds. Thus it can be concluded that at low wind speeds the wing is highly cambered, with a pronounced bending of the TE and creating a high C_L but with a drawback in C_D. When dynamic pressure gets higher, the kite inflates more and the bending reduces to give an aerodynamic shape closer to the fully-inflated design-shape. This brings a lower C_L but a higher L/D ratio.

The trend in Lift force vs q is very close to linear. The unconventional feature is the non-zero

intercept. This means that if data was extrapolated to q = 0 (no wind) the kite in this Run would create 3.5 N of Lift force. As this is not possible (the readings at q = 0, in fact, gave L = 0.0 N) there must be some non-linearities in the lowest region of wind speed. This is confirmed by the fact that the kite was not properly inflated at such low wind speed values, and hence it was an aerodynamically different object that was creating Lift. The link between the non-zero intercept in the L vs q plot and the decreasing trend in C_L vs q is theoretically derived from the equation of the linear fit:

$$L = 0.85q + 3.5 \tag{3.3}$$

which combining with Eq. 3.2 (Lift equation),

$$C_L = \frac{L}{qA}$$

gives:

$$C_L = (0.85 + \frac{3.5}{q})\frac{1}{A} \tag{3.4}$$

That is, C_L is inversely proportional to q in the second term in Eq. 3.4. That equation is the equivalent curve of the linear fit for the C_L vs q plot. Note that a zero intercept of the Lift curve would make the second term disappear and C_L would become independent of dynamic pressure, i.e., constant. Note also that this is a purely mathematical relation that is not representative of any physics of the kite. Wing surface is considered constant, but as for the calculation of the C_L values it has also been considered so, it can be a mathematical representation of the C_L curve, and can give an idea of the converged value of the coefficient at high values of q. Beyond that it has no practical value.

Drag and Drag Coefficient

According to the Drag force, the trends are similar: linear distribution of force and decreasing C_D with dynamic pressure. Figure 3.11 shows both Drag and C_D values against dynamic pressure for Run 002. It can be seen that the Drag force has also a non-zero intercept. The drag computed here is the sum of the canopy drag and the tether drag (drag coming from the H frame is substracted by tare corrections).
Both Figure 3.10 and Figure 3.11 are not showing the standard deviation of the Lift and Drag forces because they are relatively very small, less than 1% of the force.

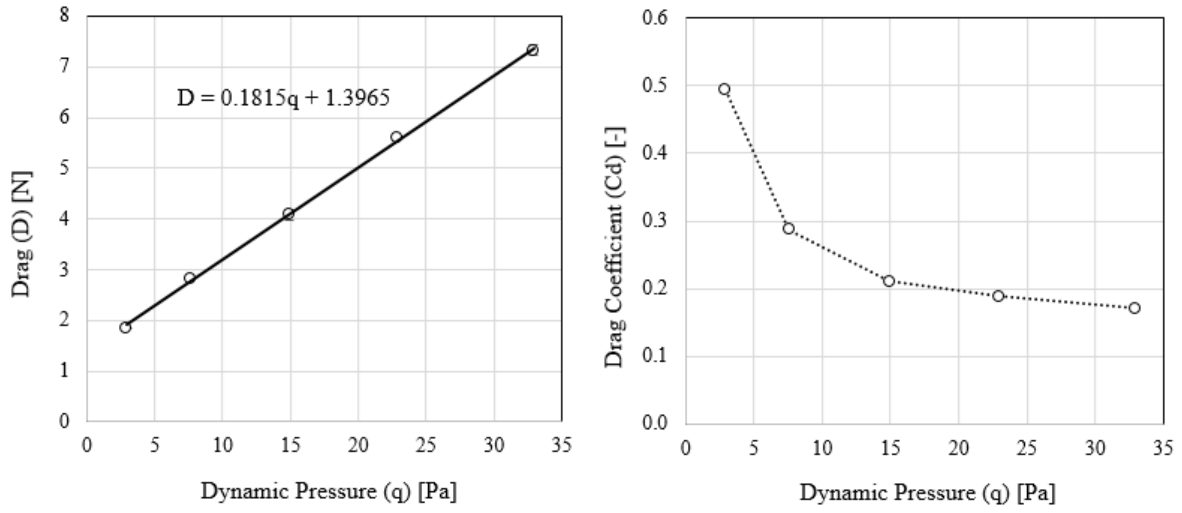

Figure 3.11: Drag vs q (left) and Drag Coefficient vs q (right) for Run 002. Pitch angle is 0 deg and spanwise spacing 61 cm.

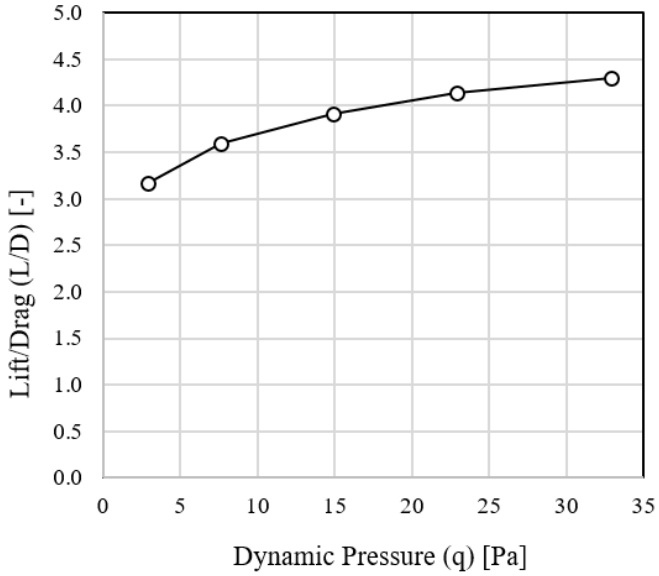

Figure 3.12: L/D against dynamic pressure for Run 002. Pitch angle is 0 degress and spanwise spacing is 61 cm.

Performance: Lift/Drag

The L/D ratio for Run 002 is given in Figure 3.12. This is the main indicative of kite performance. It is seen that L/D increases with wind speed, as it has been explained before, most likely because of a better inflation of the kite and a smaller effect of the brakes. L/D values range from 3.2 to 4.3, which are of a comparable order with other low-AR inflatable parafoil performance values. For example Nicolaides, in wind tunnel tests at Langley, measures maximum L/D values below 5 for a real inflatable kite of wing area 13.5 m^2 and AR 3 taking into account the tether drag ([**Nicolaides1971**], Figure V-4). Other literature get L/D values of the same order with inflatable kites, typically between 3 and 8 [62] [44] [48] [10].

This trend is similar for Runs with pitch angles 0, 10 and 15 degrees at all the spanwise spacings. The effect of changing the pitch angle is later explained.

Pitching Moment

Last the Pitching Moment My is discussed. It is important to understand the meaning of the output value My. This is not the aerodynamic pitching moment created in the wing, but the pitching moment recorded in the mathematical centre of the wind tunnel and translated to the centre of the H frame. Figure 3.13 is a sketch simplifying the kite-frame model to a 2D, 2-line system. T_1 (LE) and T_2 (TE) are the line tensions transmitted from the kite to the H frame, and δ_1 and δ_2 are their respective vertical angles with the handle bars.
L and D output forces result in:

$$\begin{aligned} L &= T_1\, cos(\delta_1 \,+\, \theta) \,+\, T_2\, cos(\delta_2 \,+\, \theta) \\ D &= T_1\, sin(\delta_1 \,+\, \theta) \,+\, T_2\, sin(\delta_2 \,+\, \theta) \end{aligned} \tag{3.5}$$

And My can be computed as:

$$M_y = T_1\, cos\delta_1\, \frac{l_H}{2} \;-\; T_2\, cos\delta_2\, \frac{l_H}{2} \tag{3.6}$$

The output value of pitching moment is dependant on both line tensions and their projection in the vertical of the H frame.

It is therefore a must to know the angles of each line with respect to the H frame if My is to be transformed into line tensions. The lateral photos have been considered unsatisfactory

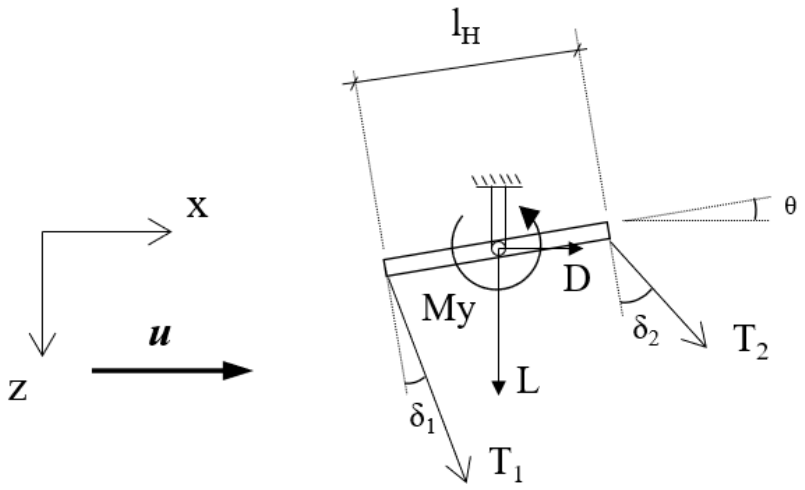

Figure 3.13: Transmission of tensions T_1 and T_2 from the kite to the H frame. As a result output values L, D and My are recorded. l_H is handle bar length and θ is handle pitch angle.

for a quantitative study of the attitude of the lines. A more sophisticated methodology needs to be implemented in order to measure the angles. That means that no relation could be obtained between My in the H frame and the force and moment distributions in the kite.

However, some information can be obtained from the readings of My. The lateral photos revealed that the LE and TE lines were almost parallel during the tests. Thus the assumption $\delta_1 = \delta_2$ helps in reducing Eq. 3.6 into:

$$M_y = T_1 \frac{l_H}{2} - T_2 \frac{l_H}{2} = \frac{l_H}{2} \Delta T \tag{3.7}$$

That is, My gives information on the tension differential created by the aerodynamic forces and moments on the kite.

Figure 3.14 is a plot of the pitching moment My around the H frame against the dynamic pressure q. The increasing linear trend of My with q is evident. That means that the differential of line tensions increases with wind speed.

It is of interest to know how the tension differential is transmitted to the kite. Figure 3.15 is a sketch of the forces applied in the kite (2D, 2 parallel lines). The Lift and Drag forces are

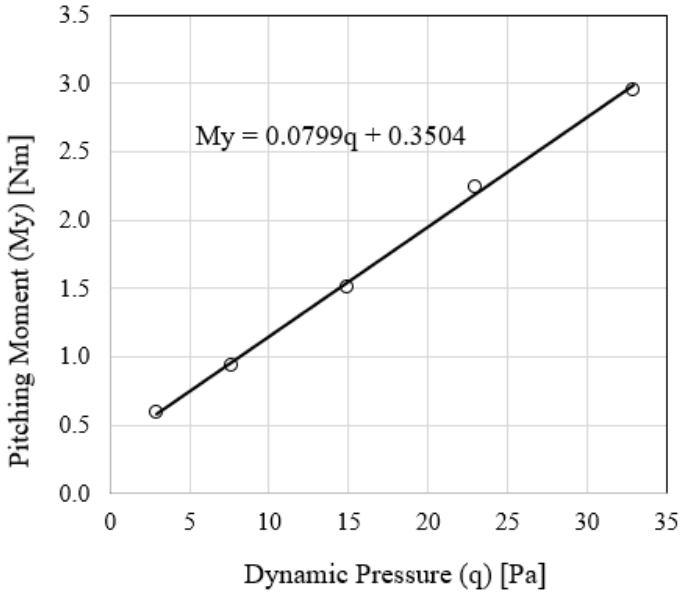

Figure 3.14: Pitching moment around the H frame against dynamic pressure for Run 002.

applied in the centre of pressure, so no pitching moment is added.

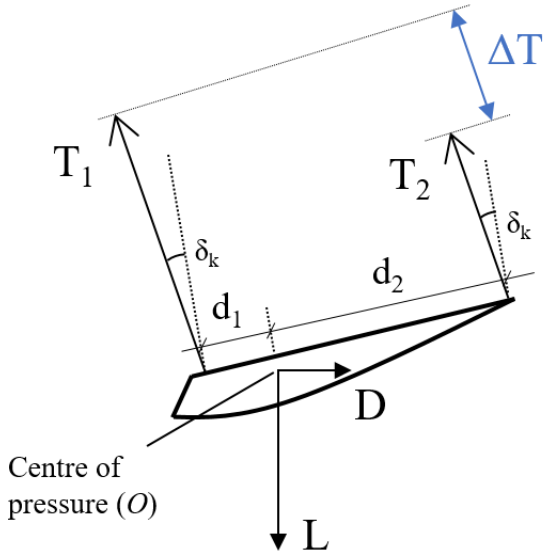

Figure 3.15: Sketch of the forces applied in a 2D model of the kite. The lines are considered parallel and have an angle with the kite δ_k.

Thus the relation between the line tensions and the aerodynamic forces originated in the kite can be computed as follows.

Applying equilibrium in the centre of pressure (denoted as A),

$$M_{y,A} = 0 \;\Rightarrow\; T_1\, d_1 \;=\; T_2\, d_2 \tag{3.8}$$

Here the projections due to the angle δ_k are are not relevant because the lines are parallel, and the displacement of the centre of pressure due to kite thickness is considered negligible. Combining Eq. 3.8 with the relation $T_1 - T_2 = \Delta T$, it is concluded

$$T_1 \left(1 - \frac{d_1}{d_2}\right) \;=\; \Delta T \tag{3.9}$$

Eq. 3.9 shows that when ΔT increases, either:

- T_1 increases. As it has been seen, an increase in dynamic pressure brings an increase in all L, D and My. My has also been seen to be directly proportional to ΔT, so it is logical that an increase in ΔT goes along with and increase in L and D, and therefore in T_1 and T_2.
- $\frac{d_1}{d_2}$ decreases. It is possible that the centre of pressure moves forward when dynamic pressure increases.

Whether the first, the second, or a combination of both happen cannot be clarified in this project. Many other effects could be taking part, but this simplistic relation helps to have a better insight on the relation between the kite and the H frame.

Stability in the output data

It has to be mentioned that the unstable and diverging data points have been included in the present study. However, there is no sign that the loads change from q = 15 Pa on (u = 5 m/s), which was the point at which the lateral and directional standard deviations rose. So even if there was a stability identifier in the side force and roll and yaw moments, there is no evidence that these instabilities affected the main forces and moments. On the contrary, the unstable and diverging data points seem to follow the linear pattern in all the three plots (L, D, My). The standard deviation of My has in some cases been found to rise in the diverging

data points, but not always.

As a general rule, from now on the last point of each Run is deleted, which is the *diverging* point that forced the shut-down of the tunnel at each Run. However, the *unstable* points have not been deleted since no sign has been found that they have a relevant effect on the output data. Furthermore, there is little data available in every Run and deleting *unstable* points would mean to reduce the data points in each Run approximately to the half.

Kite inflation

It has been observed from the digital pictures that the dynamic pressure inflates the kite. It is intuitive that a higher dynamic pressure increases the positive stagnation pressure of the air inside the cells. It can be concluded that increased wind speed slightly increases the thickness of the kite cells. Possible effects of the inflation are:

- Separation along the ribs [41] is most likely to appear sooner due to a higher ballooning effect. Trailing edge separation is most likely more severe.
- The effect of the brakes can be smaller.
- The deformations can be smaller due to a stiffer geometry, but the higher dynamic pressure could also overcome that factor and induce higher deformations. A FSI study is recommended for this analysis.

Kite attitude

The kite attitude is defined as the angle of the tethers with the vertical (z axis).

In order to understand the relation between the attitude of the kite and the aerodynamic forces, a simple, 2D model given in Brown (1989) [45] is used. The paper presents an experimental test technique that allows to measure the L/D ratio of a 2-line kite in real flight tests. The following expression is obtained from the simple sketch in Figure 3.17:

$$\frac{D}{L} = tan(tether\ angle) \Rightarrow \frac{L}{D} = tan^{-1}(tether\ angle) \tag{3.10}$$

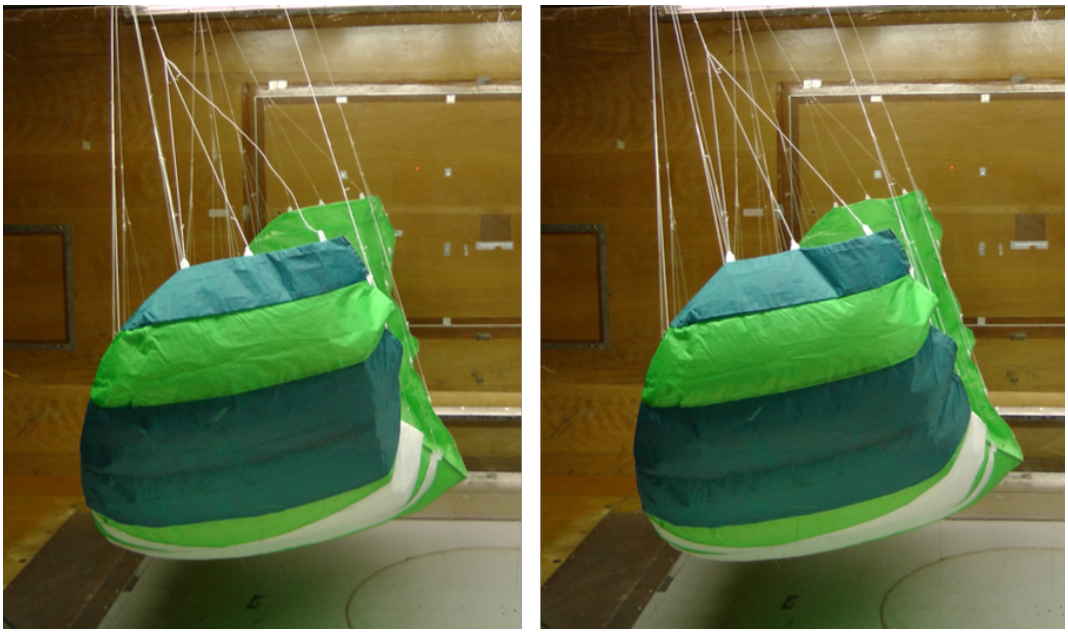

Figure 3.16: Two lateral photos of the kite during Run 032. Left: 40 rpm. Right: 60 rpm. Inflation of the kite is slightly noticeable from left to right photos.

The equation relies on the idea that the kite, depending on its L/D ratio, will fly at a given attitude (*tether angle*) because the line tension and the resultant aerodynamic force must be in the same direction to meet the equilibrium condition. Such a simple relation allows to have a preliminary insight on the kite performance just by measuring the angle of the lines.

There is a number of simplifications and discrepancies with the experiments that most likely make Eq. 3.10 inaccurate. The L and D forces will not be the aerodynamic forces of the canopy as Figure 3.17 shows due to 3D effects, wind tunnel turbulence and wall interactions, deformation effects, scalability, tether drag, kite and tether weights... However, all these considerations can be corrected in an equivalent resultant force. The system can be taken as a black box, and only the forces in the tether point be taken as output, whatever the complexity of the system is. Thus the following should not be altered: the higher the L/D ratio is, the lower the tether angle will be.

There is however a factor that makes the wind tunnel experiment differ from the model in Figure 3.17. In that model there is no transmission of pitching moments because it is a 1-line system. Any pitching moment will alter the attitude of the kite, which will find another equilibrium point (if longitudinally stable) where no pitching moments take place. For the

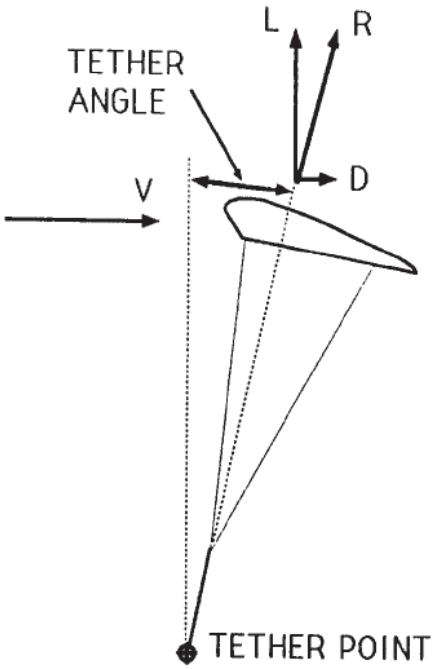

Figure 3.17: A simple 2D kite-tether model with main aerodynamic forces on it. Source: *Tethered Parafoil Test Technique (Brown, 1989)*

same reason, the force R and the tether must be aligned when the kite is at equilibrium point. That is different in the 4-line kite tested in the wind tunnel, or a simplified 2D, 2-line kite model. There can be a pitching moment acting on the kite, or in other words, the forces can be applied displaced from the centre of pressure. A differential in line tensions will counter this moment, as has been seen in the discussion of My.

It has also been seen in Figure 3.12 that L/D increased with dynamic pressure during the tests. According to the simplistic 2D model of the 1-line kite, an increase in L/D should decrease the attitude of the kite (angle of tethers with the vertical). However, photos taken from the lateral reveal that the attitude is increased instead. Somehow the logic behind the presented model is not met in the wind tunnel tests. The main reason for this phenomenon is considered to be the fact that there is 4 lines attached to the H frame. The TE lines mean an extra constrain to the system, as it has already been explained, a constrain that was necessary for a stable flight. It is possible that a nose-up pitching moment on the kite is making the attitude to increase with wind speed even with an increase in L/D. The hypothesis is in accordance with the increasing My with wind speed, that is, the line tension differential

increase with wind speed.

3.5.3 Effect of handle pitch angle on kite performance

First it has to be noted that the handle pitch angle, or the pitch angle of the H frame, is neither inputting the angle of attack of the kite, neither the attitude of the kite. It is essentially an input of the amount of brakes pulled. This input has two effects. First, it changes the bending of the brakes, and second, it changes the attitude of the kite. Both effects are coupled and the exact amount of each parameter has not been measured during the tests. Only the input (handle pitch angle) has been measured, and denoted as before with the Greek letter θ.

The best configuration to understand the effect of handle pitch angle on kite aerodynamics is the spanwise distance 61 cm since it allowed more data points to be measured. Therefore Runs 034, 001, 006, 002, 007, 003 and 004 are compared.

Lift and Lift Coefficient

First L is plotted against dynamic pressure for pitch angles ranging from -10 deg to 20 deg (Figure 3.18). The main effect with an increase of dynamic pressure is found to be a increase in the lift curve slope. Note that every pitch angle shows a linear trend with a non-zero positive intercept, which brings a decreasing C_L with dynamic pressure, as explained before. The intercept also rises in magnitude when pitch angle is increased. Thus a steeper decreasing slope of C_L is expected for the highest pitch angles.

This trend is confirmed in Figure 3.19. In addition, the main effect of increasing the handle pitch angle is to increase the C_L value at every q. The Run at θ = -10 deg shows the most reasonable values of C_L (below 1). This is the only configuration that allowed a full inflation of the kite, since it is equivalent to a very small pull of the brakes. However, the stability dramatically worsened as soon as the kite fully inflated, so there is not a lot of available data. This confirms the idea that pulling the brakes increases C_L.

For the rest of handle pitch angles, C_L values are very high, especially at the lowest q-s. The accuracy of these values is doubtful because the dynamic pressures are too low. The slope of

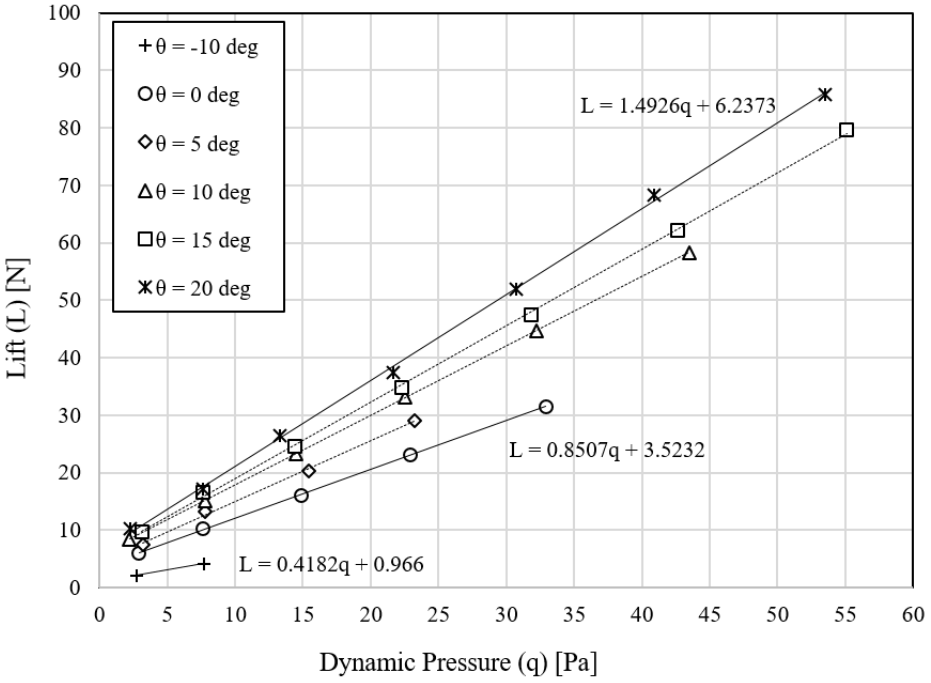

Figure 3.18: Lift force against dynamic pressure for pitch angles (θ) equal to -10, 0, 5, 10, 15 and 20 degrees. Equations of linear fit are given for θ-s -10, 0 and 20 degrees.

the curves is seen to stabilise with increasing dynamic pressure, so the points at lowest q-s are most likely coming from a transition state where the wing is not flying as a proper ram-air kite. The points of interest are the ones at higher dynamic pressures. It has to be mentioned that even these data points show very high lift coefficients, with values above 1 for θ-s 10, 15 and 20 degrees.

The weight of the kite could be acting as an extra force that increases the Lift force. Furthermore, it would be more relevant at the lowest Lift force values (lowest q), and thus might be the reason for the very high C_L values at lowest wind speeds. However, the weight of the kite was calibrated so that the balance gave L = 0.0 N at q = 0 Pa. So any lift created must be independent of the weight, and this theory is not considered valid unless the calibration has not been well done.

There is another source of error in the calculation of C_L, it is the wing surface used. As mentioned, instead of the projected area, which is the one effectively creating lift force, the flattened area of the wing has been used. As can be expected, the area used is bigger than

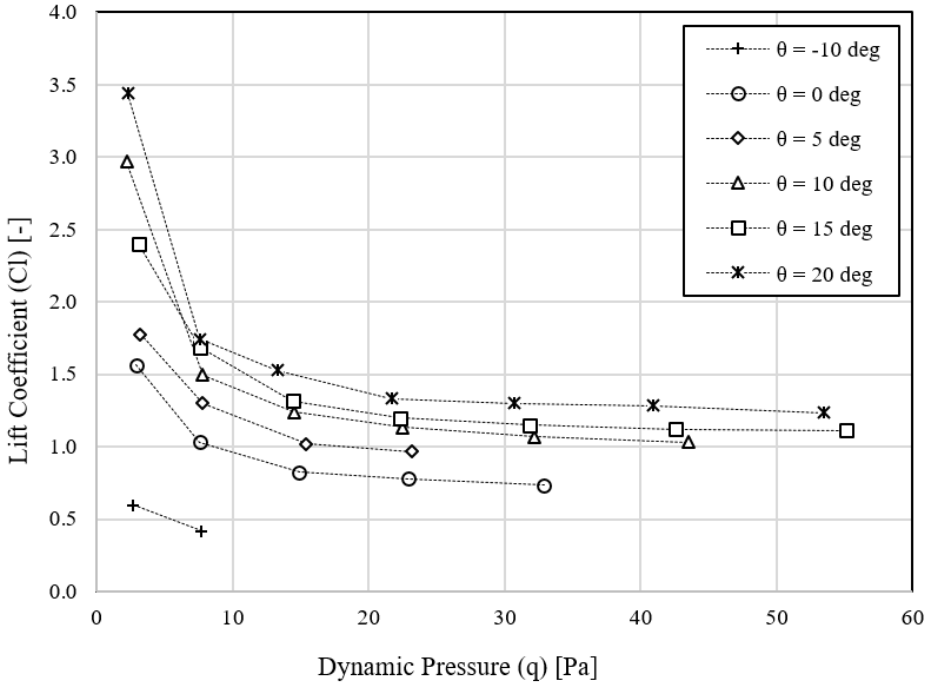

Figure 3.19: Lift coeffcient against dynamic pressure for pitching angles (θ) equal to -10, 0, 5, 10, 15 and 20 degrees.

the projected, and thus C_L is smaller. The use of the projected area would further increase the already high values in Figure 3.19, so the phenomenon cannot be explained by this effect.

The kite is considered to be operating at those high values of C_L. The reason for the high values is taken as the pull of brakes, which make the kite similar to a wing with high-lift devices. The values, even if high, are similar to those obtained by de Wachter [44] (C_L between 0.7 and 1.3). The results can be correct and correspond to the flight of a ram-air kite at different brake positions.

Lift-Drag polar, L/D

In order to measure the effect of handle pitch angle on the performance, a Lift-Drag polar is plotted in Figure 3.20. Here the trend of each value of θ is almost linear, and the increase in θ shows a decrease in L/D, i.e., a smaller slope of the linear fit. The brakes are confirmed to be designed to worsen the performance of the kite.The blue arrows show the effect of pulling the brakes (increase θ) at points with similar wind speeds. The pattern is similar for all the

wind speeds: an initial slow decrease of L/D and a more rapid decrease of L/D at higher θ-s. The upper limit of L/D = 5 and the lower limit of L/D = 2 are guides to understand the range of performance values of the kite.

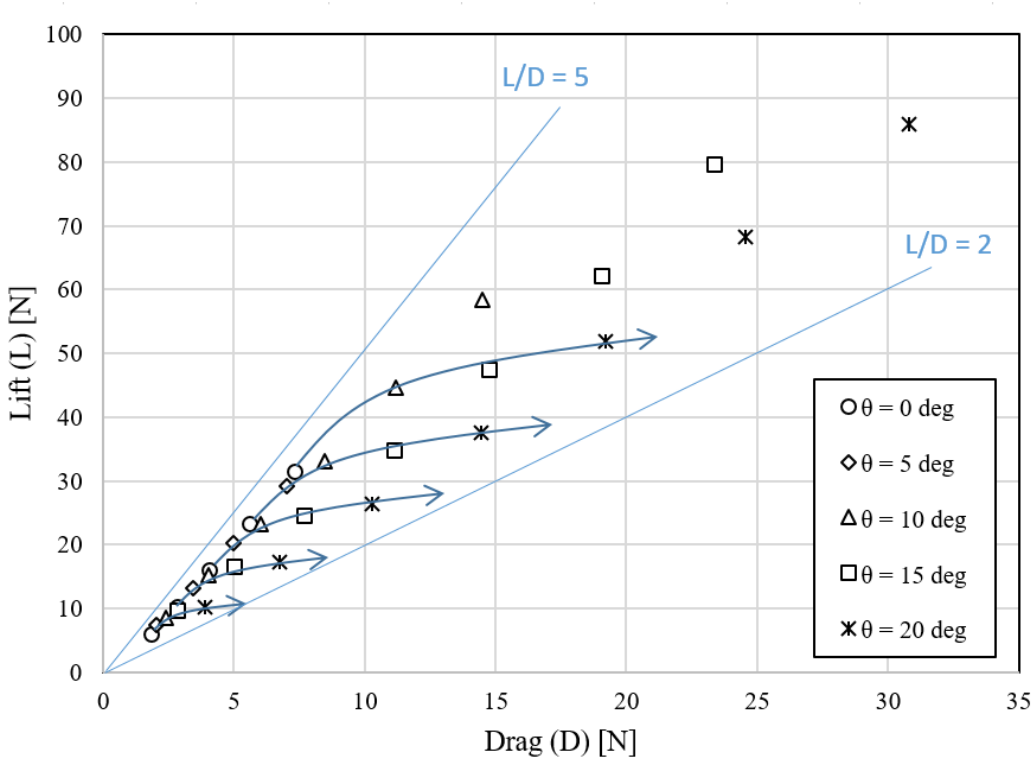

Figure 3.20: Lift-Drag polar for handle pitch angles 0, 5, 10, 15 and 20 degrees. Blue arrows denote the transition of data points at similar wind speeds when increasing pull of brakes.

It has been said that the trends of each handle pitch angle in Figure 3.20 are almost linear. For a better insight into the development of L/D with dynamic pressure Figure 3.21 is presented. It has been previously commented that L/D increases with dynamic pressure for the majority of Runs. Here, the difference between handle pitch angles can be seen as well as the general trend for each Run.

The data in this plot can be splitted into three groups:

- θ = -10 deg. It is the singular case of the negative handle pitch angle. L/D increases, but there is little information about higher wind speeds.
- θ = 0, 5, 10 deg. L/D increases and stabilises with increased wind speed at L/D values above 4. This is the case studied in Chapter 3.5.2. They are the Runs with highest

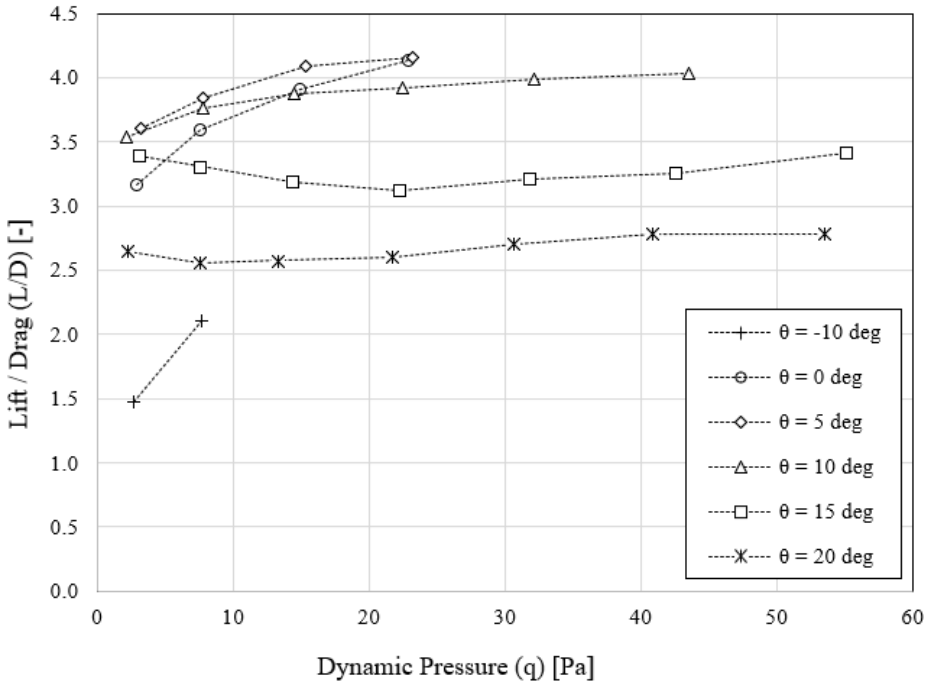

Figure 3.21: Lift over Drag ratio against dynamic pressure for Runs in *SET 01*.

L/D and can be considered the configurations with optimum brake position for the wind tunnel tests. There is however no clue on how the performance develops at higher wind speeds.

- θ = 15, 20 deg. L/D fluctuates around a nearly constant L/D mean value between 2.5 and 3.5. The performance can be defined as insensitive to wind speed, which can be a sign of good effectiveness of the brakes.

3.5.4 Effect of line lateral spacing on kite performance

The last input parameter during the wind tunnel tests has been the spanwise or lateral spacing that the two handle bars had (defined as l). The spacing between lines is a way of varying the spanwise curvature or anhedral of the kite, which is the parameter of interest in the present project. As a reminder, *SET 01* was run at a 61 cm spacing, *SET 02* at 90 cm and *SET 03* at 105 cm. These three Sets are compared for the present discussion.

The first thing to comment is the amount of data points available for each lateral spacing. The 61 cm spacing, the smallest one, allowed to make measurements at higher wind speeds. As mentioned before, an hypothesis is that the kite is too big for the wind tunnel section and

that the wakes create interference with the wind tunnel walls. In addition, the wind tunnel is closed-loop and the turbulence generated by that interaction can spread through the tunnel until it gets again upwind from the kite, further altering the free stream turbulence level. This hypothesis can explain the fact that the Set of tests that had the wing tips further from the walls maintained stable for longer.

Lift and Lift Coefficient

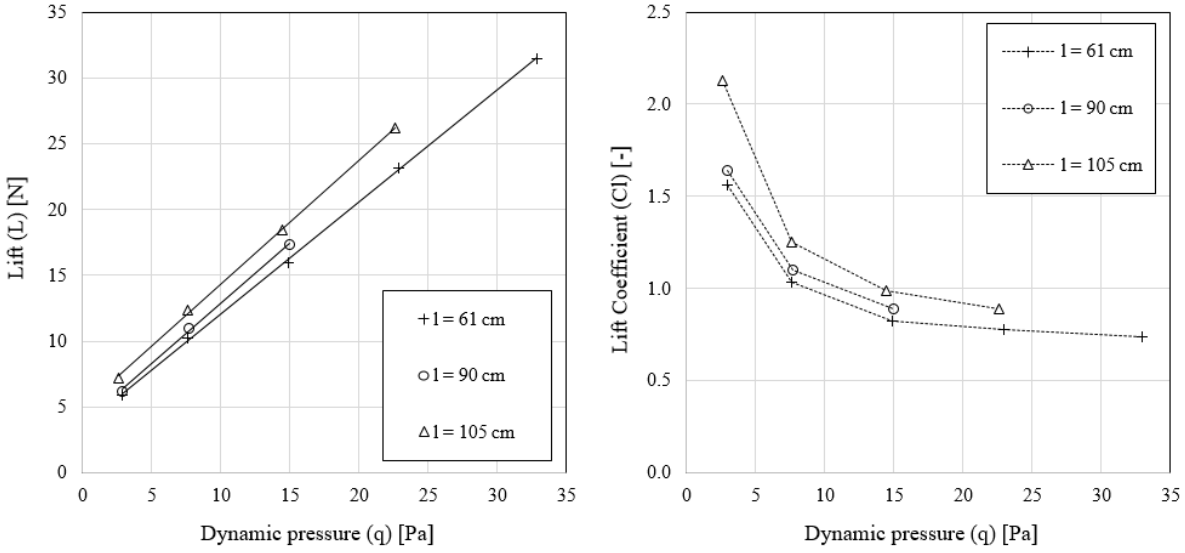

Figure 3.22: Lift and Lift Coefficient against dynamic pressure at $\theta = 0$ degrees for different spanwise spacings (l).

As Figure 3.22 shows, the Lift created by the kite increases as the spanwise spacing increases. This is logical because the lower the anhedral the more horizontal the surface of the wing is. On the other side, the kite with highest anhedral (l = 61 cm) has a smaller horizontal root and more surface pointing sideways.

It is worth to mention that the slopes of the three curves are similar and it is the intercepts that vary. This brings three curves of C_L that converge to a similar value and have different decreasing slopes. However there is no enough data points to ensure that the C_L curves will properly converge.

Other handle pitch angles also give the same trend: similar lift curve slopes and different

intercepts, the highest spanwise spacing having always the highest lift.

Drag and Drag Coefficient

In the case of the Lift, the force is related to the vertical component of the normal forces, so the spanwise curvature is directly involved, but the effect of the spanwise curvature on Drag is less intuitive.

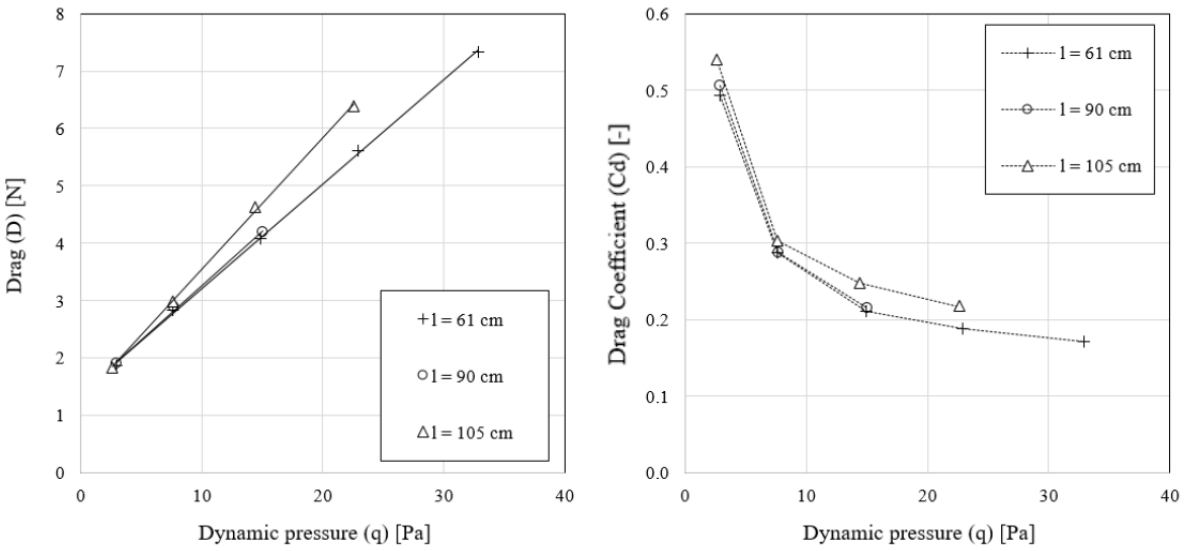

Figure 3.23: Drag and Drag Coefficient against dynamic pressure at $\theta = 0$ degrees for different spanwise spacings (l).

Figure 3.23 is presented to understand the effect of the spanwise curvature on the total Drag. It is seen that l = 61 cm and l = 90 cm have very similar Drag distributions, but that l = 105 cm has a higher slope. Therefore the latter has an extra Drag penalty. The Runs at $\theta = 10$ deg and $\theta = 15$ deg also give higher drag values for l = 105 cm, but with a parallel distribution instead of having a higher slope. A possible source of the extra Drag at l = 105 cm is that the tips are closer to the wind tunnel walls creating a highly turbulent interaction of the wake with the kite. In addition, the smaller anhedral makes the wake vortices to extend closer to the wing and induce a higher downwash. This idea is claimed and theoretically calculated in [63]. According to the paper, the Induced Drag can be written as follows:

$$C_{D_i} = \frac{{C_L}^2}{\pi\, k\, A} \tag{3.11}$$

The expression is equal to the well-known equation of the Induced Drag as a function of Lift, where A is the aspect ratio of the reference planar wing with elliptical lift distribution. Here the efficiency factor k is added to account for the effect of anhedral. The curvature parameters are defined as in Figure 3.24. k is calculated for two particular cases, the circular-arc anhedral and the elliptic anhedral:

$$k = \frac{1 + 0.5\beta^2}{\psi^2} \quad (Circular\ arc) \tag{3.12}$$

$$k = \frac{\beta + 1}{\psi^2} \quad (Elliptic) \tag{3.13}$$

where:

$$\psi = \frac{b}{b'} = \frac{flattened\ span}{curved\ span} \tag{3.14}$$

$$\beta = \frac{d}{b'/2} \quad 0 \leq \beta \leq 1 \tag{3.15}$$

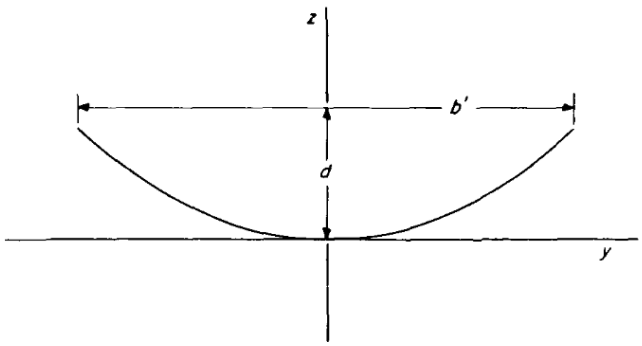

Figure 3.24: Parameters used to define the spanwise curvature of the wing. Source: *The theory of induced lift and minimum induced drag of nonplanar lifting systems (Cone 1962)*

The wing surface used for the calculation of coefficients is the same for the planar and the non-planar wing, which is S. Thus under the same q both wings will generate the same L and D forces if they have the same C_L and C_D, and the two wings can be compared at the same conditions. However, k can change while C_L remains constant, and if $k \geq 1$ for the non-planar wing, the induced drag will be lower than the drag of the equivalent flat wing.

In order to know if what has been seen in the wind tunnel results matches this theory, the equations are computed for the case plotted in Figure 3.23. For that purpose the pictures

taken inside the wind tunnel are used to have an approximate idea of the anhedral of the wing at each spanwise spacing l. Table 3.5 gives the main geometry characteristics of the kite at l = 61 cm and l = 105 cm.

Table 3.5: Main spanwise geometry parameters of the kite at l = 61 cm and l = 105 cm.

spanwise spacing (l)	61 cm	105 cm
curve type	circular arc	ellipse
b	2.08 m	2.08 m
b'	1.44 m	1.85 m
d	0.63 m	0.33 m

Calculations are done introducing the values of Table 3.5 into Equations 3.12 to 3.15. The following values for k are obtained:

$$\psi_{61cm} = 1.44 \quad ; \quad \beta_{61cm} = 0.87 \quad \Rightarrow \quad k_{61cm} = 0.66$$

$$\psi_{105cm} = 1.13 \quad ; \quad \beta_{105cm} = 0.36 \quad \Rightarrow \quad k_{105cm} = 1.07$$

The result of k_{61cm} somehow alters the statement that curved wings have lower Induced Drag. The reason of the $k \leq 1$ is the value of ψ. The induced drag is certainly reduced when ψ is equal to one, i.e., the flattened and the projected span are equal. That is evidently not possible with the kite, and ψ becomes higher than the unit.

The theoretical results neither match the trends seen in the Drag plots, where the l = 105 cm had higher Drag than the l = 61 cm. According to the theoretical method the trend is the opposite ($k_{105cm} \geq k_{61cm}$). Either the method is not accurate, or the change in induced drag is overcome by changes in other Drag components like the pressure or viscous drag.

There is other points that can justify the mismatch. First, the theoretical method comes from a Lifting Line Theory method, where no viscosity, no thickness, no chordwise distributions and no deformations are taken into account. The method is quite far from the reality. Furthermore, the kite deforms when q is increased, so the photos are not representative of all the instants during a Run.

Performance: Lift/Drag

Figure 3.25 accounts for the effect of spanwise spacing l on the Lift / Drag ratio. The general trend is that L/D improves with increased l, however it allows to take less measurements. At $\theta = 0$ deg, the data at l = 105 cm differs from the other two, which can be expected due to the different drag distribution already commented (Figure 3.23).

There is no clear information about the optimal spanwise spacing regarding L/D. The biggest separation, i.e., the lowest anhedral has better performance, but there is no data to see what is the trend all the way up to the flat wing. It needs to be mentioned that the kite is designed to fly closer to l = 61 cm than l = 105 cm. Again, it is noticed that more data is available for l = 61 cm. Apart from the wall interaction, it is possible that the kite is more stable in nature at that spanwise spacing. In that case it would be preferable to fly the kite at l = 61 cm because of it is designed to fly that way.

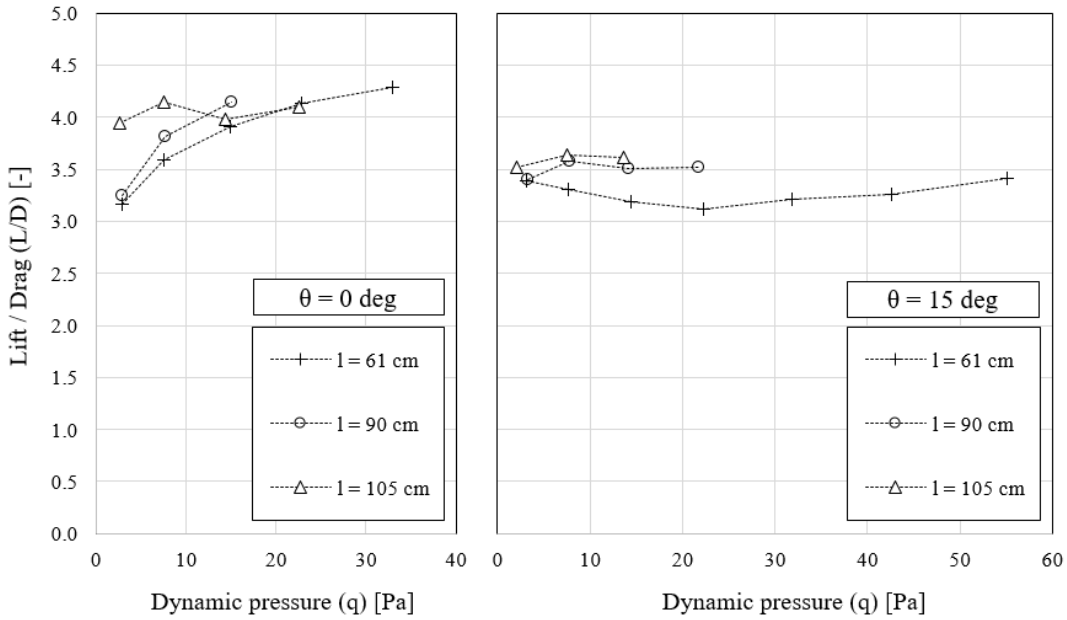

Figure 3.25: Lift / Drag ratio against dynamic pressure at handle pitch angles 0 and 15 degrees for different spanwise spacings.

Another point of view is that the brakes should be designed to reduce the performance. In that sense, it can be said that in the l = 61 cm case the brakes are more effective in doing so. The reduction in L/D caused by increasing θ is more evident in that case than in l = 105

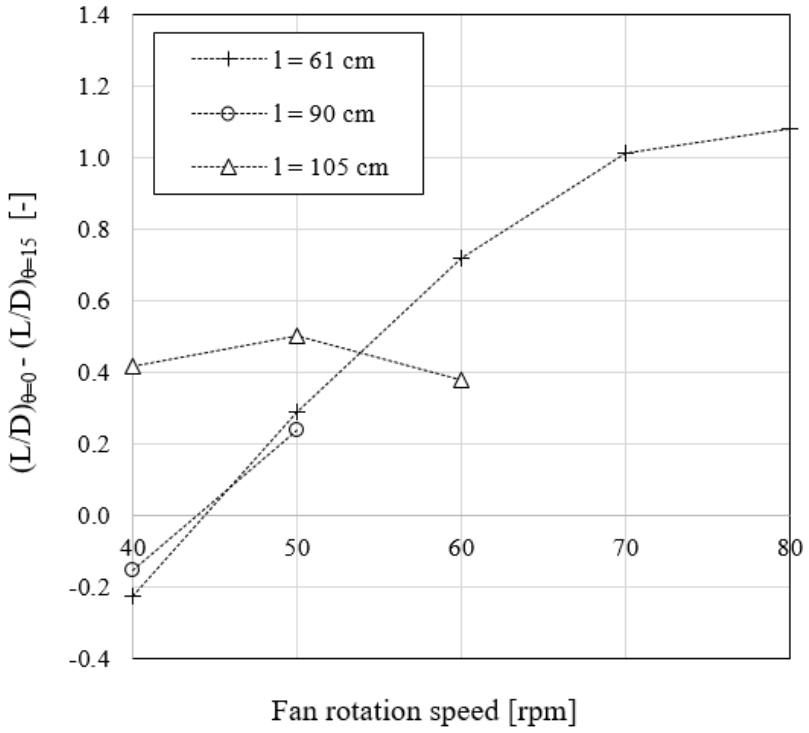

Figure 3.26: Drop in L/D due to the pull of brakes from $\theta = 0$ deg to $\theta = 15$ deg. Comparison between different spanwise spacings l.

cm. Figure 3.26 presents the drop in L/D that pulling the brakes from $\theta = 0$ deg to $\theta = 15$ deg means. Here, for the sake of simplicity, the same rpm-s have been matched instead of the same velocities. The error in that assumption can be considered small. The plot confirms that the drop in L/D due to a pull of brakes reaches higher values when l = 61 cm than when l = 90 cm and l = 105 cm. The difference lies on two factors. First, the slope is always positive, which is not satisfied in l = 105 cm. Second, the measurements last longer, which lets the drop in L/D to grow more. There is no clue of what the evolution of l = 90 cm would be at higher wind speeds.

3.5.5 No-brakes case: full inflation

The only configuration that allowed a proper inflation of the kite was the θ = -10 degrees. Instead of inflating from the beginning, however, it needed certain amount of dynamic pressure. Run 052 was tested from 40 rpm to 60 rpm, where the kite fully inflated and directly destabilised. Once inflated, the wind speed was decreased to see if the full-inflated geometry could be maintained stable at lower wind speeds. The kite remained inflated, but it showed to

be more unstable than with brakes. Records were taken only for 40 rpm and 50 rpm. These values are now compared to the data of same configuration and wind speed but with brakes applied.

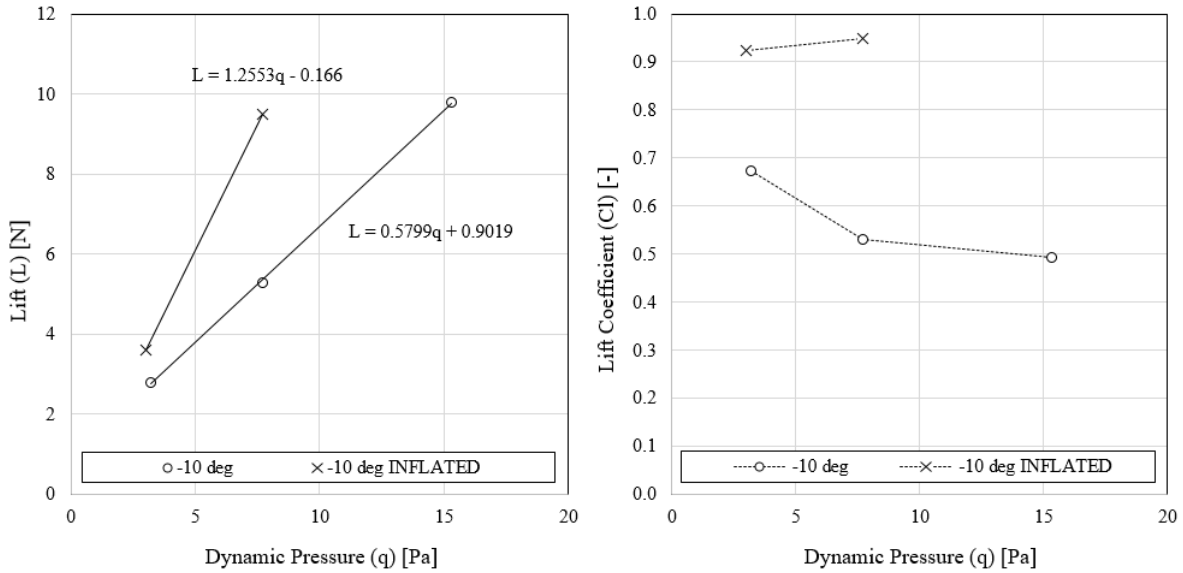

Figure 3.27: Lift force against dynamic pressure (left) and Lift Coefficient against dynamic pressure (right) for Run 052. Comparison between the fully inflated flight and the flight with brakes.

Figure 3.27 is a comparison between the two scenarios regarding the Lift force and the Lift Coefficient. The main difference is that the fully inflated case has higher L and C_L values. That makes sense because the kite is flying at its optimum, aerofoil-shaped geometry. Note that the intercept in the fully inflated case is also smaller in magnitude. That makes the C_L distribution more stable. There is now less deformation as wind speed increases because the kite is fully inflated from the beginning. It is concluded that the kite is closer to a rigid wing, which is the aim of the ram-air kite when it is inflated. Even more, the slightly increasing C_L can be due to the increase in angle of attack of the kite (attitude always increases with q, and attitude is directly related to AoA).

Drag and Pitching Moment plots have also smaller intercepts, i.e., the kite is closer to a wing with a fully developed, constant geometry.

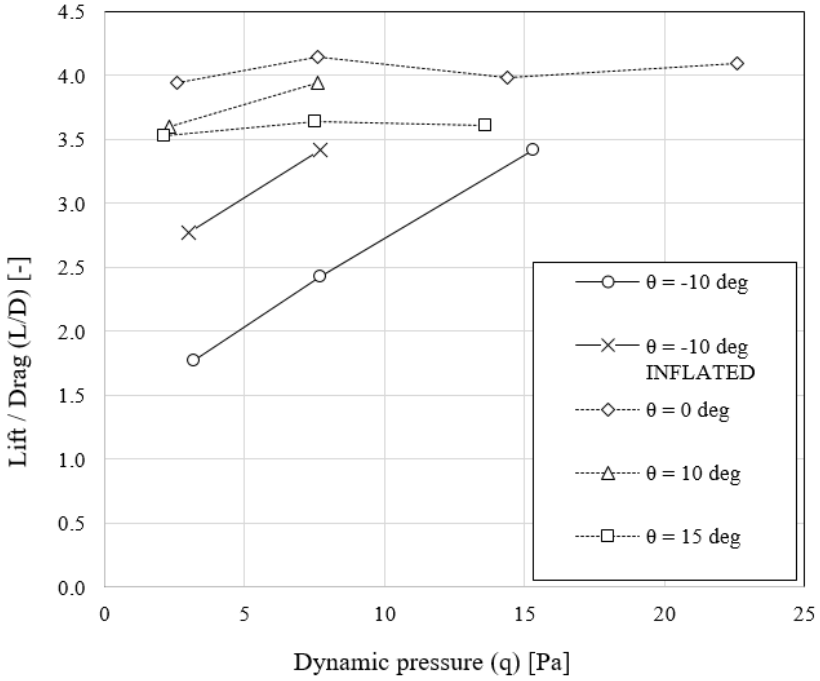

Figure 3.28: L/D ratio against dynamic pressure for a variety of Runs at spanwise spacing = 105 cm.

According to the performance, the L/D ratio also improves when the kite has been fully inflated. Figure 3.28 shows that L/D value increases a unit but still maintains the same trend. The increase is not enough to overcome the L/D values at handle pitch angles 0, 10 and 15 degrees, but it presents a considerable improvement when compared to the same flight condition with brakes.

All in all, there is little data available to get firm conclusions. Further work is needed to test a stable flight while the kite is fully inflated.

3.5.6 Repeatability

Some tests were run twice to check the repeatability of the experimental setup. It is the case of l = 105 cm at θ = -10, 0 and 10 degrees.

Lift Coefficient for the repeated Runs is plotted in Figure 3.29. The high values of C_L have already been described as non-reliable in previous analyses. This plot further suggests that

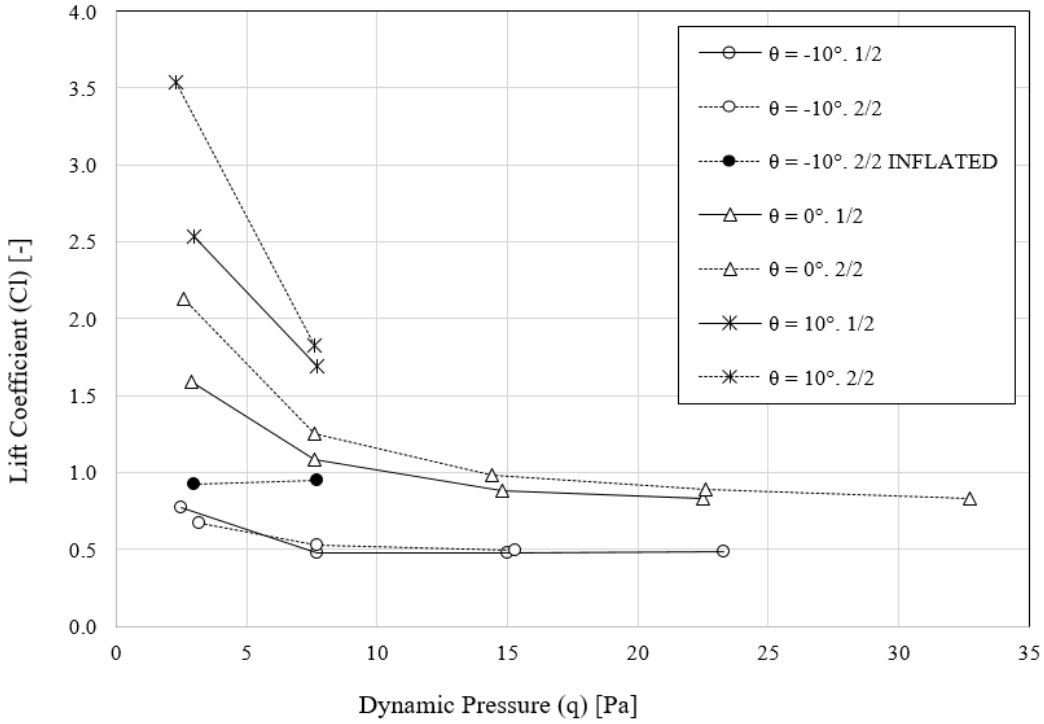

Figure 3.29: Lift Coefficient against dynamic pressure at handle pitch angles -10, 0 and 10 degrees. Assessment of repeatability.

these points are the less repeatable of all the data, somehow confirming that the values are less reliable. At higher wind speeds the difference from Run to Run decreases, but there is still a small error. That error is also smaller at θ = -10 degrees, and increases as θ increases.

The variance in the L/D distribution is plotted in Figure 3.30. The second set of measurements (2/2) has higher values at every data point, but the distributions are similar.
Regarding the numbers, the errors in C_L, C_D and L/D from one Run to the other are given in Table 3.6. They are presented as the difference in percentage relative to the first set of Runs (δ). The rpm-s are matched instead of the exact wind speed for simplicity. As can be seen, the major errors happen at 40 rpm, the lowest speed tested. The error tends to decrease at higher wind speeds. Overall, the difference from Run to Run at the same conditions can be small for some cases (δ = 1-3 %) and quite high for other cases (δ = 10-40 %). It can be concluded that the deformation is a major factor in the repeatability of the tests, because better inflated (higher speed) tests tend to be more repeatable. For repeatable tests it is of interest that the kite has a fixed geometry, which is managed when it is well inflated.

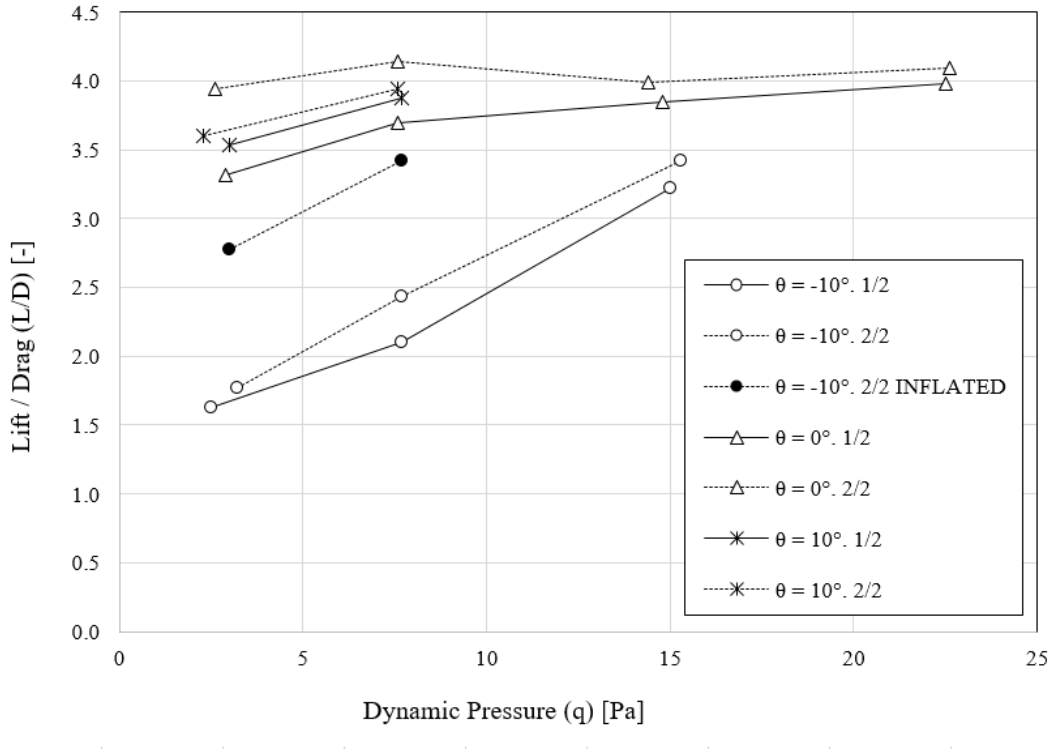

Figure 3.30: L/D ratio against dynamic pressure at handle pitch angles -10, 0 and 10 degrees. Assessment of repeatability.

Table 3.6: Errors generated from repeated tests for C_L, C_D and L/D at θ = -10, 0 and 10 degrees. l = 105 cm. $\delta = \frac{X_{1/2} - X_{2/2}}{X_{1/2}} * 100$

Fan rotation speed [rpm]		40	50	60	70
θ = -10°	δC_L [%]	-12.5	10.4	3.3	
	δC_D [%]	-19.2	-4.4	-2.6	
	δ(L/D) [%]	8.3	15.5	6.1	
θ = 0°	δC_L [%]	33.9	15.9	11.9	7.4
	δC_D [%]	12.8	3.5	8.1	4.4
	δ(L/D) [%]	18.7	12	3.5	2.9
θ = 10°	δC_L [%]	39.7	7.9		
	δC_D [%]	37.3	6.1		
	δ(L/D) [%]	1.8	1.7		

3.5.7 Asymmetric flight

The kite used in AWE technologies is typically flying crosswind in "8" shaped patterns. Thus good lateral and directional manoeuvrability is important. During the wind tunnel tests some extra Runs have been done to simulate a turning kite. This is achieved by warping the wing through an asymmetric control input, as Wright Brothers did with their first kite-glider (Chapter 2.2.4). In the case of the present experimental setup, the parameter that has been varied is the handle pitch angle θ. The Runs undertaken are given in Figure 3.31 as a function of the left and right handle angles.

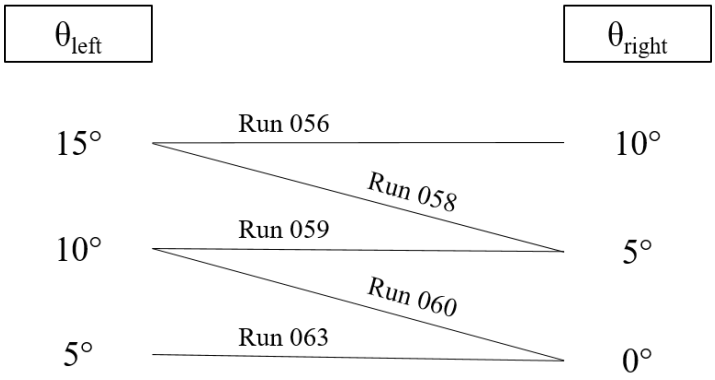

Figure 3.31: Asymmetric test plan. Handle pitch angles from 0 to 15 degrees have been tested, with steps of 5 and 10 degrees of difference between left and right handle (looking upwind from the kite). In total 5 Runs were done with their respective tare-correction measurements. l = 105 cm.

The asymmetric flight differs from the previous tests in the fact that Sideforce (Fy), Roll Moment (Mx) and Yaw Moment (Mz) are not necessarily equal to zero. During the symmetric flight these values remained below or close to 1N (or 1Nm), which were considered to be zero. Once the asymmetric tests were carried out, it was seen that Fy, Mx and Mz did not vary a lot. Their values were still below the Newton, which does not allow to do a proper study. There is neither a clear trend with increasing θ, or any pattern to distinguish the 5-deg θ difference from the 10-deg θ difference.

In any case, the results are plotted in Figure 3.32. The fastest rise in Sideforce happens at θ: left 15 deg, right 10 deg and at θ: left 15 deg, right 5 deg. However, the symmetric flight reaches similar and higher values, even if at higher wind speeds. These values were considered

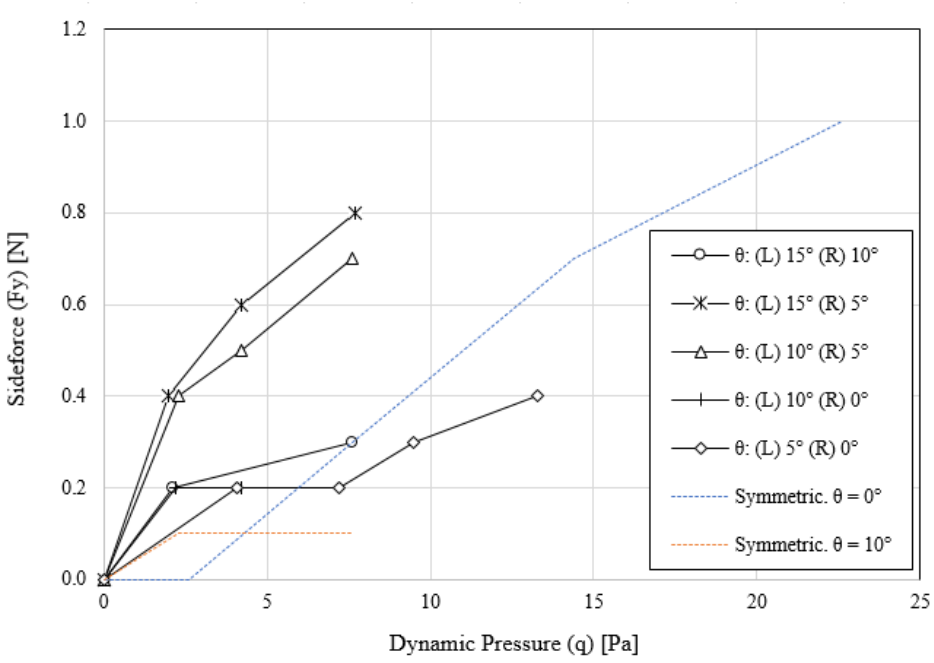

Figure 3.32: Sidforce against dynamic pressure for all the asymmetric configurations and the equivalent data from $\theta = 0$, 10 degree symmetric flights. l = 105 cm.

null during the main tests as they must come from the mean value of the fluctuations, even if small. Note that the Sideforces are very low, always lower than 1N. There is therefore no clear sign that the Sideforce values of the asymmetric tests do not have the same origin. The values are too low to build a discussion on them.

Rolling Moment and Yawing Moment plots give similar results (Figure 3.33). The moments in the symmetric flight are of the same order than in the asymmetric flight.

A possible reason for the lack of asymmetric loads is the spanwise spacing l = 105 cm. The rest of spanwise spacings have not been tested. This is considered important for future work if asymmetric loads are to be tested. As until now the spanwise spacing that allowed most measurements is l = 61 cm, it is recommended that at least this position is studied.

Higher differences between the left and right handle pitch angles were also not tested. It is of interest to extend the set of asymmetric tests in this sense because one reason for the low loads could be the little difference between the handle angles.

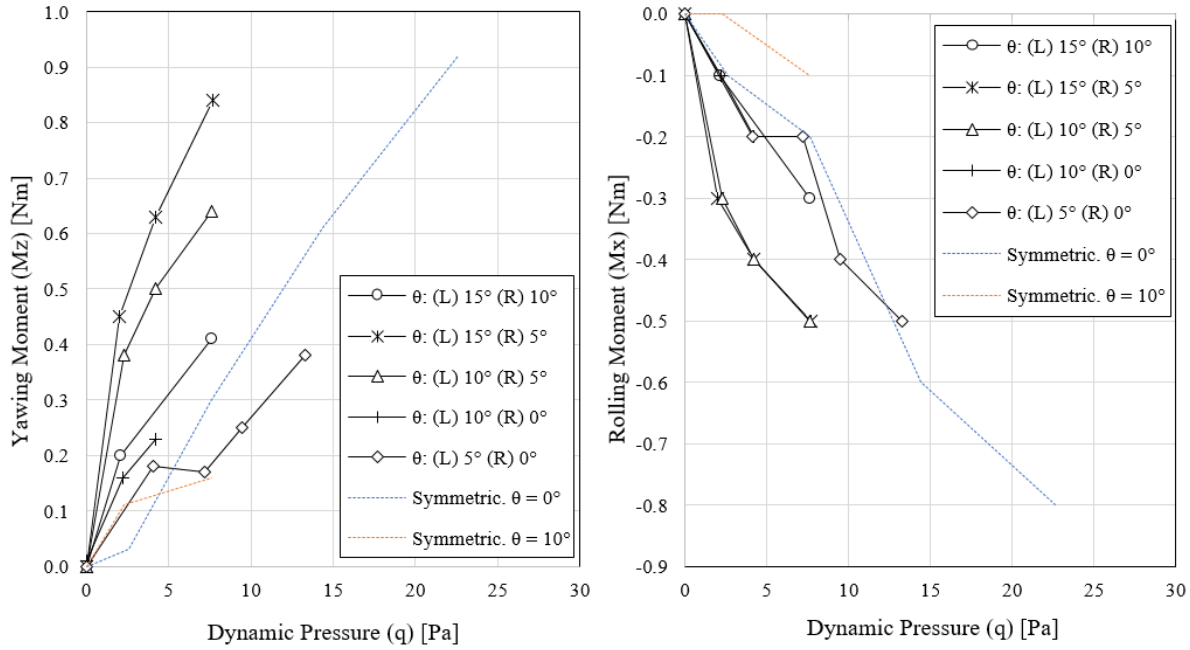

Figure 3.33: Rolling and Yawing Moment against dynamic pressure for all the asymmetric configurations and the equivalent data from $\theta = 0$, 10 degree symmetric flights. l = 105 cm.

Chapter 4

Numerical approach

It is of interest to compare the experimental results from the wind tunnel tests with theoretical results of a similar simulated environment. That way, if the numerical approach is validated with the experiments it can be used for a preliminary design optimisation process. In this chapter analytical tests are undertaken and the similarities and differences with the wind tunnel tests are discussed.

4.1 Choice of an analytical method

In the case of fully flexible kites the ideal approach is the Fluid Structure Interaction (FSI) problem. This method is introduced in the Literature Review (Chapter 2.4) as a way of taking into account the interaction between the aerodynamic loads and the deformation of the object. Apart from the aerodynamic calculations a structural model is used (FEM), which gives the relation between the aerodynamic loads (input) and the consequent displacements of the solid (output). This output is introduced into the aerodynamic model which gives new aerodynamic loads with the displaced solid. The process is continued iteratively until the loads and displacements stabilise.

However, a complete FSI study is out of the scope of this project. The main part of the project is the experimental approach, and the aim of the analytical part is only to give preliminary results of a simplified version of the experimental problem. The implementation of a FSI problem was considered too time consuming and it is preferred that a hole future project focuses in that area, including a more comprehensive research on the topic. A good

introduction to the FSI method, as mentioned in the literature, is [36].

The effect of deformation is therefore discarded in the present study and left for future work. Rather, a rigid model is analysed. There will be an error in the analysis, but it will be simpler. The problem is now more similar to the one of conventional, rigid aeroplanes, so the availability of analytical methods increases. The main choices are already discussed in the Literature Review (Chapter 2.5.2), and range from the simplest Lifting Line Theory (LLT) to the higher-fidelity RANS simulations (CFD).

A CFD analysis is also considered to be out of the scope of this project, since it is preferred that a separate project focuses on this area. A CFD study would be too time consuming and at the same time could be a rushed approach taking into account that a FSI method is not implemented. The CFD with a rigid model could be an over-complicated method that still does not give accurate results.

Potential Methods are considered to fit better into the project. They are fast and valid for a preliminary insight of the problem. It is true that the results are not likely to be close to the experiments. However, it can be useful for a parametric study of factors such as: spanwise camber (anhedral), wind speed and aspect ratio. These parameters can be then compared with the experimental results to find any matches in trends.

In order to choose the Potential Method that best fits the kite problem, first the characteristics of the tested geometry are given:

- The wing has a low aspect ratio. $AR = \frac{b^2}{S} = 3.33$.
- It is fully made of non-rigid material. It is highly deformable.
- The spanwise curvature is high. It shows both circular-arc and elliptical anhedrals.
- The kite has a relatively high thickness to chord ratio. $t/c_{rib,root} = 15\%$, but due to ballooning it is higher at the cell centers.
- There is a relatively high separated area, around the LE intakes and along the ribs (according to [41]).

The Potential Method should cover as much of these characteristics. The deformation has

already been discarded, so all the methods that are now presented take the wing as a rigid body. These are the possibilities considered by the author:

- LLT modified for low AR and anhedral [64]. Not considered: elasticity, thickness, viscous effects, chordwise distributions.
- VLM. Not considered: elasticity, thickness, viscous effects. But according to [36] corrections can be done to account for the thickness and viscosity.
- Panel Method with panels along the upper and lower surfaces. Not considered: elasticity and viscous effects. But [36] and [57] develop a Multiple-Wake Panel Method that accounts for the separation and reattachment problem.

From the previous list, VLM (with thickness correction) or Panel Methods are preferred since they cover more of the singular characteristics of the ram-air kite. The following have been chosen as the main options for the practical implementation of the analytical approach:

- Multi-Wake Panel Method by [36] and [57].
- *PANAIR* free software: A high-order Panel Method for arbitrary geometries.
- *FlightStream* commercial software: A surface vorticity solver for arbitrary input geometries with an additional viscous calculator.
- A panel method from scratch using the code in [58] (*Matlab* code).

After considering these options, the software *FlightStream* has been chosen as it is the most complete. Any other choices listed above can be implemented but they are more time consuming and do not take into account the viscosity of the fluid (with exception of the separation by Multi-Wake Panel Method). The details of the program are given in the following chapter.

4.1.1 *FlightStream* software

FlightStream is developed by the US company *Research In Flight*. It is a Potential Flow solver that computes the vorticity along the surface of a finite-thickness 3D object. As the method is vorticity-based instead of pressure-based, the mesh is less sensitive to the fidelity or perturbations of the as well as to the mesh refinement [65]. The mesh in *FlightStream* is unstructured, it is built from triangular elements that are then converted into quadrilaterals when possible. A powerful characteristic of the software is that it has a flow separation calculator and a

viscous drag calculator by means of the Reynold number. This locates *FlightStream* between typical potential methods and CFD methods.

The program allows an arbitrary geometry input, which helps a lot in the case of the unconventional kite shape. It can be a CAD model, which will then be meshed inside *FlightStream*, or can be directly inputted as a meshed object. The latter has been preferred because of the good compatibility of the program with *OpenVSP*, an open source software designed by the NASA to build a large variety of geometries used in the aerospace industry. As a simple geometry of the kite could be developed in *OpenVSP*, the software was chosen to create a set of geometry inputs. Other geomerty inputs have also been tested using *CATIA*, but the simplicity that the compatibility between *OpenVSP* and *FlightStream* supposed made that choice preferable.

4.2 Methodology

4.2.1 Test plan

As it has been said, it is not expected to find similar results to the experimental. However, some parameters can be isolated and studied independently inside the analytical approach. The following parameters have been assessed:

- STUDY 1: The effect of increased anhedral. For this study the same model of kite has been modified to several anhedral angles. A set of wings with different anhedral have been built in *OpenVSP*.
- STUDY 2: The effect of aspect ratio (AR) and taper ratio on models of high anhedral.

Then, it has been possible to compare the trends of the effect of increased anhedral (STUDY 1) with experimental results.

In addition, a fast mesh-independency test has been done to prove the statement that the results in *FlightStream* are not as dependent on the grid refinement level (as a CFD would be, for example).

4.2.2 Geometry input

Two different kite models have been built in *OpenVSP*. A description of each model and their variants is given now, as well as an explanation of which model corresponds to which STUDY.

Wing v1

This is the first and most simplistic kite modelled for STUDY 1 and STUDY 2. It is a planar wing built with Clark-Y aerofoil shapes at the root and the tips. This is the aerofoil shape most widely used in ram-air kites, and it has been preferred to use this as a standard for all the analytical studies than the not-so-well known aerofoil shape of the kite used in the wind tunnel tests. The Clark-Y aerofoil used in all the analytical studies has a maximum thickness-to-chord ratio of 11.7% at 28% of the chord [66]. In the case of this kite model (*Wing v1*), the thickness of the wing is constant along the span, and has no taper, sweep or twist.

Table 4.1 gives the main geometry characteristics of the original wing (v1.1) as well as the variants of different anhedral (v1.2-v1.7). The anhedral angle is defined as the angle that the wing would have if it had a straight anhedral instead of an arched one.

The tests made with these models are part of the scope of STUDY 1.

Table 4.1: Main geometry characteristics of wings v1.1 to v1.7. Anhedral variations of the original wing v1.

	Wing area [m]	Projected span [m]	AR [-]	Root chord [m]	Taper ratio [-]	ANHEDRAL [deg]	Chordwise tesselation	Spanwise tesselation
v1.1	1.2	1.50	1.88	0.8	1	0	61	35
v1.2	”	1.49	1.86	”	”	5	”	”
v1.3	”	1.48	1.82	”	”	10	”	”
v1.4	”	1.45	1.75	”	”	15	”	”
v1.5	”	1.41	1.66	”	”	20	”	”
v1.6	”	1.36	1.54	”	”	25	”	”
v1.7	”	1.30	1.41	”	”	30	”	”

Table 4.2 presents four extra variants with increased AR, two for v1.1 and two for v1.7. These models serve as part of STUDY 2.

Table 4.2: Main geometry characteristics of wings v1.1 and v1.7 with AR variations.

	Wing area [m2]	Projected span [m]	AR [-]	Root chord [m]	Taper ratio [-]	ANHEDRAL [deg]	Chordwise tesselation	Spanwise tesselation
v1.1	1.2	1.50	1.88	0.8	1	0	61	35
v1.1_ARx2	2.4	3.00	3.75	”	”	”	”	”
v1.1_ARx4	4.8	6.00	7.50	”	”	”	”	”
v1.7	1.2	1.30	1.41	0.8	1	30	61	35
v1.7_ARx2	2.4	2.60	2.81	”	”	”	”	”
v1.7_ARx4	4.8	5.20	5.63	”	”	”	”	”

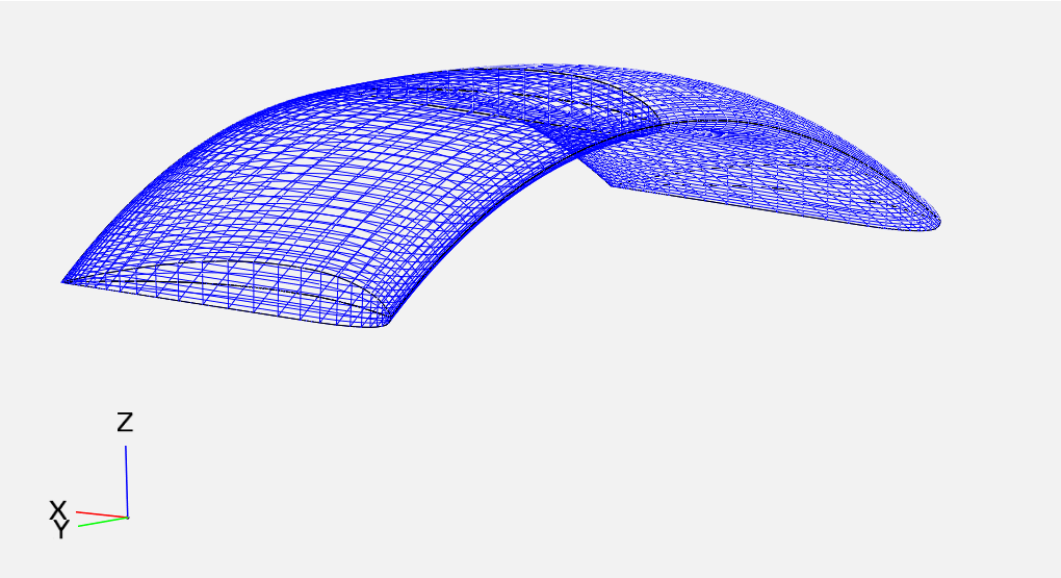

Figure 4.1: *OpenVSP* kite wing v1.5 (anhedral 20 deg).

Wing v2

The second kite model has a higher fidelity to the kite tested in the wind tunnel. The aerofoil is still Clark-Y, but the span, chord at the root, taper ratio and planview shape have been matched closer. The thickness-to-chord ratio of the aerofoil has been maintained constant, so the tips, which now have smaller chord, have a smaller thickness too. The wing area and AR are also closer to the real kite. Some variations have been done to the anhedral of the wing for STUDY 1.

Table 4.3 shows the main characteristics of the original wing (v2.1) and its variants.

Table 4.3: Main geometry characteristics of wings v2.1 to v2.4. Anhedral variations of the original wing.

	Wing area [m2]	Projected span [m]	AR [-]	Root chord [m]	Taper ratio [-]	ANHEDRAL [deg]	Chordwise tesselation	Spanwise tesselation
v2.1	1.33	2.08	3.92	0.78	0.36	0	61	20
v2.2	”	2.05	3.80	”	”	10	”	”
v2.3	”	1.95	3.46	”	”	20	”	”
v2.4	”	1.80	2.94	”	”	30	”	”

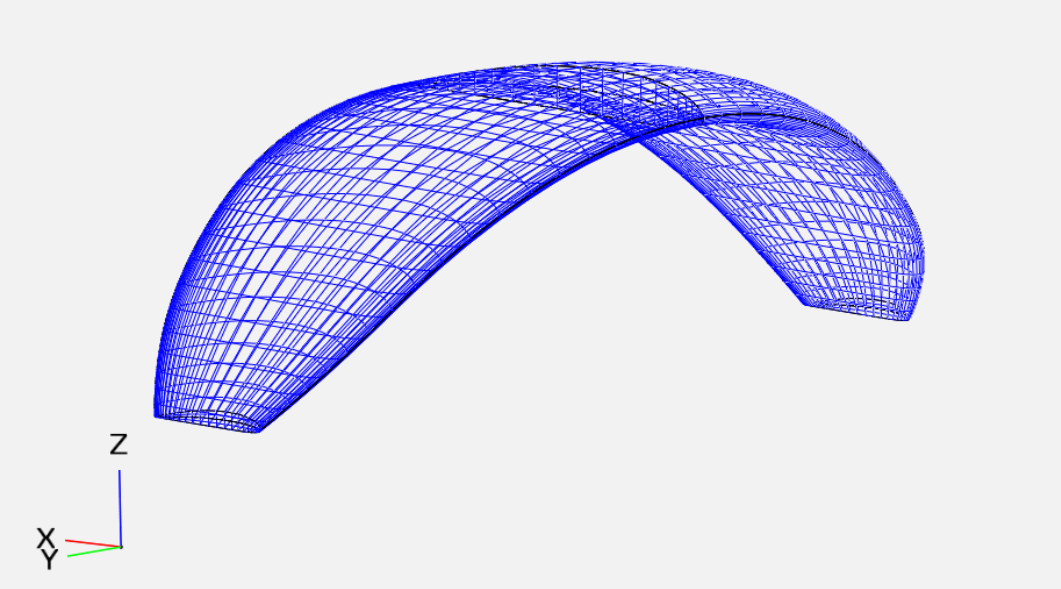

Figure 4.2: *OpenVSP* kite wing v2.4 (anhedral 30 deg).

Mesh Independency Study

The mesh in *OpenVSP* is built in quadrilaterals. The total number of cells is divided into the spanwise tesselation and the chordwise tesselation, i.e., the number of cells. In order to know the optimal tesselation a mesh independency study has been done in *FlightStream*. The process of getting the results is explained in the next section.

For the mesh independency test four different tesselations have been created. Table 4.4 gives the details about the different versions of the same model (v2.1).

Table 4.4: Chordwise and spanwise tesselation used for the mesh independency study. All the models are built from the wing v2.1.

Version of v2.1	chordwise tess.	spanwise tess.	total num. of cells
1	33	10	330
2	41	10	410
3	41	20	820
4	61	20	1220
5	61	35	2135
6	73	35	2555

It can be seen that the chordwise and the spanwise tesselations have been increased alternatively to capture any difference in the results due to an isolated increase of tesselation in a single direction. The chordwise tesselation was suggested by the program developer not to exceed the amount of 70. The spanwise, on the other hand, was maintained lower than 35 because these models showed a drastic increase in computation time. As *FlightStream* computes a relaxed wake for every spanwise node, it can be that the increase of spanwise nodes makes the computation heavier than the increase of chordwise nodes. Therefore the finest mesh was set to 73x35 tesselation, and the coarsest to 33x10.

Figure 4.3 presents the variation (drop) in C_L and C_D that the increase of total number of cells mean. The coarsest mesh is used as reference for the calculation of the relative errors. It is seen that the relative error from mesh to mesh decreases and the curves stabilise. But this is more evident in the C_D plot than in the C_L one. Note also that the data points of the finest mesh move off the converging trend. It has to be said that this mesh presented convergence problems in *Flightstream*, possibly because of the high chordwise tesselation (higher than 70). Thus the finest mesh is discarded for the calculations and finer meshes are considered invalid. The level of refinement used for the calculations has been the previous finest mesh, i.e., the 61x35 tesselation mesh. For some cases the 61x20 mesh has been preferred because of the high computation cost of the 35 spanwise tesselation. Note the small relative error between 61x20 and 61x35 and the high reduction in number of cells.

Once the geometries are built with the corresponding tesselation, they are remeshed and the quadrilaterals are splitted into triangles by diagonal edges. Then the final mesh is exported

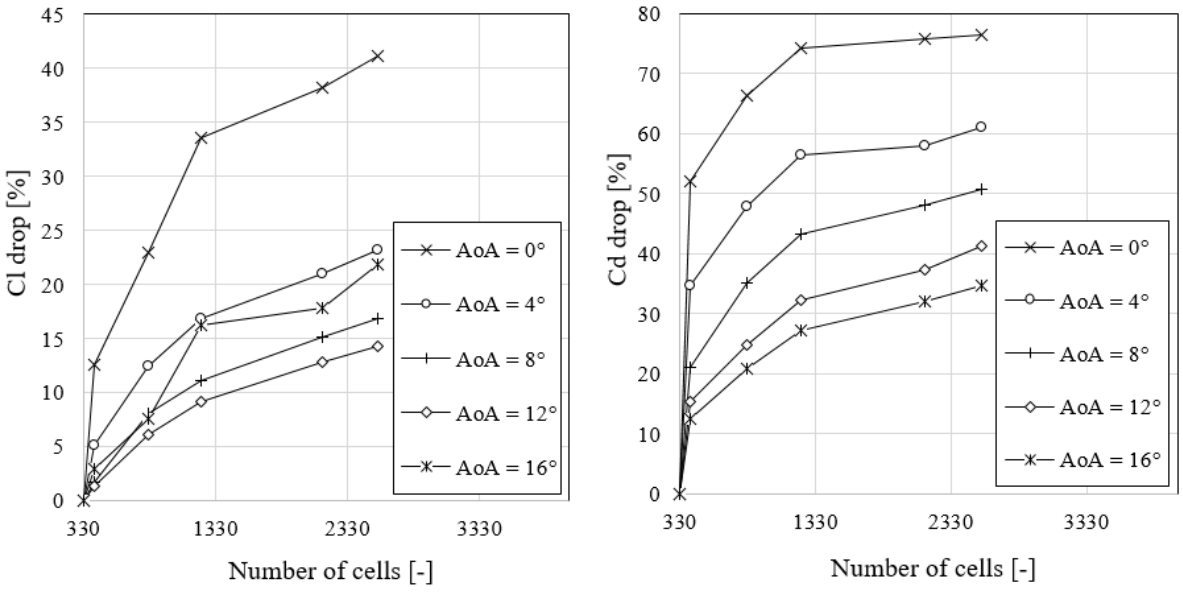

Figure 4.3: Cl and Cd drops (%) against number of cells (spanwise x chordwise) at different angles of attack. All are versions of the same wing, v2.1.

with the file extension *Stereolith* (.stl), which is a compatible input format of *FlightStream*.

4.2.3 *FlightStream* setup

Imported under the *Stereolith* (.stl) file extension, the geometry in *FlightStream* is already meshed in triangular cells. Then, the program needs to know the location of the trailing edge, which is selected and marked by the user.

FlightStream allows slight modifications to the mesh. The most useful tools have been found to be: split a surface into several with user-defined boundaries, swap the diagonal edges that divide the quadrilaterals and invert the cell normals in case they are inverted.

FlightStream has an option to run the calculations for a range of angles of attack, sideslip angles and wind speeds. The wing v1 has been tested for a variety of AoA and wind speeds, so a matrix of runs has been done with these two variables. The AoA has ranged from 0 to 22 degrees with a 2 degree step. The wind speed has ranged from 1 to 11 m/s with a step of 2 m/s, which is similar to the range of the wind tunnel tests. For a further analysis of the effect of wind speed on the aerodynamic coefficients, tests ranging from 20 to 50 m/s have

been undertaken with a 10 m/s step. The effect of wind speed was seen to be negligible on the coefficients, as would be expected from a rigid wing. Therefore the wing v2 has been tested for a single wind speed, 10 m/s. The AoA range has also been reduced, now from 0 to 16 degrees with a 2 degree step.

The coefficients were calculated with a reference wing area equal to 1.2 m^2 for wing v1 and equal to 1.34 m^2 for wing v2. Those are the wing areas with the kite flattened (0 anhedral). The projected area decreases when anhedral is increased, but it has been preferred to use the same reference area for a better comparison. The flow is treated as incompressible, as it is evident at such low wind speeds. The convergence threshold for the residuals has been set to 1e-4.

4.2.4 *FlightStream* output

The output is given as CL, CDi, CDo and CM. The sum of the two drag coefficients gives the total drag coefficient ($CDi + CDo = CD$). CDi is called "induced drag", but it is not representative of the lift-induced drag. It is rather the summation of all the inviscid drag components + the drag coming from flow separation. Here it is called "pressure drag". CDo, on the other hand, is the skin friction drag. CL and CM are lift and pitching moment coefficients respectively.

The coefficients can be outputted into a .txt extension file. The consequent post-processing of the data is easily done in *Excel*.

4.3 Results and Discussion

4.3.1 STUDY 1: The effect of anhedral

The change in CL induced by an increased anhedral in shown in Figure 4.4. Here, the wing with 30 degrees anhedral has a lower curve slope and a smaller intercept. Thus a higher angle of attack is needed if the same lift is to be generated. The trend matches the fact that a planar wing has all of its surface in the horizontal plane, thus creating the aerodynamic forces in the vertical plane. The wing with anhedral, on the other hand, creates forces out of the vertical plane that in the sense of generating lift are also effective with their vertical

component. The root will be the area with highest lift coefficient, while the tips will generate a combination of lift and side force. The side forces are cancelled because of the symmetry.

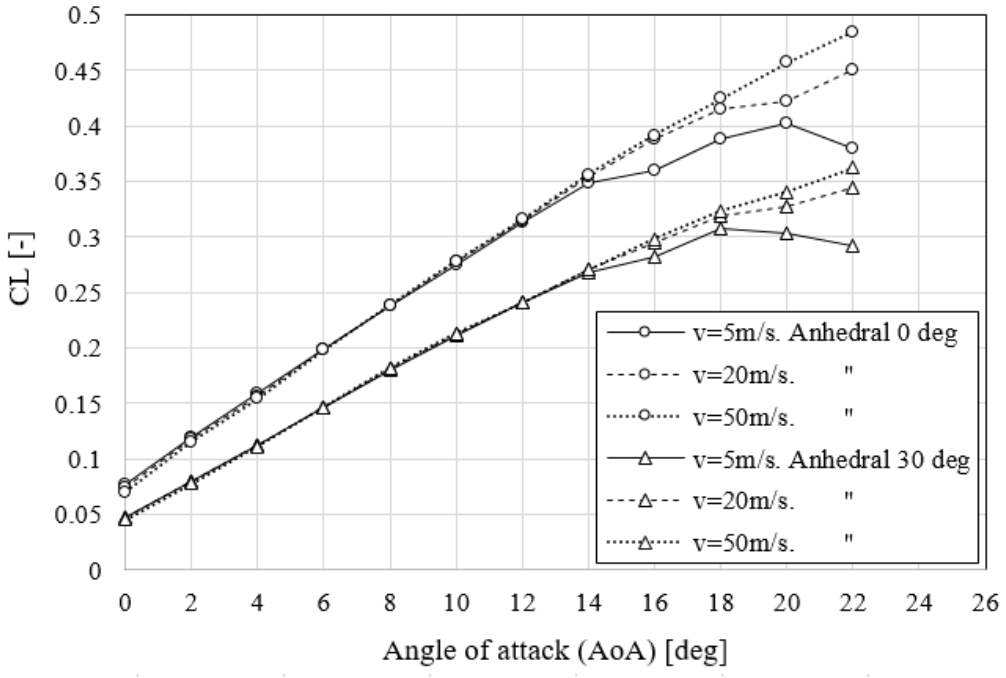

Figure 4.4: CL against angle of attack for two versions of wing v1: a 0-deg anhedral and a 30-deg anhedral. Both wings are presented at 5, 20 and 50 m/s.

There is an extra effect recognisable in Figure 4.4. It is the wind speed. As during the wind tunnel tests the lift and drag coefficients were highly dependant on the wind speed, it was considered interesting to check that this effect was due to the deformation that the wing suffered with increased wind speed. The plot confirms that there is little effect of the wind speed on the coefficients at angles of attack lower than 14 degrees. The highest angles of attack show differences due to a different flow separation scenario. The higher Reynolds number at 50 m/s makes the flow to suffer stall later than the 5 m/s case. This is a well known phenomenon, however no special features have been seen due to the anhedral: the non-linear region of the plot starts at 14 degrees for both planar and non-planar wings.

Figure 4.5 presents the drag coefficient against angle of attack. The wind speed has a higher effect on the 0-deg anhedral wing. It can be due to a higher effect of the reduced separation area, or it can be due to computational errors. However the highest difference is seen between the planar wing and the high anhedral wing. Clearly the anhedral reduces the CD consider-

ably. It can be due to a reduction in induced drag as it is claimed in [63], but the magnitude of this drag has not been possible to isolate from the rest of the drag components. It can also be that the 30-deg anhedral wing does not show such an increase in angle of attack at the areas closer to the tips. Thus the form drag could be smaller than in the planar wing.

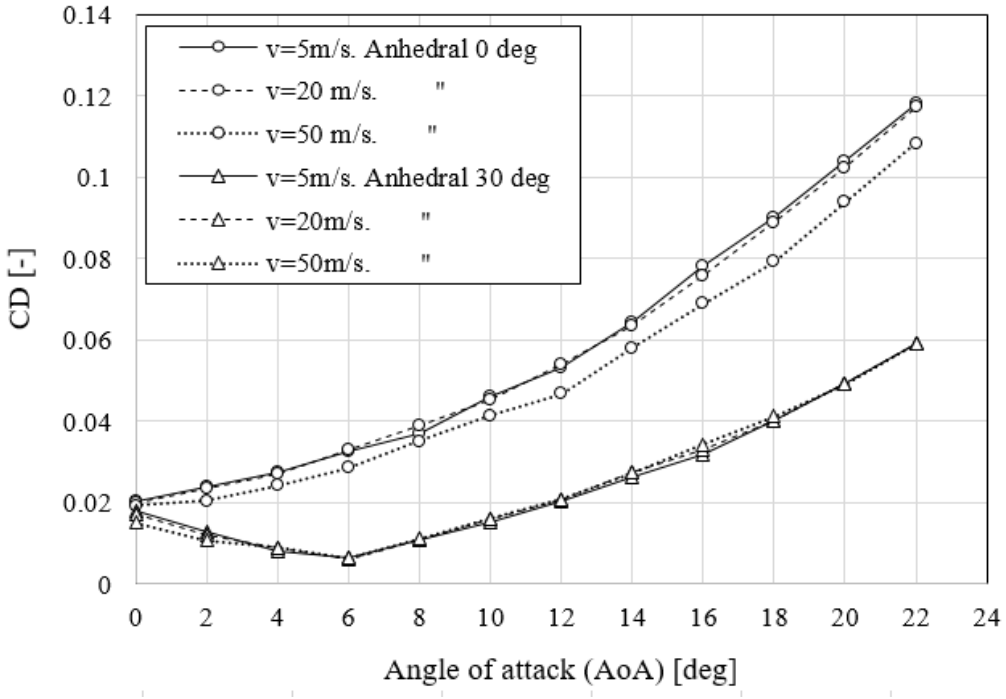

Figure 4.5: CD against angle of attack for two versions of wing v1: a 0-deg anhedral and a 30-deg anhedral. Both wings are presented at 5, 20 and 50 m/s.

An interesting detail in the 30-deg anhedral wing is that the minimum CD is displaced to an angle of attack of 6 degrees. That can be a feature of this particular wing, because the wing v2 does not show the same trend. It can be discarded that this is purely due to an increased anhedral, but the general reduction in drag due to the anhedral is clear.

Finally the L/D is plotted against angle of attack in Figure 4.6. Windspeed is not compared here, as it has been seen that it has little effect. The windspeed 5 m/s has been selected, and more anhedral cases are presented. The anhedral clearly increases L/D for this wing. The reason is that the reduction in CD overcomes the reduction in CL. As the wing has a low AR it must have a considerable penalty in induced drag. It may be possible that the high anhedral angles are effective in cases of low AR. This statement motivates the STUDY 2.

Another mention is the peak that the 30-deg anhedral has at 6 degrees AoA. This is coming from the minimum CD value that has already been seen at 6 degrees.

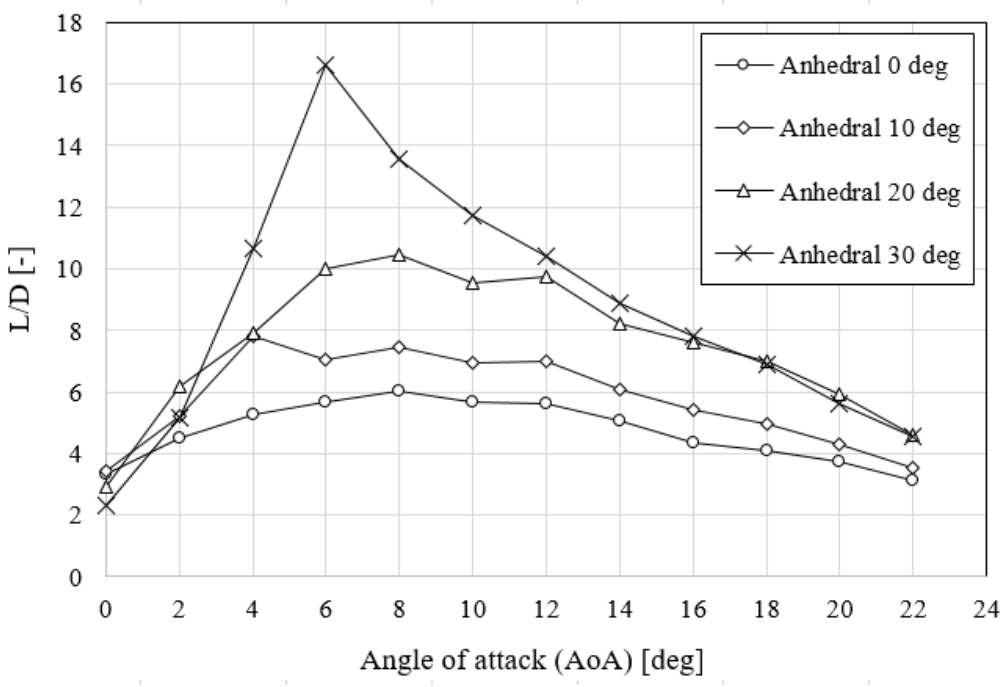

Figure 4.6: L/D against angle of attack for two versions of wing v1: a 0-deg anhedral and a 30-deg anhedral. Both wings are presented at 5, 20 and 50 m/s.

Now the results obtained with the wing v2 are presented in Figure 4.7. Wind speed is 5 m/s and only the linear trend has been plotted (up to 16 deg AoA). The same trends are seen: a reduction in CL and CD values. If compared to wing v1, wing v2 has a higher slope of CL and a lower CD. It can be said that it is an aerodynamically more efficient wing. As can be expected, L/D values are also higher, with maximum values higher than 20. Not only that, L/D is seen to increase with increased anhedral, as happened with wing v1. The only difference is the peak at 6 degrees of AoA that had wing v1, which is no existant here. Rather, the maximum L/D occurs sooner, between 0 and 4 degrees.

4.3.2 STUDY 2: The effect of aspect ratio

As it has been mentioned, the improvement of L/D due to the application of anhedral to a wing can be related to the AR of the wing. Most inflatable kites have low AR because

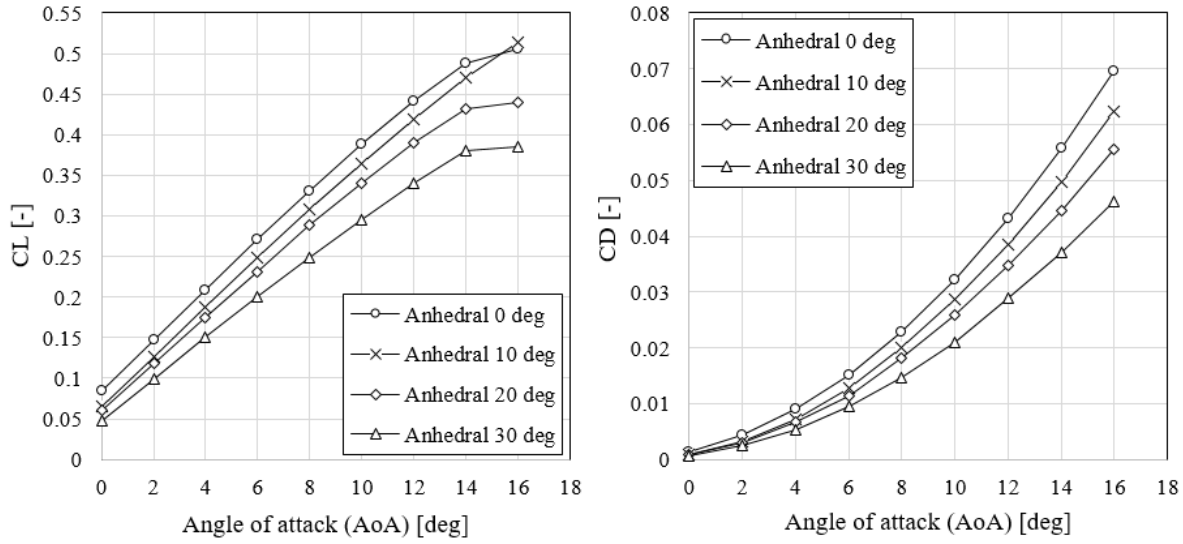

Figure 4.7: CL and CD against AoA at different wing anhedral versions of wing v2.

stiffness to bending moment is lost at high spans. It is the case of the kite tested in the wind tunnel, and it is the case of the present simulations. Now various versions of the wing v1 are modelled with increased wing span while maintaining the root chord. The result is a wing with doubled AR and a wing with quadrupled AR for each v1.1 (0-deg anhedral) and v1.7 (30-deg anhedral). Table 4.2 summarises their geometry characteristics. The aim of the present test is to see the effectiveness of the anhedral in L/D with a kite that has higher AR. A comparison with STUDY 1 will provide a conclusion on the effect AR.

L/D of the variants of increased AR is plotted against AoA in Figure 4.8. The results with the original AR are presented in the same plot for the comparison. The factor to compare is the capability of the anhedral (0 to 30 deg) to increase L/D.

The original AR sees the increase in L/D that has already been mentioned (dotted lines). The increase with the ARx2 is smaller, first because the planar wing has a better L/D and second because the 30-deg anhedral wing has a lower L/D. It can be said that the increased AR has made the anhedral less effective in increasing the L/D value. Last, the ARx4 has clearly worsened the capability of anhedral to improve the performance of the wing. Here, the curve of the planar wing has dropped probably because of an increase in profile drag overcoming the decrease in induced drag [63]. The curve of the 30-deg anhedral is not much better, and shows an erratic distribution. A more detailed study of the correlation between anhedral and

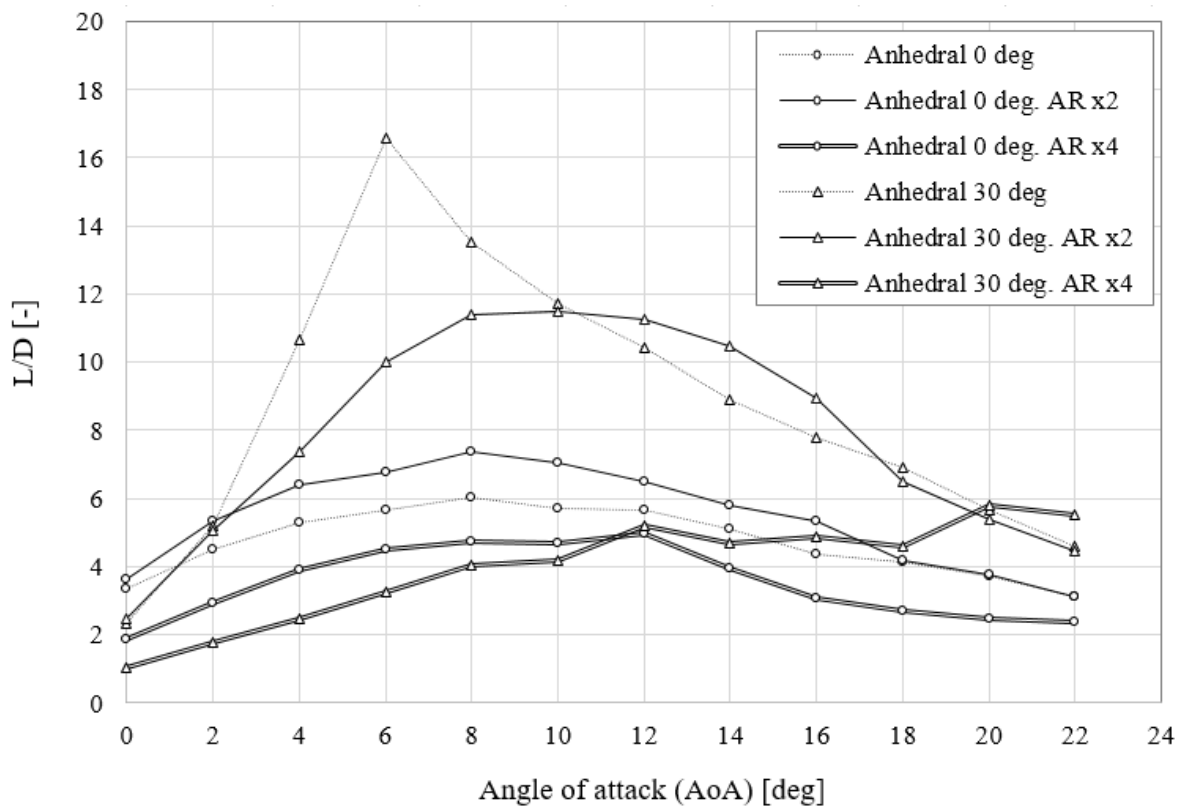

Figure 4.8: L/D against AoA for anhedrals 0 and 30 deg. Comparison between original AR, twice AR and four times AR.

AR is left for future work.

4.4 Validation with wind tunnel tests

It has been previously noted that the analytical approach and the wind tunnel tests were most likely not giving similar results. The two problems are too far to compare the absolute values of their results. This is easily confirmed if the C_L and C_D plots are compared. Similarities have rather been searched in the trends of aerodynamic forces with respect to several parameters. Note that these parameters have been defined slightly different in the experimental and the numerical approaches. The main parameters are listed below and an evaluation is given on the relation between the experimental and the numerical.

- Wind speed has been the same for the two approaches. They are completely equivalent.
- Lateral spacing (exp) vs Anhedral angle (num). The definitions are different, but they

have the same significance. Qualitatively, they are inversely proportional: the higher the anhedral angle, the closer is the lateral spacing. Quantitatively, however, it has not been possible to set a clear relation.

- Handle pitch angle (exp) vs Angle of attack (num). The definitions are different, and they do not have the same significance. But it has been seen in the experiments that every time the handle pitch angle increased under a constant wind speed, the attitude of the kite and therefore the angle of attack also increased. The two definitions can therefore be considered directly proportional. A quantitative relation has been found very difficult to find.

Thus a comparison of the experimental and the numerical approaches can only be done qualitatively, not only in the magnitude of the output values but also in the parameters on which they are compared.

It has been seen that the aerodynamic coefficients did not change with wind speed in the numerical approach, but they did in the experiments. Thus equivalent values of C_L and C_D had to be obtained. The best way of doing so, according to the author, was to suppose the dynamic pressure (q) so high that the coefficient plots converged to a certain value. This value is not recorded in the tests, but it is a $[q \to \infty]$ extrapolation of the curve showed by the experimental aerodynamic coefficients (see Figure 3.19, for example). The curves clearly converge when dynamic pressure increases.

In essence, the procedure lies on the supposition that the kite will be rigid when dynamic pressure is high enough, so that it can be compared to the numerical results. The values of C_L and C_D were obtained using the equation $C_L = \frac{L}{qA}$ in combination with the linear trend of the lift vs q curve (an example is given in Section 3.5.2). Table 4.5 shows the converged C_L and C_D for every lateral spacing (l) and handle pitch angles (θ) equal to 0, 10 and 15 degrees. The values with a " $*$ " are considered not reallistic as they are very high. Therefore the spanwise distance l = 90 cm has been discarded from the actual study. The converged values are plotted against θ, which is claimed to be related to AoA. That way the experimental results are compared with the CL vs AoA and CD vs AoA plots in Figure 4.4 and Figure 4.5 (for the case of v = 5 m/s). The comparison is presented in Figure 4.9 and Figure 4.10.

First, note that the vertical scale is not the same for the numerical and experimental results.

Table 4.5: Converged values of C_L and C_D when $[q \to \infty]$.

l [cm]	θ [deg]	C_L $[q \to \infty]$	C_D $[q \to \infty]$
61	0	0.65	0.14
	10	0.93	0.23
	15	1.02	0.30
90	0	0.71	0.14
	10	3.77*	0.89*
	15	5.74*	1.62*
105	0	0.72	0.18
	10	1.08	0.24
	15	1.23	0.34

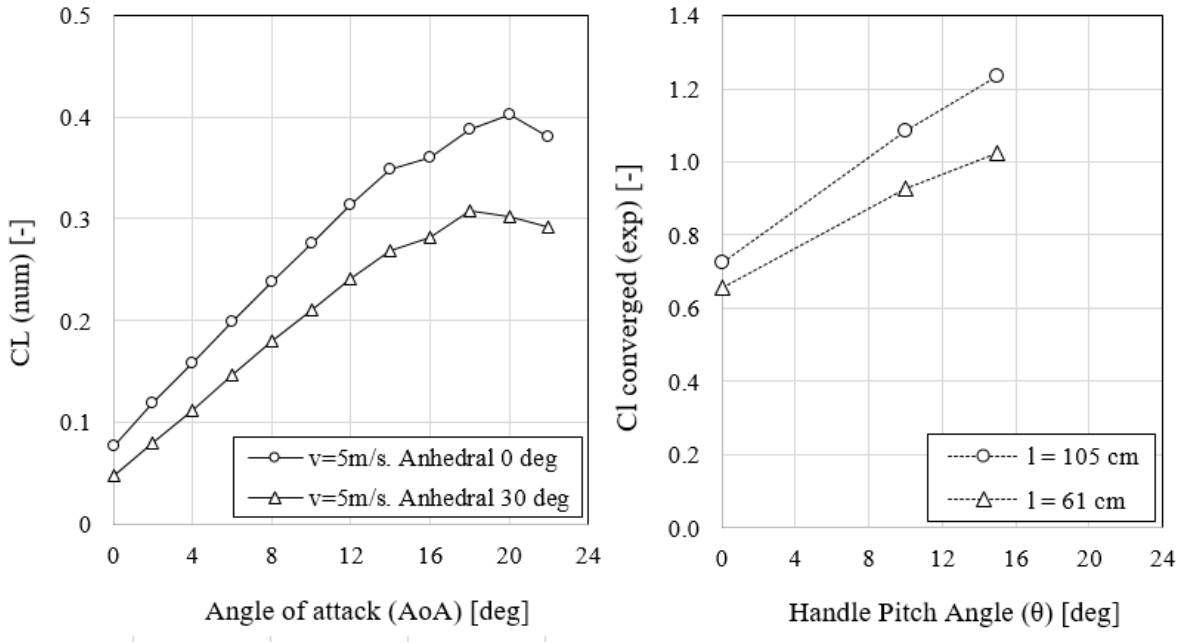

Figure 4.9: Numerical CL against AoA (left) and converged experimental C_L against θ (right).

The experimental plots give higher values of C_L and C_D. The number of data available in the experimental plots is also small, and it has to be reminded that their calculation comes from an extrapolation. The two studies, the numerical and the experimental, are remote in a sense. The numerical takes a simplified kite without the geometry characteristics such as balooning, air intakes... and deformation, and it carries the inaccuracies of a potential method. The experimental, on the other hand, has had stability problems and the chance that there is a

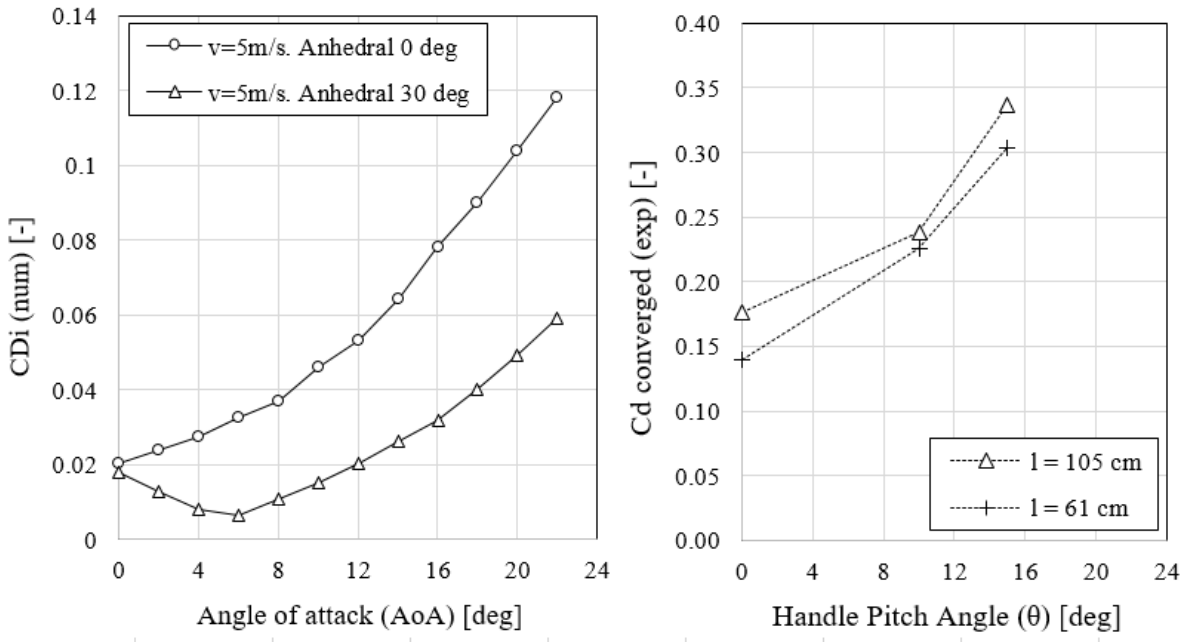

Figure 4.10: Numerical CD against AoA (left) and converged experimental C_D against θ (right).

high interaction with the wind tunnel walls is high. Taking into account every difference between the two studies, the similarity is considered reasonable. Both plots in Figure 4.9 show increasing C_L curve slopes and the effect of the increased anhedral is the same: decrease the slope of the curve and decrease the intercept. The similarities are easily seen in the plots. The C_D curves also show similar patterns, an increasing value with a growing slope. The effect of the increased anhedral is also that of decreasing the magnitude of the drag coefficient at every AoA.

It is not considered that the numerical approach has been properly validated, but the trends regarding the effect of anhedral on a low-AR wing can be claimed to match.

Chapter 5

Conclusions and Future Work

Wind tunnel tests of a scaled inflatable kite have been undertaken in the *8x6 Low Speed Wind Tunnel* at Cranfield University as a means of assessing the aerodynamic loads in such a scarcely studied wing. The context of the project is the application of non-rigid kites for wind energy harvesting, a branch of the novel, though promising technology defined as *Airborne Wind Energy*. A self-standing literature review has been included to introduce the topic to the reader as well as to give a base to future work.

The kite tested is a low aspect ratio, high arch-anhedral and fully flexible wing that is self inflated under wind pressure by openings along its leading edge. An experimental setup has been implemented where the kite is tethered upside down with its four lines to a "H frame". The frame emulates the control input of the kite and transmits the aerodynamic loads to an external, six-component strain-gauge balance.

A set of tests has been carried out over a range of wind speeds for various flight configurations. The main input parameters driving the different configurations have been the lateral or spanwise spacing between the lines and the pitch angle of the handles. These parameters have been manually adjusted in the H frame.

The experimental results have been compared to numerical simulations in a surface vorticity VLM solver. For the numerical approach two simplified wings have been modelled with their respective variations in anhedral and aspect ratio. The simulations have been run over a range of wind speeds and angles of attack.

The following observations have been done regarding the quality of the experimental approach. has been concluded regarding the quality of the experimental approach and its validity for the data extrapolation to full-scale power kites.

- **The kite showed lateral and directional instabilities** from a wind speed threshold on. This supposed an upper limit to the range of wind speeds, which varied with the configuration of each run. The kite was longitudinally stable.

- The best lateral spacing for the stability problem has been the smallest one ($l = 61cm$). As this is the spacing that brings the tips furthest from the walls, it has been concluded that **the main driver of instabilities is the interaction of the aerodynamic wake with the wind tunnel walls**.

- The best handle pitch angles for the stability problem have been the highest ones ($10deg \leq \theta \leq 20deg$). The handle pitch angle has been found to be directly related to two different parameters, the attitude of the kite and the pull of brakes. **The high pull of brakes has been found to be a way of increasing kite stability**.

- The quality of the wind tunnel tests has been penalised by the need of applying brakes to achieve a stable flight, which prevented the kite to fully inflate. **The experimental approach has had a compromise between kite stability and data quality**.

- C_L and C_D are found to converge to a constant value with increased wind speed. This trend confirms the flexible nature of the kite and suggests that **rigidity is gained with wind speed**.

- The kite flies at high C_L and C_D values. C_L converges to values around the unit. The highest L/D ratios converge in values between 4 and 4.5. **The performance of the kite is inside the range of typical L/D-s of low AR, flexible kites**.

- The brakes are seen to act as high-lift devices, as they induce an extra camber to the wing. **An increase in pull of brakes increases both C_L and C_D, but reduces L/D. This is a sign of good effectiveness of the brakes**.

- **A smaller lateral spacing (higher wing anhedral) has been seen to reduce both C_L and C_D.**. The effect of wing anhedral has been compared to the numerical approach and the trends match qualitatively.

Overall, the experimental tests have been found useful for a parametric study but not successful in providing quantitative data that can be extrapolated to full-scale power kites. The stability problem is identified as the main responsible for the reduced quality or results. **It is concluded that the dimensions of the kite are too big for the 8x6 Wind Tunnel**.

The numerical approach has not been properly validated. The only successful comparison was a qualitative one involving the effect of anhedral in C_L and C_D. **The numerical and experimental approaches are considered to be too far for a proper comparison**.

The project has been the first involving a kite in a wind tunnel in Cranfield University. The not-as-satisfactory results are considered overcome by the knowledge obtained on the flight of the flexible kite. The limitations of testing a kite in a wind tunnel have also been understood. Several tips for future work are given now.

Regarding the continuation of the present experimental approach:

- If the stability is guarantied, the two trailing edge lines (brakes) are not necessary. Instead of a four-line kite a simpler two-line kite can be purchased. This will make the kite to fully inflate and fly as designed. Thus the challenge is to find a way of stabilising the kite in order to avoid the use of brakes.
- A possible way of increasing stability is to test different kites with smaller wing span. That way the interaction with the wind tunnel walls can be reduced.
- A better imaging setup can help in reading more accurately the attitude, or even the angle of attack of the kite at every flight configuration and wind speed. The extraction of data would see a big improvement.
- Flow-visualisation tests can determine the regions of separated flow, and allow a study of the effects that different flight configurations have on the flow separation.

According to alternative approaches of the research line:

- A different wind tunnel setup can be that of testing a rigid model. That way the stability can be guaranteed, the input can be more controllable and the output more reliable. A parametric study of isolated factors is also easier to undertake, since the coupled effects are reduced. In addition, it would mean an easier validation of the numerical approach.

- Another alternative is that of testing a semi-rigid model, i.e., a rigid structure with a fabric coating. This would bring the benefits of the rigid model combined with a partial account for the deformations. This procedure is also more common in the literature.

- Another alternative to the wind tunnel tests is the atmospheric flight. Even if a whole new grounding would have to be set for this approach, it has to be reminded that the flight tests are closer to the real application of power generation.

- Instead of simplifying the wind tunnel model to a rigid one, the numerical approach can be modified to a higher-fidelity level to stand closer to the behaviour of the fully-flexible kite. It is suggested that the first step to take into account when building a comprehensive numerical approach is the FSI problem. A CFD study could also help in obtaining more detailed results. A FSI approach combined with the use of CFD could represent a bridge between the complex wind tunnel environment and the simplified VLM environment. For that a FEM model could be used to account for the surface displacements due to aerodynamic loads.

- Building a dynamic model of the experimental setup can help in understanding the unstable behaviour of the kite. In addition it can set the relations between the static flight of the wind tunnel and the more complex crosswind motion of the full-scale power kites. Instead of time-averaged measurements in the wind tunnel, measurements over time could be preferred for this approach.

Bibliography

[1] Clive Hart. *Kites: An Historical Survey*. Faber and Faber Ltd., 1967.

[2] John D. Jr. Anderson. *A History of Aerodynamics and Its Impact on Flying Machines*. Cambridge University Press, 1997.

[3] Stephen E. Hobbs. "A Quantitative Study of Kite Performance in Natural Wind with Application to Kite Anemometry". PhD thesis. Cranfield University, 1986.

[4] C. F. Marvin. *The Mechanics and Equilibrium of Kites*. Tech. rep. Weather Bureau, 1897. URL: https://archive.org/details/amonographonmec00buregoog/page/n5.

[5] S. B. Jackson. *Free-Flight Tests on Kites in the 24-ft Wind Tunnel*. Tech. rep. Aeronautical Research Council (ARC), 1951.

[6] Francis M. Rogallo. *Preliminary Investigation of a Paraglider*. Tech. rep. NASA, 1960.

[7] Edward C. Polhamus and Rodger L. Naeseth. *Experimental and Theoretical Studies of the Effects of Camber and Twist on the Aerodynamic Characteristics of Parawings having Nominal Aspect Ratios of 3 and 6*. Tech. rep. NASA, 1963. URL: https://ntrs.nasa.gov/search.jsp?R=19630002411.

[8] Francis M. Rogallo, William C. Sleeman, and Delwin R. Croom. *Resume of Recent Parawing Research*. Tech. rep. NASA, 1965.

[9] Charles E. Libbey, George M. Ware, and Rodger L. Naeseth. *Wind-tunnel investigation of the static aerodynamic characteristics of an 18-foot (5.49-meter) all-exible parawing*. Tech. rep. NASA, 1967.

[10] John D. Nicolaides, Ralph J. Speelman, and George L. C. Menard. "A Review of Para-Foil Applications". In: *Journal of Aircraft* 7.5 (1970), pp. 423–431.

[11] John D. Nicolaides. *Parafoil Wind Tunnel Tests*. Tech. rep. Air Force Flight Dynamics Laboratory (AFFDL), 1971.

[12] John D. Nicolaides and Michael A. Tragarz. *Parafoil Flight Performance*. Tech. rep. June 1971.

[13] Payne et al. *Self-Erecting Windmill*. 1976.

[14] Miles L. Loyd. "Crosswind Kite Power". In: *Journal of Energy* 4.3 (1980), pp. 106–111.

[15] Antonello Cherubini et al. "Airborne Wind Energy Systems: A review of the technologies". In: *Renewable and Sustainable Energy Reviews* 51 (Aug. 2015), pp. 1461–1476.

[16] Lorenzo Fagiano. "Control of Tethered Airfoils for High-Altitude Wind Energy Generation". PhD thesis. Politecnico di Torino, 2009, pp. 76–80.

[17] I. Argatov, P. Rautakorpi, and R. Silvennoinen. "Estimation of the mechanical energy output of the kite wind generator". In: *Renewable Energy* 34.6 (2009), pp. 1525–1532.

[18] Marcelo De Lellis et al. "The Betz limit applied to Airborne Wind Energy". In: *Renewable Energy* 127 (Nov. 2018), pp. 32–40.

[19] Rachel Leuthold, Sébastien Gros, and Moritz Diehl. "Induction in Optimal Control of Multiple-Kite Airborne Wind Energy Systems". In: *IFAC-PapersOnLine* 50.1 (2017), pp. 153–158.

[20] Mojtaba Kheiri et al. "On the aerodynamic performance of crosswind kite power systems". In: *Journal of Wind Engineering and Industrial Aerodynamics* 181 (Oct. 2018), pp. 1–13.

[21] C. M. Madsen and C. J. Cerimele. "Flight Performance, Aerodynamics, and Simulation Development for the X-38 Parafoil Test Program". In: *17th AIAA Aerodynamic Decelerator Systems Technology Conference and Seminar*. Monterey: American Institute of Aeronautics and Astronautics (AIAA), May 2003.

[22] KiteGen. *KiteGen webpage (last entry July 2019)*.

[23] SkySails. *SkySails webpage (last entry July 2019)*.

[24] KitePower. *KitePower webpage (last entry July 2019)*. URL: `https://kitepower.nl/%7B%5C%%7D0Aresearch/`.

[25] AWEC. *Airborne Wind Energy Conference (AWEC) 2019 webpage (last entry July 2019)*. URL: `https://www.awec2019.com/`.

[26] Leo Bruinzeel et al. "Ecological Impact of Airborne Wind Energy Technology: Current State of Knowledge and Future Research Agenda". In: *Airborne Wind Energy: Advances in Technology Development and Research*. Springer, 2018. Chap. 28, pp. 679–701.

[27] C Wang and R G Prinn. “Climatic impacts and reliability of very large-scale wind farms”. In: *Atmos. Chem. Phys* 10.4 (2010), pp. 2053–2061. URL: www.atmos-chem-phys.net/10/2053/2010/.

[28] L. M. Miller, F. Gans, and A. Kleidon. “Jet stream wind power as a renewable energy resource: little power, big impacts”. In: *Earth System Dynamics* 2.2 (2011), pp. 201–212.

[29] D. W. Keith et al. “The influence of large-scale wind power on global climate”. In: *Proceedings of the National Academy of Sciences* 101.46 (Nov. 2004), pp. 16115–16120.

[30] Paul Williams, Bas Lansdorp, and Wubbo Ockesl. “Optimal Cross-Wind Towing and Power Generation with Tethered Kites”. In: *AIAA Guidance, Navigation and Control Conference and Exhibit*. Hilton Head: American Institute of Aeronautics and Astronautics (AIAA), Aug. 2007.

[31] Bas Lansdorp et al. “Modeling, Simulation, and Testing of Surf Kites for Power Generation”. In: *Modeling and Simulation Technologies Conference and Exhibit*. Honolulu: American Institute of Aeronautics and Astronautics (AIAA), Aug. 2008.

[32] M.B. Ruppert. “Development and validation of a real time pumping kite model”. PhD thesis. Delft University of Technology, 2012.

[33] Jelte Van Til et al. “Dynamic Model of a C-shaped Bridled Kite Using a few Rigid Plates”. In: *Airborne Wind Energy: Advances in Technology Development and Research*. Springer, 2018. Chap. 5, pp. 99–115.

[34] G. Sánchez-Arriaga, M. García-Villalba, and R. Schmehl. “Modeling and dynamics of a two-line kite”. In: *Applied Mathematical Modelling* 47 (July 2017), pp. 473–486.

[35] Rolf van der Vlugt et al. “Quasi-steady model of a pumping kite power system”. In: *Renewable Energy* 131 (Feb. 2019), pp. 83–99. ISSN: 18790682.

[36] Rachel Leuthold. “Multiple-Wake Vortex Lattice Method for Membrane-Wing Kites”. PhD thesis. Delft University of Technology, 2015.

[37] Allert Bosch et al. “Dynamic Nonlinear Aeroelastic Model of a Kite for Power Generation”. In: *Journal of Guidance, Control, and Dynamics* 37.5 (Sept. 2014), pp. 1426–1436.

[38] Michael Erhard and Hans Strauch. “Control of Towing Kites for Seagoing Vessels”. In: *IEEE Transactions on Control Systems Technology* 21.5 (Sept. 2013), pp. 1629–1640.

[39] Uwe Fechner and Roland Schmehl. “Design of a Distributed Kite Power Control System”. In: *IEEE International Conference on Control Applications*. Dubrovnik, 2012, pp. 800–805.

[40] R. G. den Boer. *Numerical and experimental investigation of the aerodynamics of double membrane sailwing airfoil sections*. Tech. rep. Delft University of Technology, 1982.

[41] H. Babinsky. “The aerodynamic performance of paragliders”. In: *The Aeronautical Journal* 103.1027 (1999), pp. 421–428.

[42] Kenneth J. Desabrais et al. “Aerodynamic Investigations of a Ram-Air Parachute Canopy and an Airdrop System”. In: *23rd AIAA Aerodynamic Decelerator Systems Technology Conference*. Daytona Beach: American Institute of Aeronautics and Astronautics (AIAA), Mar. 2015.

[43] H. Belloc. “Wind Tunnel Investigation of a Rigid Paraglider Reference Wing”. In: *Journal of Aircraft* 52.2 (Jan. 2015), pp. 703–708. ISSN: 0021-8669.

[44] Aart de Wachter. “Deformation and aerodynamic performance of a ram-air wing”. PhD Thesis. Delft University of Technology, 2008, p. 110.

[45] Glen J. Brown. “Tethered parafoil test technique”. In: *10th Aerodynamic Decelerator Conference*. AIAA, 1989. URL: `www.aiaa.org`.

[46] Johannes Oehler, Van Reijen Marc, and Roland Schmehl. “Experimental investigation of soft kite performance during turning maneuvers”. In: *Journal of Physics: Conference Series*. Vol. 1037. 5. Institute of Physics Publishing, 2018.

[47] S. E. Hobbs. “Kite performance measurements in natural wind”. In: *Aeronautical Journal* 94.932 (Feb. 1990), pp. 59–66.

[48] C. Iacomini and C. Cerimele. “Lateral-directional aerodynamics from a large scale parafoil test program”. In: *15th Aerodynamic Decelerator Systems Technology Conference*. Reston, Virigina: American Institute of Aeronautics and Astronautics (AIAA), 1999. URL: `http://arc.aiaa.org/doi/10.2514/6.1999-1731`.

[49] C. Iacomini and C. J. Cerimele. “Longitudinal aerodynamics from a large scale parafoil test program”. In: *15th Aerodynamic Decelerator Systems Technology Conference*. American Institute of Aeronautics and Astronautics (AIAA), 1999.

[50] Thomas Jann. “Aerodynamic model identification and GNC design for the parafoil-load system ALEX”. In: *16th AIAA aerodynamic decelerator systems technology conference and seminar*. American Institute of Aeronautics and Astronautics (AIAA), 2001.

[51] Bas Lansdorp, B Remes, and W J Ockels. “Design and testing of a remotely controlled surfkite for the Laddermill”. In: *submissiion to World Wind Energy Conference*. 2005.

[52] Wubbo J. Ockels. “Laddermill, a novel concept to exploit the energy in the airspace”. In: *Aircraft Design* 4.2-3 (June 2001), pp. 81–97.

[53] M. Gonzalez. “Prandtl theory applied to paraglider aerodynamics”. In: *Aerospace Design Conference*. American Institute of Aeronautics and Astronautics (AIAA), 1993.

[54] Thomas Jann. “Aerodynamic Coefficients for a Parafoil Wing with Arc Anhedral - Theoretical and Experimental Results”. In: *17th AIAA Aerodynamic Decelerator Systems Technology Conference and Seminar*. American Institute of Aeronautics and Astronautics (AIAA), 2003.

[55] Alain De Solminihac et al. “Kite as a Beam: A Fast Method to get the Flying Shape”. In: *Airborne Wind Energy: Advances in Technology Development and Research*. Springer, 2018. Chap. 4, pp. 79–97.

[56] M. Gaunaa et al. “A computationally efficient method for determining the aerodynamic performance of kites for wind energy applications”. In: *Proceedings European Wind Energy Association (EWEA)*. 2011.

[57] Prabu Sal Manoj. *Multiple-Wake Vortex Method for Leading Edge Inatable Tube Kites used in Airborne Wind Energy Systems*. 2017. URL: `https://bitbucket.org/rschmehl/awec%7B%5C_%7Dlatex%7B%5C_%7Dboa`.

[58] Teresa Rodrigo Rey. “Development of a 3D Panel Method Code for Wing Design”. PhD thesis. Cranfield University, 2014.

[59] W. Strang et al. “Evaluation of four panel aerodynamic prediction methods (MCAERO, PANAIR, QUADPAN, and VSAERO)”. In: *AIAA 3rd Applied Aerodynamics Conference*. Colorado Springs: American Institute of Aeronautics and Astronautics (AIAA), Oct. 1985.

[60] Gianmauro Maneia et al. “Aerodynamics of a rigid curved kite wing”. In: (June 2013). arXiv: `1306.4148`. URL: `http://arxiv.org/abs/1306.4148`.

[61] Florian Bauer et al. “Drag power kite with very high lift coefficient”. In: *Renewable Energy* 118 (2018), pp. 290–305.

[62] S. E. Hobbs. “Kite performance measurements in natural wind”. In: *Aeronautical Journal* 94 (1990), pp. 59–66.

[63] Clarence D. Jr. Cone. *The Theory of Induced Lift and Minimum Induced Drag of Nonplanar Lifting Systems*. Tech. rep. NASA, 1962.

[64] M. Gonzalez. "Prandtl theory applied to paraglider aerodynamics". In: *Aerospace Design Conference*. AIAA, 1993.

[65] Vivek Ahuja. "Aerodynamic Loads over Arbitrary Bodies by Method of Integrated Circulation". PhD thesis. Auburn University, 2013.

[66] Airfoil Tools. *Clark-Y aerofoil geometry (webpage, last entry August 2019)*. URL: `http://airfoiltools.com/airfoil/details?airfoil=clarky-il`.